TRANSIENT ELECTRIC FIELD RADIATION FROM HIGH–SPEED INTERCONNECTS WITHIN A SINGLE DIELECTRIC, PRINTED CIRCUIT STRUCTURE

by

Ralph Dennis Lohse

A Thesis Presented to the

Faculty of Graduate Studies

University of Manitoba

In Partial Fulfillment of the Requirements for the Degree of

Master of Science (EE)

August, 1996

ISBN 0-612-16197-8

Canada

Name ___

Dissertation Abstracts International and *Masters Abstracts International* are arranged by broad, general subject categories. Please select the one subject which most nearly describes the content of your dissertation or thesis. Enter the corresponding four-digit code in the spaces provided.

Electronics and Electrical — SUBJECT TERM

0544 — SUBJECT CODE

UMI

Subject Categories

THE HUMANITIES AND SOCIAL SCIENCES

COMMUNICATIONS AND THE ARTS
- Architecture 0729
- Art History 0377
- Cinema 0900
- Dance 0378
- Fine Arts 0357
- Information Science 0723
- Journalism 0391
- Library Science 0399
- Mass Communications 0708
- Music 0413
- Speech Communication 0459
- Theater 0465

EDUCATION
- General 0515
- Administration 0514
- Adult and Continuing 0516
- Agricultural 0517
- Art 0273
- Bilingual and Multicultural 0282
- Business 0688
- Community College 0275
- Curriculum and Instruction 0727
- Early Childhood 0518
- Elementary 0524
- Finance 0277
- Guidance and Counseling 0519
- Health 0680
- Higher 0745
- History of 0520
- Home Economics 0278
- Industrial 0521
- Language and Literature 0279
- Mathematics 0280
- Music 0522
- Philosophy of 0998
- Physical 0523
- Psychology 0525
- Reading 0535
- Religious 0527
- Sciences 0714
- Secondary 0533
- Social Sciences 0534
- Sociology of 0340
- Special 0529
- Teacher Training 0530
- Technology 0710
- Tests and Measurements 0288
- Vocational 0747

LANGUAGE, LITERATURE AND LINGUISTICS
- Language
  - General 0679
  - Ancient 0289
  - Linguistics 0290
  - Modern 0291
- Literature
  - General 0401
  - Classical 0294
  - Comparative 0295
  - Medieval 0297
  - Modern 0298
  - African 0316
  - American 0591
  - Asian 0305
  - Canadian (English) 0352
  - Canadian (French) 0355
  - English 0593
  - Germanic 0311
  - Latin American 0312
  - Middle Eastern 0315
  - Romance 0313
  - Slavic and East European 0314

PHILOSOPHY, RELIGION AND THEOLOGY
- Philosophy 0422
- Religion
  - General 0318
  - Biblical Studies 0321
  - Clergy 0319
  - History of 0320
  - Philosophy of 0322
- Theology 0469

SOCIAL SCIENCES
- American Studies 0323
- Anthropology
  - Archaeology 0324
  - Cultural 0326
  - Physical 0327
- Business Administration
  - General 0310
  - Accounting 0272
  - Banking 0770
  - Management 0454
  - Marketing 0338
- Canadian Studies 0385
- Economics
  - General 0501
  - Agricultural 0503
  - Commerce-Business 0505
  - Finance 0508
  - History 0509
  - Labor 0510
  - Theory 0511
- Folklore 0358
- Geography 0366
- Gerontology 0351
- History
  - General 0578
  - Ancient 0579
  - Medieval 0581
  - Modern 0582
  - Black 0328
  - African 0331
  - Asia, Australia and Oceania 0332
  - Canadian 0334
  - European 0335
  - Latin American 0336
  - Middle Eastern 0333
  - United States 0337
- History of Science 0585
- Law 0398
- Political Science
  - General 0615
  - International Law and Relations 0616
  - Public Administration 0617
- Recreation 0814
- Social Work 0452
- Sociology
  - General 0626
  - Criminology and Penology 0627
  - Demography 0938
  - Ethnic and Racial Studies 0631
  - Individual and Family Studies 0628
  - Industrial and Labor Relations 0629
  - Public and Social Welfare 0630
  - Social Structure and Development 0700
  - Theory and Methods 0344
- Transportation 0709
- Urban and Regional Planning 0999
- Women's Studies 0453

THE SCIENCES AND ENGINEERING

BIOLOGICAL SCIENCES
- Agriculture
  - General 0473
  - Agronomy 0285
  - Animal Culture and Nutrition 0475
  - Animal Pathology 0476
  - Food Science and Technology 0359
  - Forestry and Wildlife 0478
  - Plant Culture 0479
  - Plant Pathology 0480
  - Plant Physiology 0817
  - Range Management 0777
  - Wood Technology 0746
- Biology
  - General 0306
  - Anatomy 0287
  - Biostatistics 0308
  - Botany 0309
  - Cell 0379
  - Ecology 0329
  - Entomology 0353
  - Genetics 0369
  - Limnology 0793
  - Microbiology 0410
  - Molecular 0307
  - Neuroscience 0317
  - Oceanography 0416
  - Physiology 0433
  - Radiation 0821
  - Veterinary Science 0778
  - Zoology 0472
- Biophysics
  - General 0786
  - Medical 0760

EARTH SCIENCES
- Biogeochemistry 0425
- Geochemistry 0996
- Geodesy 0370
- Geology 0372
- Geophysics 0373
- Hydrology 0388
- Mineralogy 0411
- Paleobotany 0345
- Paleoecology 0426
- Paleontology 0418
- Paleozoology 0985
- Palynology 0427
- Physical Geography 0368
- Physical Oceanography 0415

HEALTH AND ENVIRONMENTAL SCIENCES
- Environmental Sciences 0768
- Health Sciences
  - General 0566
  - Audiology 0300
  - Chemotherapy 0992
  - Dentistry 0567
  - Education 0350
  - Hospital Management 0769
  - Human Development 0758
  - Immunology 0982
  - Medicine and Surgery 0564
  - Mental Health 0347
  - Nursing 0569
  - Nutrition 0570
  - Obstetrics and Gynecology 0380
  - Occupational Health and Therapy 0354
  - Ophthalmology 0381
  - Pathology 0571
  - Pharmacology 0419
  - Pharmacy 0572
  - Physical Therapy 0382
  - Public Health 0573
  - Radiology 0574
  - Recreation 0575
  - Speech Pathology 0460
  - Toxicology 0383
- Home Economics 0386

PHYSICAL SCIENCES
Pure Sciences
- Chemistry
  - General 0485
  - Agricultural 0749
  - Analytical 0486
  - Biochemistry 0487
  - Inorganic 0488
  - Nuclear 0738
  - Organic 0490
  - Pharmaceutical 0491
  - Physical 0494
  - Polymer 0495
  - Radiation 0754
- Mathematics 0405
- Physics
  - General 0605
  - Acoustics 0986
  - Astronomy and Astrophysics 0606
  - Atmospheric Science 0608
  - Atomic 0748
  - Electronics and Electricity 0607
  - Elementary Particles and High Energy 0798
  - Fluid and Plasma 0759
  - Molecular 0609
  - Nuclear 0610
  - Optics 0752
  - Radiation 0756
  - Solid State 0611
- Statistics 0463

Applied Sciences
- Applied Mechanics 0346
- Computer Science 0984
- Engineering
  - General 0537
  - Aerospace 0538
  - Agricultural 0539
  - Automotive 0540
  - Biomedical 0541
  - Chemical 0542
  - Civil 0543
  - Electronics and Electrical 0544
  - Heat and Thermodynamics 0348
  - Hydraulic 0545
  - Industrial 0546
  - Marine 0547
  - Materials Science 0794
  - Mechanical 0548
  - Metallurgy 0743
  - Mining 0551
  - Nuclear 0552
  - Packaging 0549
  - Petroleum 0765
  - Sanitary and Municipal 0554
  - System Science 0790
- Geotechnology 0428
- Operations Research 0796
- Plastics Technology 0795
- Textile Technology 0994

PSYCHOLOGY
- General 0621
- Behavioral 0384
- Clinical 0622
- Developmental 0620
- Experimental 0623
- Industrial 0624
- Personality 0625
- Physiological 0989
- Psychobiology 0349
- Psychometrics 0632
- Social 0451

Nom _____

Dissertation Abstracts International est organisé en catégories de sujets. Veuillez s.v.p. choisir le sujet qui décrit le mieux votre thèse et inscrivez le code numérique approprié dans l'espace réservé ci-dessous.

_____ ☐☐☐ U·M·I

SUJET — CODE DE SUJET

Catégories par sujets

HUMANITÉS ET SCIENCES SOCIALES

COMMUNICATIONS ET LES ARTS
Architecture 0729
Beaux-arts 0357
Bibliothéconomie 0399
Cinéma 0900
Communication verbale 0459
Communications 0708
Danse 0378
Histoire de l'art 0377
Journalisme 0391
Musique 0413
Sciences de l'information 0723
Théâtre 0465

ÉDUCATION
Généralités 515
Administration 0514
Art 0273
Collèges communautaires 0275
Commerce 0688
Économie domestique 0278
Éducation permanente 0516
Éducation préscolaire 0518
Éducation sanitaire 0680
Enseignement agricole 0517
Enseignement bilingue et multiculturel 0282
Enseignement industriel 0521
Enseignement primaire. 0524
Enseignement professionnel 0747
Enseignement religieux 0527
Enseignement secondaire 0533
Enseignement spécial 0529
Enseignement supérieur 0745
Évaluation 0288
Finances 0277
Formation des enseignants 0530
Histoire de l'éducation 0520
Langues et littérature 0279
Lecture 0535
Mathématiques 0280
Musique 0522
Orientation et consultation 0519
Philosophie de l'éducation 0998
Physique 0523
Programmes d'études et enseignement 0727
Psychologie 0525
Sciences 0714
Sciences sociales 0534
Sociologie de l'éducation 0340
Technologie 0710

LANGUE, LITTÉRATURE ET LINGUISTIQUE
Langues
- Généralités 0679
- Anciennes 0289
- Linguistique 0290
- Modernes 0291

Littérature
- Généralités 0401
- Anciennes 0294
- Comparée 0295
- Médiévale 0297
- Moderne 0298
- Africaine 0316
- Américaine 0591
- Anglaise 0593
- Asiatique 0305
- Canadienne (Anglaise) 0352
- Canadienne (Française) 0355
- Germanique 0311
- Latino-américaine 0312
- Moyen-orientale 0315
- Romane 0313
- Slave et est-européenne 0314

PHILOSOPHIE, RELIGION ET THÉOLOGIE
Philosophie 0422
Religion
- Généralités 0318
- Clergé 0319
- Études bibliques 0321
- Histoire des religions 0320
- Philosophie de la religion 0322

Théologie 0469

SCIENCES SOCIALES
Anthropologie
- Archéologie 0324
- Culturelle 0326
- Physique 0327

Droit 0398
Économie
- Généralités 0501
- Commerce-Affaires 0505
- Économie agricole 0503
- Économie du travail 0510
- Finances 0508
- Histoire 0509
- Théorie 0511

Études américaines 0323
Études canadiennes 0385
Études féministes 0453
Folklore 0358
Géographie 0366
Gérontologie 0351
Gestion des affaires
- Généralités 0310
- Administration 0454
- Banques 0770
- Comptabilité 0272
- Marketing 0338

Histoire
- Histoire générale 0578
- Ancienne 0579
- Médiévale 0581
- Moderne 0582
- Histoire des noirs 0328
- Africaine 0331
- Canadienne 0334
- États-Unis 0337
- Européenne 0335
- Moyen-orientale 0333
- Latino-américaine 0336
- Asie, Australie et Océanie 0332

Histoire des sciences 0585
Loisirs 0814
Planification urbaine et régionale 0999
Science politique
- Généralités 0615
- Administration publique 0617
- Droit et relations internationales 0616

Sociologie
- Généralités 0626
- Aide et bien-être social 0630
- Criminologie et établissements pénitentiaires 0627
- Démographie 0938
- Études de l' individu et de la famille 0628
- Études des relations interethniques et des relations raciales 0631
- Structure et développement social 0700
- Théorie et méthodes. 0344
- Travail et relations industrielles 0629

Transports 0709
Travail social 0452

SCIENCES ET INGÉNIERIE

SCIENCES BIOLOGIQUES
Agriculture
- Généralités 0473
- Agronomie. 0285
- Alimentation et technologie alimentaire 0359
- Culture 0479
- Élevage et alimentation 0475
- Exploitation des pâturages 0777
- Pathologie animale 0476
- Pathologie végétale 0480
- Physiologie végétale 0817
- Sylviculture et faune 0478
- Technologie du bois 0746

Biologie
- Généralités 0306
- Anatomie 0287
- Biologie (Statistiques) 0308
- Biologie moléculaire 0307
- Botanique 0309
- Cellule 0379
- Écologie 0329
- Entomologie 0353
- Génétique 0369
- Limnologie 0793
- Microbiologie 0410
- Neurologie 0317
- Océanographie 0416
- Physiologie 0433
- Radiation 0821
- Science vétérinaire 0778
- Zoologie 0472

Biophysique
- Généralités 0786
- Medicale 0760

SCIENCES DE LA TERRE
Biogéochimie 0425
Géochimie 0996
Géodésie 0370
Géographie physique 0368
Géologie 0372
Géophysique 0373
Hydrologie 0388
Minéralogie 0411
Océanographie physique 0415
Paléobotanique 0345
Paléoécologie 0426
Paléontologie 0418
Paléozoologie 0985
Palynologie 0427

SCIENCES DE LA SANTÉ ET DE L'ENVIRONNEMENT
Économie domestique 0386
Sciences de l'environnement 0768
Sciences de la santé
- Généralités 0566
- Administration des hôpitaux 0769
- Alimentation et nutrition 0570
- Audiologie 0300
- Chimiothérapie 0992
- Dentisterie 0567
- Développement humain 0758
- Enseignement 0350
- Immunologie 0982
- Loisirs 0575
- Médecine du travail et thérapie 0354
- Médecine et chirurgie 0564
- Obstétrique et gynécologie 0380
- Ophtalmologie 0381
- Orthophonie 0460
- Pathologie 0571
- Pharmacie 0572
- Pharmacologie 0419
- Physiothérapie 0382
- Radiologie 0574
- Santé mentale 0347
- Santé publique 0573
- Soins infirmiers 0569
- Toxicologie 0383

SCIENCES PHYSIQUES
Sciences Pures
Chimie
- Généralités 0485
- Biochimie 487
- Chimie agricole 0749
- Chimie analytique 0486
- Chimie minérale 0488
- Chimie nucléaire 0738
- Chimie organique 0490
- Chimie pharmaceutique 0491
- Physique 0494
- PolymÈres 0495
- Radiation 0754

Mathématiques 0405
Physique
- Généralités 0605
- Acoustique 0986
- Astronomie et astrophysique 0606
- Électronique et électricité 0607
- Fluides et plasma 0759
- Météorologie 0608
- Optique 0752
- Particules (Physique nucléaire) 0798
- Physique atomique 0748
- Physique de l'état solide 0611
- Physique moléculaire 0609
- Physique nucléaire 0610
- Radiation 0756

Statistiques 0463

Sciences Appliqués Et Technologie
Informatique 0984
Ingénierie
- Généralités 0537
- Agricole 0539
- Automobile 0540
- Biomédicale 0541
- Chaleur et thermodynamique 0348
- Conditionnement (Emballage) 0549
- Génie aérospatial 0538
- Génie chimique 0542
- Génie civil 0543
- Génie électronique et électrique 0544
- Génie industriel 0546
- Génie mécanique 0548
- Génie nucléaire 0552
- Ingénierie des systèmes 0790
- Mécanique navale 0547
- Métallurgie 0743
- Science des matériaux 0794
- Technique du pétrole 0765
- Technique minière 0551
- Techniques sanitaires et municipales 0554
- Technologie hydraulique 0545

Mécanique appliquée 0346
Géotechnologie 0428
Matières plastiques (Technologie) 0795
Recherche opérationnelle 0796
Textiles et tissus (Technologie) 0794

PSYCHOLOGIE
Généralités 0621
Personnalité 0625
Psychobiologie 0349
Psychologie clinique 0622
Psychologie du comportement 0384
Psychologie du développement 0620
Psychologie expérimentale 0623
Psychologie industrielle 0624
Psychologie physiologique 0989
Psychologie sociale 0451
Psychométrie 0632

THE UNIVERSITY OF MANITOBA

FACULTY OF GRADUATE STUDIES

COPYRIGHT PERMISSION

TRANSIENT ELECTRIC FIELD RADIATION FROM HIGH-SPEED INTERCONNECTS WITHIN A SINGLE DIELECTRIC, PRINTED CIRCUIT STRUCTURE

BY

RALPH DENNIS LOHSE

A Thesis/Practicum submitted to the Faculty of Graduate Studies of the University of Manitoba in partial fulfillment of the requirements for the degree of

MASTER OF SCIENCE

IN LOVING MEMORY OF MY FATHER

MARTIN GOTTFRIED LOHSE

1927–1995

ABSTRACT

Simulation of the electromagnetic fields radiated from high speed printed circuits is becoming increasingly important in electronic system design as well as to ensure compliance with present electromagnetic compatibility standards. Furthermore, increasing complexities in the printed circuits and electronic systems being considered have created a need for quick and efficient techniques for the calculation of such radiated emissions. In this thesis, electromagnetic radiation due to high speed transient signals on printed circuit board, multi–chip module, and integrated circuit interconnects is examined using a simple closed form solution for the time domain radiated fields due to an arbitrary, single–dielectric interconnect geometry. The developed technique is intended to use currents generated by common, time domain circuit simulation softwares to calculate the desired transient fields. The development of the method is described in detail and then demonstrated by considering several interconnect examples involving transmission line mismatches and ringing. The accuracy of the method is addressed and found to be excellent for far field distances.

ACKNOWLEDGEMENTS

I would like to express my gratitude to Dr. Greg Bridges for his suggestion of this project as well as for his valuable advice given during our many discussions.

Financial support by NSERC and Micronet is gratefully acknowledged.

I would also like to express my thanks to Dr. Jasmin Roy for his detailed reading and editing of the original document as well as for the many useful recommendations which he made.

I would further like to thank all of my colleagues who made my work enjoyable and who many times kept me interested.

Finally, I would like to thank my mother for always encouraging me to succeed.

TABLE OF CONTENTS

LIST OF FIGURES

LIST OF TABLES

CHAPTER 1

INTRODUCTION

1.1 Motivation and Previous Work

In the past, the calculation of radiation from printed circuit structures, (usually in terms of microstrip and stripline transmission lines), was largely the domain of the academic or the microstrip antenna designer. However, in the last several years, with the advent of ever increasingly fast electronics, radiation from a growing variety of printed circuits has become of great concern to the electronics industry. The reason for this is due in part to environmental and health concerns but is for the most part, due to the unwanted interference of high speed printed circuits with other electronic products. Because of this, most industrialized countries have now instituted strict standards dealing with these concerns, the most recent of these having come into full effect on January 1st 1996. This was the European Community's CISPR 22 standard concerning radiation from electronic and computing devices.

To adhere to these new standards, electronics designers and manufacturers now require some sort of numerical, radiation calculation software so they can design for EMC from the beginning of their product development cycle. Because of this, many numerical, radiation calculation softwares are now being developed. Many of these are based on numerical methods such as the Boundary Element Method, the Finite Element Method and the Finite–Difference Time–Domain Method [Archambeault], which are all fairly rigorous and accurate but are therefore also time consuming. Furthermore, software tools based on these methods are usually quite expensive [Cabral], and because of this, there is a lot of interest in quick yet reasonably accurate approximate methods.

Much research into radiation from printed structures has employed a complete frequency domain approach for determining the currents on, and subsequent radiation from, a printed circuit structure ([Aksun], [Naishadham]), using a spectral domain approach in one form or another. Another standard approach to calculating radiated emissions is to use a

circuit simulator to solve for the structure currents and voltages in the time–domain [Goyal], and then evaluate the radiated emissions in the frequency domain through a Fourier transform ([Gravelle], [Herault]). Because of this many electromagnetic software companies, (who up to this time have been calculating voltages and currents in the time domain for the purposes of signal integrity and cross–talk), are now making the logical leap toward the development of tools which calculate electromagnetic radiation from real physical products based on the voltages and currents which they already have available to them. An added advantage in the use of a time–domain approach to the circuit simulation, is that such a method also provides the capability of directly modeling the non–linear elements present in active circuits which complete frequency domain methods have difficulties with.

The numerical Fourier transforms required in the above approach are time consuming however, and so, as an alternative, several researchers have recently formulated the radiated fields in the time–domain ([Cicchetti], [Felsen2]). This enables the emissions to be determined directly from the transient current data without the need of a Fourier transform. This is obviously very beneficial when considering time domain currents with wide band frequency domain characteristics since in the frequency domain one complete analysis must be done for each frequency component of the current spectra. Furthermore, if only the far zone fields are required an approximate closed form solution is available for a single dielectric, printed circuit geometry and has been shown to give good accuracy [Cicchetti].

1.2 Objective and Document Summary

Herein will be presented a method, based on the work of [Cicchetti], [Bridges2] and [Lohse1], whereby a user can have an approximate but fast time domain solution of the radiation from general, single dielectric, printed circuit structures. This method requires the availability of a signal integrity tool, or some other kind of current simulation software, and

the writing of a short bit of code to calculate the actual radiation due to these currents. The radiation code is based on a closed form solution of the spectral–frequency to frequency domain Fourier transform integral for single dielectric, printed circuit structures. The printed circuit interconnects are assumed to be horizontal or vertical thin wire structures located on or within a single dielectric, grounded substrate, although the theory can be extended to multilayered substrates of different dielectric constants as well.

In Chapter 2 we will rigorously develop the spectral–frequency domain magnetic vector potential dyadic Green function, where this work is based on preceding works by [Bridges1], [Choi], [Harington], [Rana], [Tai], [Tsandoulas] and [Uzunoglu]. This development begins with the use of the Maxwell equations and the magnetic vector potential and proceeds to calculate the spectral–frequency domain magnetic vector potential dyadic Green function for a single dielectric, printed circuit structure.

Section 3.1 of Chapter 3 then proceeds to calculate a closed form solution of the inverse Fourier transform integration of the magnetic vector potential dyadic Green function from the spectral–frequency domain into the frequency domain. This work was based on preceding works by [Barkeshli], [Collin], [Felsen1], [Kong], and [Mosig] as well as some of the ones mentioned above for the previous chapter. The closed form result is obtained via the method of steepest descents (or the saddle point method) and includes much discussion about integration in the complex plane and the problems caused by the poles and branch cuts which are inherently present. Section 3.2 then transforms the above closed form frequency domain result into the time domain and a complete closed form expression for the fields radiated from a transient current source on or within a single dielectric, printed circuit structure are given.

Then in Chapter 4 section 4.1 the exact inverse Fourier transform integration, which converts from the spectral–frequency domain into the frequency domain, is evaluated numerically for all non–zero components of the electric field dyadic Green function in the

E–plane. These are then compared graphically with the approximate solutions obtained from the saddle point method and error results are given. Following this, section 4.2 examines several interesting printed circuit problems by discussing their radiated electric field E–plane results and then gives some algorithmic timing information. Finally, the work and its results are briefly summarized, appropriate conclusions are drawn and future work is discussed.

Before proceeding with this extensive formulation and discussion, it is important to note that throughout this thesis the convention of Maxwell Equations and a Green Function has been used as opposed to Maxwell's Equations and a Green's Function for similar reasons to those of [Jackson].

CHAPTER 2

DERIVATION OF THE SPECTRAL–FREQUENCY DOMAIN DYADIC GREEN FUNCTION

2.1 The 'Wave' Equations

The calculation of electric and magnetic fields in space due to the existence of electric or magnetic sources can be performed through proper application of the time honored Maxwell equations. These differential equations are shown below for homogeneous, isotropic and lossless regions [Harrington], and define the instantaneous electric ($\tilde{\mathbf{E}}$) and magnetic ($\tilde{\mathbf{H}}$) vector fields at a particular point in space due to the instantaneous electric and magnetic vector currents ($\tilde{\mathbf{J}}$ and $\tilde{\mathbf{M}}$) and scalar charges ($\tilde{q}$ and $\tilde{m}$) at a given source point. Be aware that, within these equations and throughout this document bold faced type denotes a vector quantity and tilde (~) denotes an instantaneous time domain quantity. The coordinate system

$$
\begin{aligned}
&a)\ \nabla \times \tilde{\mathbf{E}} = -\mu \frac{\partial \tilde{\mathbf{H}}}{\partial t} - \tilde{\mathbf{M}} \qquad b)\ \nabla \times \tilde{\mathbf{H}} = \varepsilon \frac{\partial \tilde{\mathbf{E}}}{\partial t} + \tilde{\mathbf{J}} \\
&c)\ \nabla \cdot \tilde{\mathbf{E}} = \frac{\tilde{q}}{\varepsilon} \qquad\qquad d)\ \nabla \cdot \tilde{\mathbf{H}} = \frac{\tilde{m}}{\mu} \\
&e)\ \nabla \cdot \tilde{\mathbf{J}} = -\frac{\partial \tilde{q}}{\partial t} \qquad\qquad f)\ \nabla \cdot \tilde{\mathbf{M}} = -\frac{\partial \tilde{m}}{\partial t}
\end{aligned}
\tag{2.1}
$$

required by these equations is shown in Fig. 1. Here the field is calculated at the point P and the outlined arrow at the source point S represents a directed (vector) current source that could be either electric or magnetic but could also be an undirected (scalar) electric or magnetic charge source. Examining these equations then, one can immediately see that equations (2.1a) and (2.1b) are coupled with respect to the vector fields which we wish to find. They can however be uncoupled by

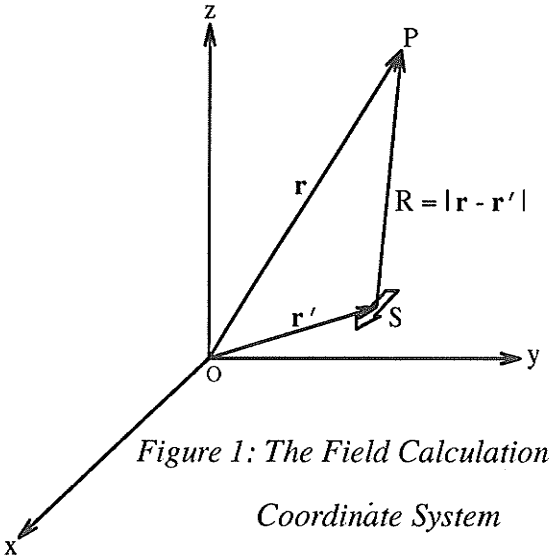

Figure 1: The Field Calculation Coordinate System

substituting equation (2.1b) into the curl of equation (2.1a) to obtain equation (2.2a) and similarly substituting equation (2.1a) into the curl of equation (2.1b) to obtain equation (2.2b). These 'wave' equations for the electric and magnetic fields are now not only uncoupled, but they are also completely defined by the sources $\tilde{\mathbf{J}}$ and $\tilde{\mathbf{M}}$ or, perhaps more exactly, they implicitly include the effect of any charge sources present. This will be shown in the next section.

$$a)\quad \left(\nabla\times\nabla\times+\mu\varepsilon\frac{\partial^2}{\partial t^2}\right)\tilde{\mathbf{E}}=-\mu\frac{\partial}{\partial t}\tilde{\mathbf{J}}-\nabla\times\tilde{\mathbf{M}} \tag{2.2}$$

$$b)\quad \left(\nabla\times\nabla\times+\mu\varepsilon\frac{\partial^2}{\partial t^2}\right)\tilde{\mathbf{H}}=-\varepsilon\frac{\partial}{\partial t}\tilde{\mathbf{M}}+\nabla\times\tilde{\mathbf{J}}$$

The similarity between equations (2.2a) and (2.2b) is immediately obvious and in general only one of these equations is solved, yielding either the electric or the magnetic field, from which the other field quantity is obtained through direct application of the appropriate Maxwell equation. For our purposes however, we will deal with both of these equations as required, the solution of which is more complicated than need be for most field problems encountered due to the time derivatives which exist within them. These derivatives can be removed and the equations thereby simplified through application of the Fourier transform which converts these equations and the resultant fields into the frequency domain. The equations are then solved in the frequency domain following which the inverse Fourier transform is applied to the resultant fields yielding the instantaneous time domain results which we desire. Taking this approach, the Fourier transform pair which we will use here is written below as appropriate for vector quantities [Trim2],

$$a)\quad \mathbf{F}(\omega)=\int_{-\infty}^{\infty}\tilde{\mathbf{F}}(t)e^{-j\omega t}dt \qquad b)\quad \tilde{\mathbf{F}}(t)=\frac{1}{2\pi}\int_{-\infty}^{\infty}\mathbf{F}(\omega)e^{+j\omega t}d\omega \tag{2.3}$$

where $\omega=2\pi f$, $\tilde{\mathbf{F}}(t)$ is any well behaved time domain function and $\mathbf{F}(\omega)$ is the corresponding frequency domain function. Note that frequency domain quantities are represented as simple vectors or scalars since most of the subsequent derivations will be in

the frequency domain. Furthermore, from here on in, function dependencies will only be included in an equation if clarification of such a dependency is warranted. Before preceding it is also worthwhile to note that since the inverse Fourier transform uses the multiplier $e^{+j\omega t}$ the frequency domain functions are said to have an $e^{+j\omega t}$ time dependance.

Now, applying the Fourier transform (equation (2.3a)) to equations (2.2) we obtain the following equations where $k = \omega\sqrt{\mu\varepsilon}$ is known as the wave–number of the medium.

$$a) \quad \left(\nabla \times \nabla \times -k^2\right)\mathbf{E} = -j\omega\mu\mathbf{J} - \nabla \times \mathbf{M} \tag{2.4}$$

$$b) \quad \left(\nabla \times \nabla \times -k^2\right)\mathbf{H} = -j\omega\varepsilon\mathbf{M} + \nabla \times \mathbf{J}$$

These equations can be further simplified by taking into account their linearity, and thereby breaking each one of them into two equations as,

$$a) \quad \left(\nabla \times \nabla \times -k^2\right)\mathbf{E}_e = -j\omega\mu\mathbf{J} \qquad b) \quad \left(\nabla \times \nabla \times -k^2\right)\mathbf{E}_h = -\nabla \times \mathbf{M} \tag{2.5}$$

$$c) \quad \left(\nabla \times \nabla \times -k^2\right)\mathbf{H}_h = -j\omega\varepsilon\mathbf{M} \qquad d) \quad \left(\nabla \times \nabla \times -k^2\right)\mathbf{H}_e = \nabla \times \mathbf{J}$$

where $\mathbf{E}_e$ and $\mathbf{H}_e$ are the electric and magnetic fields due to electric sources ($\tilde{\mathbf{J}}$) and $\mathbf{E}_h$ and $\mathbf{H}_h$ are the electric and magnetic fields due to magnetic sources ($\tilde{\mathbf{M}}$). The desired total electric and magnetic fields are then simply the superposition of these single source fields.

2.2 The Method of Potentials

Equations (2.5), simplified as they are, are still formidable equations due to the double curl of the fields, which exists within them. Because of this, a simplified method is usually employed ([Harrington], [Tai]), which takes an intermediate step using equations that are easier to solve. These intermediate equations make use of the theory of potentials. As it turns out, electric sources make use of the magnetic vector potential $\mathbf{A}$ while magnetic sources use the electric vector potential $\mathbf{F}$. This is perhaps a partial justification for bothering to separate equations (2.4) into electric and magnetic source parts.

To derive the definitions of these potentials we begin by examining equation (2.5a) from which we notice that, it looks exactly like equation (2.4a) with no magnetic sources present. Similarly (2.5c) looks exactly like (2.4b) with no electric sources present. Because of this we can look back to the Maxwell equations and, without magnetic sources present, the divergence of the magnetic field (equation (2.1d)) is seen to be zero while without electric sources present, the divergence of the electric field is zero, (equation (2.1c)). These results immediately remind us of the identity which says that any divergence–less vector can be represented by the curl of another arbitrary vector, namely,

$$\nabla\cdot\mathbf{U} = \nabla\cdot(\nabla \times \mathbf{V}) = 0 \quad . \tag{2.6}$$

Because of this we can represent the magnetic field due to electric sources and the electric field due to magnetic sources in terms of their still unknown vector potentials as,

$$a) \quad \overline{\mathbf{H}}_e = \nabla \times \mathbf{A} \qquad\qquad b) \quad \overline{\mathbf{E}}_h = -\nabla \times \mathbf{F} \tag{2.7}$$

where the negative sign was chosen on the curl of the electric vector potential so as to be consistent with accepted methodology [Balanis].

Now, knowing one field quantity for both electric and magnetic sources we need to find the other field quantity as well as the equations defining the vector potentials. To do this we begin by taking the divergence of equations (2.5a) and (2.5c) and once more apply identity (2.6) to obtain divergences of the fields $\mathbf{E}_e$ and $\mathbf{H}_h$ as follows,

$$a) \quad -k^2\nabla\cdot\mathbf{E}_e = -j\omega\mu\nabla\cdot\mathbf{J} \qquad b) \quad -k^2\nabla\cdot\mathbf{H}_h = -j\omega\varepsilon\nabla\cdot\mathbf{M} \quad . \tag{2.8}$$

It is encouraging to note that by substituting the frequency domain versions of the continuity equations (equations (2.1e) and (2.1f)) into equations (2.8a) and (2.8b) we obtain the frequency domain divergences of the electric and magnetic fields given in equations (2.1c) and (2.1d). This suggests that if the currents and charges obey the continuity equations, as they must, equations (2.5a) and (2.5c) implicitly satisfy the divergence equations for the corresponding fields as expected.

If we now apply the following identity to equations (2.5a) and (2.5c),

$$\nabla \times \nabla \times \mathbf{V} = \nabla(\nabla \cdot \mathbf{V}) - \nabla^2 \mathbf{V} \tag{2.9}$$

we obtain,

$$a) \quad \left(\nabla\nabla\cdot - \nabla^2 - k^2\right)\mathbf{E}_e = -j\omega\mu\mathbf{J} \qquad b) \quad \left(\nabla\nabla\cdot - \nabla^2 - k^2\right)\mathbf{H}_h = -j\omega\varepsilon\mathbf{M} \tag{2.10}$$

and substituting equations (2.8) into equations (2.10) we find,

$$a) \quad \left(\nabla^2 + k^2\right)\mathbf{E}_e = -\frac{1}{j\omega\varepsilon}\left(\nabla\nabla\cdot + k^2\right)\mathbf{J} \quad b) \quad \left(\nabla^2 + k^2\right)\mathbf{H}_h = -\frac{1}{j\omega\mu}\left(\nabla\nabla\cdot + k^2\right)\mathbf{M} \ . \tag{2.11}$$

Now, since only the curl of the vector potentials has been defined up to this point there is still some arbitrariness to these vector potentials. To make the potentials unique we must then also define their divergences. Keeping this in mind we can immediately see, observing equations (2.11), that if the fields $\mathbf{E}_e$ and $\mathbf{H}_e$ are defined in terms of their vector potentials as,

$$a) \quad \mathbf{E}_e = \frac{1}{j\omega\varepsilon}\left(\nabla\nabla\cdot + k^2\right)\mathbf{A} \quad b) \quad \mathbf{H}_h = \frac{1}{j\omega\mu}\left(\nabla\nabla\cdot + k^2\right)\mathbf{F} \tag{2.12}$$

and these equations are substituted back into equations (2.11) we can, upon rearranging the linear partial derivative operators slightly, write,

$$a) \quad \frac{1}{j\omega\varepsilon}\left(\nabla\nabla\cdot + k^2\right)\left[\left(\nabla^2 + k^2\right)\mathbf{A} = -\mathbf{J}\right] \quad b) \quad \frac{1}{j\omega\mu}\left(\nabla\nabla\cdot + k^2\right)\left[\left(\nabla^2 + k^2\right)\mathbf{F} = -\mathbf{M}\right]. \tag{2.13}$$

The equations defining the vector potentials are thereby seen to be,

$$a) \quad \left(\nabla^2 + k^2\right)\mathbf{A} = -\mathbf{J} \qquad b) \quad \left(\nabla^2 + k^2\right)\mathbf{F} = -\mathbf{M} \ . \tag{2.14}$$

As we can now see, the electric and magnetic fields due to both electric and magnetic sources can be defined in a much easier way than the double curl equations of equation (2.5) by using equations (2.7), (2.12) and (2.14). That is, using equations (2.7) and (2.12), we can define the total electric and magnetic fields due to both electric and magnetic sources through

superposition, as mentioned previously, to obtain,

$$\mathbf{E} = \mathbf{E}_e + \mathbf{E}_h = \frac{1}{j\omega\varepsilon}\left(\nabla\nabla\cdot + k^2\right)\mathbf{A} - \nabla \times \mathbf{F} \tag{2.15}$$

$$\mathbf{H} = \mathbf{H}_e + \mathbf{H}_h = \nabla \times \mathbf{A} + \frac{1}{j\omega\mu}\left(\nabla\nabla\cdot + k^2\right)\mathbf{F} \tag{2.16}$$

and use equations (2.14) to define the potentials [Balanis]. Comparing equations (2.15) and (2.16) with the original equations, (2.4), we can see that the new equations have been significantly simplified since we have managed to remove the fields from being a direct part of these equations. These fields are now simply dependent on the divergence and curl of the magnetic and electric vector potentials, which are both obtainable through simple partial differential equations.

2.3 The Green Function

In the previous section we derived a simplified solution methodology which defines the electric and magnetic fields in terms of electric and magnetic vector potentials. These potentials were in turn defined in terms of the electric and magnetic currents existing anywhere in the problem space. Such currents however can be completely arbitrary so solution of the vector potentials would seem to be dependent on the unknown or changing location of an unknown or changing current. To reconcile this it is necessary to make use of a Green function. Such a function defines the required vector potential at a particular observation point due to a unit current existing at a particular source point. To do this the Green function assumes that the current distribution for the vector potentials is a three dimensional dirac delta function, $\delta(\mathbf{r} - \mathbf{r}')$, in each of the three vector directions. This delta function is defined as follows [MyintU],

$$\delta(\mathbf{r} - \mathbf{r}') = 0 \quad , \quad \mathbf{r} \neq \mathbf{r}' \tag{2.17}$$

and has the following properties,

$$a) \quad \iiint_V \delta(\mathbf{r} - \mathbf{r}')dV = 1 \qquad b) \quad \iiint_V \mathbf{F}(\mathbf{r})\delta(\mathbf{r} - \mathbf{r}')dV = \mathbf{F}(\mathbf{r}') \tag{2.18}$$

assuming that the point $\mathbf{r}'$ is contained within the volume of integration. Furthermore, $\mathbf{F}(\mathbf{r})$ is an arbitrary function defined throughout this volume and $\mathbf{F}(\mathbf{r}')$ is the value of this function at the point $\mathbf{r}'$. Using one dirac delta excitation for each of the three component current directions, equations (2.14) can be written in three similar sets as,

$$a)\quad \left(\nabla^2 + k^2\right)\mathbf{G}_A^{(u)} = -\delta(\mathbf{r}-\mathbf{r}')\hat{u} \qquad b)\quad \left(\nabla^2 + k^2\right)\mathbf{G}_F^{(u)} = -\delta(\mathbf{r}-\mathbf{r}')\hat{u} \qquad (2.19)$$

where $\mathbf{G}_A$ is the vector Green function for the magnetic vector potential, $\mathbf{G}_F$ is the vector Green function for the electric vector potential and the superscript u attached to these Green functions represents the direction of the forcing dirac delta which can be either of x, y or z in cartesian coordinates. From these equations we can see that each vector Green function always results from one inhomogeneous equation, having a homogeneous as well as a particular solution, due to the singly directed source and two homogeneous equations for each of the two remaining component directions. The solution of equations (2.19) now depends on the boundary conditions of the problem space, where the homogeneous equations are used to represent the fields scattered from the problem geometry and, obviously, the inhomogeneous equation represents the source function residing within this problem geometry.

It is convenient to first rewrite the three equations for each of the vector potentials in a more compact manner by defining the Dyadic or Tensor Green functions as in equation (2.20) [Tai]. Note that dyadic functions are denoted by variables in bold faced type with a bar since they contain several vector functions.

$$a)\quad \overline{\mathbf{G}}_A = \mathbf{G}_A^{(x)}\hat{x} + \mathbf{G}_A^{(y)}\hat{y} + \mathbf{G}_A^{(z)}\hat{z} \qquad b)\quad \overline{\mathbf{G}}_F = \mathbf{G}_F^{(x)}\hat{x} + \mathbf{G}_F^{(y)}\hat{y} + \mathbf{G}_F^{(z)}\hat{z}\ . \qquad (2.20)$$

These dyadic Green functions are each simply a collection of the three appropriate vector Green functions for the three component directions of field and are usually written in matrix form with the three vector Green functions being the three columns of the three by three

dyadic. In this form, equations (2.20) would look as follows,

$$a)\quad \overline{\mathbf{G}}_A = \begin{bmatrix} \mathbf{G}_{Ax}^{(x)}\hat{x}\hat{x} & \mathbf{G}_{Ax}^{(y)}\hat{x}\hat{y} & \mathbf{G}_{Ax}^{(z)}\hat{x}\hat{z} \\ \mathbf{G}_{Ay}^{(x)}\hat{y}\hat{x} & \mathbf{G}_{Ay}^{(y)}\hat{y}\hat{y} & \mathbf{G}_{Ay}^{(z)}\hat{y}\hat{z} \\ \mathbf{G}_{Az}^{(x)}\hat{z}\hat{x} & \mathbf{G}_{Az}^{(y)}\hat{z}\hat{y} & \mathbf{G}_{Az}^{(z)}\hat{z}\hat{z} \end{bmatrix} \quad b)\quad \overline{\mathbf{G}}_F = \begin{bmatrix} \mathbf{G}_{Fx}^{(x)}\hat{x}\hat{x} & \mathbf{G}_{Fx}^{(y)}\hat{x}\hat{y} & \mathbf{G}_{Fx}^{(z)}\hat{x}\hat{z} \\ \mathbf{G}_{Fy}^{(x)}\hat{y}\hat{x} & \mathbf{G}_{Fy}^{(y)}\hat{y}\hat{y} & \mathbf{G}_{Fy}^{(z)}\hat{y}\hat{z} \\ \mathbf{G}_{Fz}^{(x)}\hat{z}\hat{x} & \mathbf{G}_{Fz}^{(y)}\hat{z}\hat{y} & \mathbf{G}_{Fz}^{(z)}\hat{z}\hat{z} \end{bmatrix} . \qquad (2.21)$$

From this construct of the dyadic, it is also useful to define a unit dyad, as $\overline{\mathbf{I}} = \hat{x}\hat{x} + \hat{y}\hat{y} + \hat{z}\hat{z}$, which we can see is simply a unit diagonal dyadic in matrix form. Therefore, using this new dyadic notation equations (2.19) can be written in the following simplified way which now includes all three of the vector Green function equations,

$$a)\quad \left(\nabla^2 + k^2\right)\overline{\mathbf{G}}_A = -\delta(\mathbf{r}-\mathbf{r}')\overline{\mathbf{I}} \qquad b)\quad \left(\nabla^2 + k^2\right)\overline{\mathbf{G}}_F = -\delta(\mathbf{r}-\mathbf{r}')\overline{\mathbf{I}} \quad . \qquad (2.22)$$

Furthermore, given these dyadic vector potential Green functions and equations (2.15) and (2.16) we can then write the electric and magnetic field dyadic Green functions as well, namely,

$$\overline{\mathbf{G}}_E = \overline{\mathbf{G}}_{E_e} + \overline{\mathbf{G}}_{E_h} = \frac{1}{j\omega\varepsilon}\left(\nabla\nabla\cdot + k^2\right)\overline{\mathbf{G}}_A - \nabla \times \overline{\mathbf{G}}_F \qquad (2.23)$$

$$\overline{\mathbf{G}}_H = \overline{\mathbf{G}}_{H_e} + \overline{\mathbf{G}}_{H_h} = \nabla \times \overline{\mathbf{G}}_A + \frac{1}{j\omega\mu}\left(\nabla\nabla\cdot + k^2\right)\overline{\mathbf{G}}_F \quad . \qquad (2.24)$$

After calculating equations (2.22) to (2.24) we can calculate the fields for an arbitrary source by directly applying the integral properties of the dirac delta function which were defined in equation (2.18). In this way the potentials can be obtained through the following equations,

$$a)\quad \mathbf{A} = \int\int\int_V \overline{\mathbf{G}}_A \cdot \mathbf{J} dV \qquad b)\quad \mathbf{F} = \int\int\int_V \overline{\mathbf{G}}_F \cdot \mathbf{M} dV \qquad (2.25)$$

and similarly the desired electric and magnetic fields can be obtained as,

$$a)\quad \mathbf{E} = \int\int\int_V \overline{\mathbf{G}}_{E_e} \cdot \mathbf{J} dV + \int\int\int_V \overline{\mathbf{G}}_{E_h} \cdot \mathbf{M} dV \qquad (2.26)$$

$$b)\quad \mathbf{H} = \int\int\int_V \overline{\mathbf{G}}_{H_e} \cdot \mathbf{J} dV + \int\int\int_V \overline{\mathbf{G}}_{H_h} \cdot \mathbf{M} dV \quad .$$

In these equations it is important to note that the dot product of a vector with a dyadic is taken simply to be a matrix multiplication where the vector is written as a column matrix.

2.4 The Single Dielectric, Printed Circuit Boundary Conditions

Now that we have defined the vector potential solution methodology along with the concept of the dyadic Green function we are free to begin the setup for the solution of an actual problem. In this thesis we will concern ourselves with a single dielectric, Printed Circuit Board (PCB) structure as shown in Fig. 2. We will assume that the dielectric layer and its ground plane extend infinitely in the transverse (x and y) directions, that the ground plane is perfectly conducting, and that the dielectric layer is homogeneous, isotropic and lossless. Note that any of these conditions can be removed at the expense of added complexity to the problem (and hence the solution), and so we will simply concern ourselves with the general idea. Before we proceed however it must also be stated that, for this type of problem, only electric sources are present and so, for our purposes, the magnetic source vector in equation (2.14b) can simply be set to zero. This leaves a homogeneous equation to define the electric vector potential but by no means requires the electric vector potential itself to be zero. Therefore, to avoid confusion the equations to be solved in this instance are repeated below.

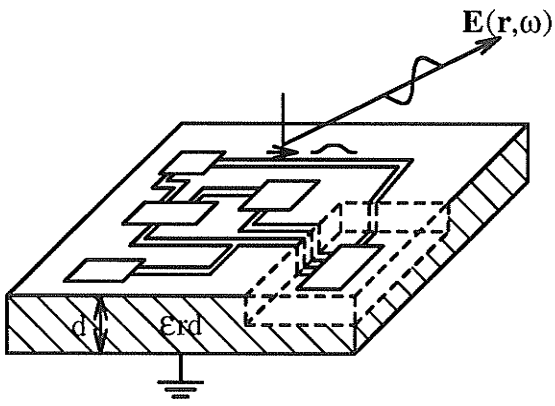

Figure 2: A Typical Single Dielectric PCB

$$a)\quad \left(\nabla^2 + k^2\right)\mathbf{A} = -\mathbf{J} \qquad b)\quad \left(\nabla^2 + k^2\right)\mathbf{F} = 0 \tag{2.27}$$

$$c)\quad \mathbf{E} = \frac{1}{j\omega\varepsilon}\left(\nabla\nabla\cdot + k^2\right)\mathbf{A} - \nabla \times \mathbf{F} \qquad d)\quad \mathbf{H} = \nabla \times \mathbf{A} + \frac{1}{j\omega\mu}\left(\nabla\nabla\cdot + k^2\right)\mathbf{F}$$

Now that we know the problem which we wish to tackle we can immediately deduce the boundary conditions which need to be satisfied. Observing the cross–sectional diagram

in Fig. 3 and applying some basic electromagnetic knowledge we know that at a perfect conductor ($\sigma = \infty$) the total tangential electric field must vanish. This yields the following boundary condition at the ground plane,

$$\mathbf{E}_{td}(z = -d) = 0 \qquad (2.28)$$

where the subscripts refer to the transverse (t) component of the field (which is either x or y in this case) within the dielectric region (d).

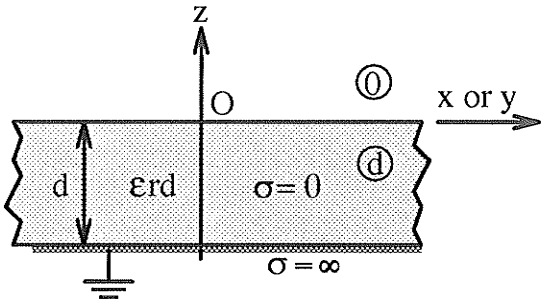

Figure 3: The PCB Cross–Section

The remaining boundary conditions which are immediately obvious from Fig. 3 are simple statements of the fact that the tangential electric and magnetic fields as well as the normal electric and magnetic flux densities must be continuous across any material boundary. It can be shown [Harrington], that enforcing any two of these conditions also enforces the third and so we write for the tangential components,

$$a)\quad \mathbf{E}_{t0}(z = 0) = \mathbf{E}_{td}(z = 0) \qquad b)\quad \mathbf{H}_{t0}(z = 0) = \mathbf{H}_{td}(z = 0)\ . \qquad (2.29)$$

Here the added subscript (0) refers to the air region above the microstrip. Beyond these conditions one other boundary condition remains, due to the open air upper half space, which effects all three components of both the electric and magnetic fields. This condition, known as the radiation condition, states that all fields must be both outward propagating and decaying as the distance from their source approaches infinity [Tai].

We now know the boundary conditions on the electric and magnetic fields for the PCB problem which we wish to solve but have no idea as to what type of currents will be present. We should therefore find the dyadic Green functions for the vector potentials and eventually for the fields themselves. Writing equations (2.27) in terms of dyadic Green functions and dirac delta excitations for both possible regions within this problem, but with the source residing inside the dielectric, we obtain the following equations for the magnetic vector potential dyadic Green function $\overline{\mathbf{G}}_A$,

$$a)\quad \left(\nabla^2 + k_d^2\right)\overline{\mathbf{G}}_{A_d} = -\delta(\mathbf{r} - \mathbf{r}')\overline{\mathbf{I}} \qquad b)\quad \left(\nabla^2 + k_0^2\right)\overline{\mathbf{G}}_{A_0} = 0 \qquad (2.30)$$

as well as the equations for the remaining three dyadic Green functions, namely,

$$a)\quad \overline{\mathbf{G}}_E = \frac{1}{j\omega\varepsilon}\left(\nabla\nabla\cdot + k^2\right)\overline{\mathbf{G}}_A - \nabla\times\overline{\mathbf{G}}_F \qquad b)\quad \overline{\mathbf{G}}_H = \nabla\times\overline{\mathbf{G}}_A + \frac{1}{j\omega\mu}\left(\nabla\nabla\cdot + k^2\right)\overline{\mathbf{G}}_F$$

$$c)\quad \left(\nabla^2 + k^2\right)\overline{\mathbf{G}}_F = 0 \quad . \tag{2.31}$$

Examining equations (2.31a) and (2.31b) we can immediately see that due to the differential operators within these equations, each component of $\overline{\mathbf{G}}_E$ and $\overline{\mathbf{G}}_H$ is defined by a total of five components of $\overline{\mathbf{G}}_A$ and $\overline{\mathbf{G}}_F$. For example, each component of $\overline{\mathbf{G}}_E$ is defined by three components of $\overline{\mathbf{G}}_A$ due to the gradient of the divergence of this dyadic and two components of $\overline{\mathbf{G}}_F$ due to the curl of this dyadic. As it turns out however, we require at most two components of the vector potentials, in both regions, to completely define the boundary conditions on the electric and magnetic fields for any single component of source direction, (x, y or z). Because of this we can set $\overline{\mathbf{G}}_F$ equal to zero and proceed with only $\overline{\mathbf{G}}_A$, (although many different choices are also possible). This simplifies equations (2.31) substantially and yields,

$$a)\quad \overline{\mathbf{G}}_E = \frac{1}{j\omega\varepsilon}\left(\nabla\nabla\cdot + k^2\right)\overline{\mathbf{G}}_A \qquad b)\quad \overline{\mathbf{G}}_H = \nabla\times\overline{\mathbf{G}}_A \qquad c)\quad \overline{\mathbf{G}}_F = 0 \quad . \tag{2.32}$$

Expanding the above partial differential equations for $\overline{\mathbf{G}}_E$ and $\overline{\mathbf{G}}_H$ in both of the two transverse directions then gives the equations which must be continuous across the dielectric–air interface while equations (2.33a) and (2.33c) must also vanish at the ground plane according to the previously derived boundary conditions.

$$a)\quad G_{Ex} = \frac{1}{j\omega\varepsilon}\left(\frac{\partial^2 G_{Ax}}{\partial x^2} + \frac{\partial^2 G_{Ay}}{\partial x\partial y} + \frac{\partial^2 G_{Az}}{\partial x\partial z} + k^2 G_{Ax}\right) \quad b)\quad G_{Hx} = \frac{\partial G_{Az}}{\partial y} - \frac{\partial G_{Ay}}{\partial z} \tag{2.33}$$

$$c)\quad G_{Ey} = \frac{1}{j\omega\varepsilon}\left(\frac{\partial^2 G_{Ax}}{\partial x\partial y} + \frac{\partial^2 G_{Ay}}{\partial y^2} + \frac{\partial^2 G_{Az}}{\partial y\partial z} + k^2 G_{Ay}\right) \quad d)\quad G_{Hy} = \frac{\partial G_{Ax}}{\partial z} - \frac{\partial G_{Az}}{\partial x}$$

Within these equations if should be noted that $\varepsilon = \varepsilon_r\varepsilon_0$ and that ε_r, the relative permittivity

of the material, will change depending on the region in which the equation occurs, (either in the air or in the dielectric itself).

Within equations (2.33) we can again see partial derivatives cropping up which reminds us of the Fourier transform which we used in section 2.1 to remove partial derivatives with respect to time. In this case a similar Fourier transform pair can be defined but only for the transverse components of the potentials. This is due to the fact that the Fourier transform integral is evaluated from $-\infty \rightarrow \infty$ and the dielectric and ground plane layers extend to infinity in these directions with the only boundary conditions being that the fields must go to zero at infinity to satisfy the radiation condition. These conditions are inherent in the Fourier transform of a derivative [MyintU], and so we can use the following double Fourier transform pair for the transversely directional potential components.

$$a)\quad \mathbf{f}(k_x,k_y) = \int_{-\infty}^{\infty}\int_{-\infty}^{\infty} \mathbf{F}(x,y)e^{-j(k_x x+k_y y)}dxdy \tag{2.34}$$

$$b)\quad \mathbf{F}(x,y) = \frac{1}{4\pi^2}\int_{-\infty}^{\infty}\int_{-\infty}^{\infty} \mathbf{f}(k_x,k_y)e^{+j(k_x x+k_y y)}dk_x dk_y$$

Applying equation (2.34a) to equations (2.33) yields the following simplified set of equations which are now no longer partial differential equations but are simply ordinary differential equations in what is known as the spectral–frequency domain.

$$a)\quad G_{Ex} = \frac{1}{j\omega\varepsilon}\left\{\left(k^2-k_x^2\right)G_{Ax} - k_x k_y G_{Ay} + jk_x\frac{dG_{Az}}{dz}\right\} \quad b)\quad G_{Hx} = jk_y G_{Az} - \frac{dG_{Ay}}{dz} \tag{2.35}$$

$$c)\quad G_{Ey} = \frac{1}{j\omega\varepsilon}\left\{\left(k^2-k_y^2\right)G_{Ay} - k_x k_y G_{Ax} + jk_y\frac{dG_{Az}}{dz}\right\} \quad d)\quad G_{Hy} = \frac{dG_{Ax}}{dz} - jk_x G_{Az}$$

For the remainder of this chapter it should be understood that we are in the spectral–frequency domain and therefore no special delimiters will be used on any vector or scalar quantities to indicate that they occur in this particular domain.

Obviously, it is now easy and straight forward to write the desired boundary

conditions in terms of equations (2.35). Doing this, condition (2.28) yields,

$$a)\ \left\{\left(k_d^2-k_x^2\right)G_{A_dx}-k_xk_yG_{A_dy}+jk_x\frac{dG_{A_dz}}{dz}\right\}_{z=-d}=0 \qquad (2.36)$$

$$b)\ \left\{\left(k_d^2-k_y^2\right)G_{A_dy}-k_xk_yG_{A_dx}+jk_y\frac{dG_{A_dz}}{dz}\right\}_{z=-d}=0$$

and because the relative permittivity of air is unity condition (2.29a) yields,

$$a)\ \varepsilon_{rd}\left\{\left(k_0^2-k_x^2\right)G_{A_0x}-k_xk_yG_{A_0y}+jk_x\frac{dG_{A_0z}}{dz}\right\}_{z=0}=\left\{\left(k_d^2-k_x^2\right)G_{A_dx}-k_xk_yG_{A_dy}+jk_x\frac{dG_{A_dz}}{dz}\right\}_{z=0} \qquad (2.37)$$

$$b)\ \varepsilon_{rd}\left\{\left(k_0^2-k_y^2\right)G_{A_0y}-k_xk_yG_{A_0x}+jk_y\frac{dG_{A_0z}}{dz}\right\}_{z=0}=\left\{\left(k_d^2-k_y^2\right)G_{A_dy}-k_xk_yG_{A_dx}+jk_y\frac{dG_{A_dz}}{dz}\right\}_{z=0}$$

and finally condition (2.29b) yields,

$$a)\quad \left\{jk_yG_{A_0z}-\frac{dG_{A_0y}}{dz}\right\}_{z=0}=\left\{jk_yG_{A_dz}-\frac{dG_{A_dy}}{dz}\right\}_{z=0} \qquad (2.38)$$

$$b)\quad \left\{\frac{dG_{A_0x}}{dz}-jk_xG_{A_0z}\right\}_{z=0}=\left\{\frac{dG_{A_dx}}{dz}-jk_xG_{A_dz}\right\}_{z=0}\ .$$

Equations (2.36) to (2.38) completely describe the boundary conditions on the electric and magnetic dyadic Green functions for our single dielectric, PCB problem. It is now left for us to transfer these, onto conditions on the magnetic vector potential dyadic Green function. Before we proceed with actually calculating this dyadic however, we must also expand equations (2.30), which are the defining equations for the magnetic vector potential, and apply the Fourier transform of equation (2.34a) as with the above boundary conditions. In doing so we must remember that the sources in this problem will always reside within the dielectric or on its surface and so we obtain the following spectral domain equations for the

two regions of our problem,

$$a)\quad \left(\frac{d^2}{dz^2}-u_d^2\right)\overline{\mathbf{G}}_{A_d}=-e^{-j(k_x x'+k_y y')}\delta(z-z')\overline{\mathbf{I}}=-E_d\delta(z-z')\overline{\mathbf{I}} \tag{2.39}$$

$$b)\quad \left(\frac{d^2}{dz^2}-u_0^2\right)\overline{\mathbf{G}}_{A_0}=0$$

where $u_0=\sqrt{k_x^2+k_y^2-k_0^2}$, $u_d=\sqrt{k_x^2+k_y^2-k_d^2}$ and we have let $E_d=e^{-j(k_x x'+k_y y')}$. In the next two sections we will proceed to define the boundary conditions on the magnetic vector potential dyadic Green function for each of the three component source directions and using these conditions we will derive this Green function in both the air and dielectric regions.

2.5 The Magnetic Vector Potential Green Function due to a Vertical Electric Source

In the previous section, the magnetic vector potential dyadic Green function equations for both possible regions were derived. It was noted that each column of this dyadic represents one of the three vector Green Functions, each one of which is due to a source directed in one of the three component directions. In this section we will concern ourselves with the last column of this dyadic whose vector Green function is due to a z–directed source and so the appropriate vector Green function equations are reiterated below for the dielectric and air regions which we are interested in.

$$a)\quad \left(\frac{d^2}{dz^2}-u_0^2\right)\mathbf{G}_{A_0}^{(z)}=0 \qquad b)\quad \left(\frac{d^2}{dz^2}-u_d^2\right)\mathbf{G}_{A_d}^{(z)}=-E_d\delta(z-z')\hat{z} \tag{2.40}$$

Splitting these two equations into component parts yields three homogeneous equations in the source–free (air) region along with two homogeneous equations and one inhomogeneous equation in the dielectric region, namely,

$$a)\quad \left(\frac{d^2}{dz^2}-u_0^2\right)G_{A_0x,y,z}^{(z)}=0 \qquad b)\quad \left(\frac{d^2}{dz^2}-u_d^2\right)G_{A_dx,y}^{(z)}=0 \tag{2.41}$$

$$c)\quad \left(\frac{d^2}{dz^2}-u_d^2\right)G_{A_dz}^{(z)}=-E_d\delta(z-z')\quad .$$

However, an inhomogeneous equation consists of a homogeneous as well as a particular solution, as was mentioned previously, and so the inhomogeneous equation above can be split into two parts as,

$$a)\quad \left(\frac{d^2}{dz^2}-u_d^2\right)G^{(z)}_{A_{dhz}}=0 \qquad b)\quad \left(\frac{d^2}{dz^2}-u_d^2\right)G^{(z)}_{A_{dpz}}=-E_d\delta(z-z') \tag{2.42}$$

where the subscript h represents the homogeneous solution while the subscript p represents the particular solution.

Now remember that in the previous section we postulated that, for our particular geometry we would need at most two components of vector potential, in each of the two regions, to completely define the boundary conditions on the electric and magnetic fields. Obviously then, we must decide how many components are required and which ones we need. In a free space problem the obvious answer would be one and the appropriate choice would be the component of potential directed parallel to the source which in our case would be the component $G^{(z)}_{Az}$. If we use this component by itself it must be able to satisfy all the required boundary conditions as well as properly represent the source where, as mentioned previously, the particular solution represents the source while the homogeneous equations are used to represent the fields scattered from the problem geometry. The simplest way to proceed in this case is then to set the components transverse to the source direction to zero and see if the source component by itself can possibly satisfy all our boundary conditions. Then if it doesn't we must add another component and try again.

Taking this approach in the case of equations (2.41) and (2.42) we will first try and set the components transverse to the source direction to zero which leaves us with the following equations,

$$a)\quad \left(\frac{d^2}{dz^2}-u_0^2\right)G^{(z)}_{A_{0z}}=0 \qquad b)\quad \left(\frac{d^2}{dz^2}-u_d^2\right)G^{(z)}_{A_{dhz}}=0 \tag{2.43}$$

$$c)\quad \left(\frac{d^2}{dz^2}-u_d^2\right)G^{(z)}_{A_{dpz}}=-E_d\delta(z-z')$$

where the following equalities were applied.

$$a)\quad G^{(z)}_{A_0x} = G^{(z)}_{A_dx} = 0 \qquad b)\quad G^{(z)}_{A_0y} = G^{(z)}_{A_dy} = 0 \tag{2.44}$$

We then proceed by trying to apply equations (2.44a) and (2.44b) to the boundary conditions derived in the previous section, (equations (2.36) to (2.38)) and in doing so we obtain the following, very simplified conditions, on $G^{(z)}_{Az}$.

$$a)\quad \left.\frac{dG^{(z)}_{A_dz}}{dz}\right|_{z=-d} = 0 \qquad b)\quad \varepsilon_{rd}\left.\frac{dG^{(z)}_{A_0z}}{dz}\right|_{z=0} = \left.\frac{dG^{(z)}_{A_dz}}{dz}\right|_{z=0} \qquad c)\quad G^{(z)}_{A_0z}\Big|_{z=0} = G^{(z)}_{A_dz}\Big|_{z=0} \tag{2.45}$$

Since these new boundary conditions on the z component of the magnetic vector potential Green function were derived with no mathematical inconsistencies and satisfying these boundary conditions will ensure the satisfaction of all the original boundary conditions on the electric and magnetic fields we can be confident that our choice of setting the transverse components to zero was correct.

Now using these simplified boundary conditions and applying them to equations (2.43) we can obtain the spectral–frequency domain magnetic vector potential Green function for a z–directed source. To do this we begin by solving the equation in the source–free air region, (equation (2.43a)). The solution of this homogeneous ordinary differential equation is very well known [Campbell], and so we just write it here without delving into the details of the solution which can be found in any basic differential equation text.

$$G^{(z)}_{A_0z} = A_0 e^{u_0 z} + B_0 e^{-u_0 z} \tag{2.46}$$

In this solution the multipliers A_0 and B_0 are unknowns which will be determined through the application of the boundary conditions of equation (2.45). Before we apply these conditions, for which we need the solution of the inhomogeneous equation as well, we can immediately enforce the radiation condition which allows us to set $A_0 = 0$ since the exponential on which it operates approaches infinity as z approaches infinity. We are now

left with the following solution of the homogeneous equation in the source–free region, which contains only one unknown.

$$G_{A_{0Z}}^{(z)} = B_0 e^{-u_0 z} \tag{2.47}$$

Moving on to the inhomogeneous equation in the source region we can immediately see that its homogeneous equation (equation (2.43b)) is very similar to that in the source free region and can therefore, simply deduce its solution from equation (2.46) to write,

$$G_{A_{dhZ}}^{(z)} = A_d e^{u_d z} + B_d e^{-u_d z} \quad . \tag{2.48}$$

Note that there is no radiation condition on z to satisfy in this region and so we are left with two unknowns to solve for.

Next, we tackle the solution of the particular equation, (equation (2.43c)). If we forget for the moment that this equation is only valid in a finite region we can use the following Fourier transform pair to simplify the solution. The finiteness of the region is then enforced along with the boundary conditions.

$$a) \quad F(k_z) = \int_{-\infty}^{\infty} f(z) e^{-j(k_z z)} dk_z \qquad b) \quad f(z) = \frac{1}{2\pi} \int_{-\infty}^{\infty} F(k_z) e^{+j(k_z z)} dk_z \tag{2.49}$$

Applying equation (2.49a) to equation (2.43c) and rearranging we obtain,

$$G_{A_{dpZ}}^{(z)}(k_z) = E_d \frac{e^{-jk_z z'}}{\left(k_z^2 + u_d^2\right)} \tag{2.50}$$

which is the solution we want in the k_z domain. To get the solution in the spectral–frequency domain we simply apply the inverse transform (2.49b) which yields the following integral to solve.

$$G_{A_{dpZ}}^{(z)} = \frac{E_d}{2\pi} \int_{-\infty}^{\infty} \frac{e^{+jk_z(z-z')}}{\left(k_z^2 + u_d^2\right)} dk_z \tag{2.51}$$

It is immediately obvious that the integrand of this integral has two poles at $\pm ju_d$, which points us in the direction of the Cauchy residue theorem [Trim1], in the complex k_z plane

as the possible means to a solution. In this complex plane equation (2.51) becomes,

$$G_{A_{dpz}}^{(z)} = \frac{E_d}{2\pi}\left\{\oint_C \frac{e^{+jk_z(z-z')}}{\left(k_z^2+u_d^2\right)}dk_z - \int_\Gamma \frac{e^{+jk_z(z-z')}}{\left(k_z^2+u_d^2\right)}dk_z\right\} \tag{2.52}$$

where the subscript C on the first integral represents the closed contour to be traversed and the subscript Γ on the second integral represents the part of this contour which does not coincide with the original path of integration along the real k_z axis. It is evident that if the integral along the Γ section of the closed contour is zero the desired Green function will simply be equal to the contour integration around the closed contour itself, which can easily be solved by the aforementioned residue theorem. As shown in Fig. 4 we can see that there are two possible choices for the contour C. The upper contour (C_u) traverses around the positive imaginary part of the complex k_z plane in a counter–clockwise direction and contains the pole ju_d while the lower contour (C_l) traverses clockwise around the negative imaginary part of this plane and contains the pole $-ju_d$. Now, letting Γ_u (the Γ section of C_u) have a radius of R we can let $k_z = Re^{j\theta}$ along this contour and substituting this relation into the integrand of the integral along Γ in equation (2.52) we obtain,

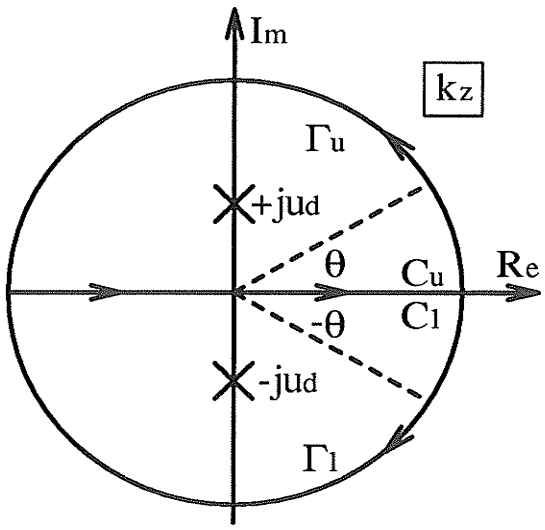

Figure 4: The Integration Paths in the k_z Plane for the Inverse Fourier Transform

$$I_{\Gamma_u} = \frac{e^{+jRe^{j\theta}(z-z')}}{\left(R^2e^{j2\theta}+u_d^2\right)} = \frac{e^{+R(j\cos\theta-\sin\theta)(z-z')}}{\left(R^2e^{j2\theta}+u_d^2\right)} \tag{2.53}$$

the magnitude of which is,

$$\left|I_{\Gamma_u}\right| = \frac{e^{-R\sin\theta(z-z')}}{\left|R^2e^{j2\theta}+u_d^2\right|} \le \frac{e^{-R\sin\theta(z-z')}}{\left|R^2e^{j2\theta}\right|-\left|u_d^2\right|} = \frac{e^{-R\sin\theta(z-z')}}{R^2-u_d^2} \tag{2.54}$$

where we have used the relation [Trim1],

$$\frac{1}{|a+b|} \leq \frac{1}{|a|-|b|} \quad , \quad |a| > |b| \quad . \tag{2.55}$$

Using this result we can immediately write the following relation for the integral along Γ_u to be,

$$\left| \int_{\Gamma_u} \frac{e^{+jk_z(z-z')}}{\left(k_z^2 + u_d^2\right)} dk_z \right| \leq \frac{e^{-R\sin\theta(z-z')}}{R^2 - u_d^2}(\pi R) \tag{2.56}$$

which we can see, upon taking the limit as $R \to \infty$, becomes zero if $z \geq z'$. In a similar manner, we can let $k_z = Re^{-j\theta}$ along Γ_l (the Γ section of C_l) and repeat equations (2.53) to (2.56) to find that as $R \to \infty$ the magnitude of the integral approaches zero if $z \leq z'$. From these two relations we can immediately rewrite equation (2.52) as,

$$G^{(z)}_{A_{dpZ}} = \frac{E_d}{2\pi} \begin{cases} \oint_{C_u^{\rightarrow}} \frac{e^{+jk_z(z-z')}}{\left(k_z^2 + u_d^2\right)} dk_z, & z \geq z' \\ \oint_{C_l^{\leftarrow}} \frac{e^{+jk_z(z-z')}}{\left(k_z^2 + u_d^2\right)} dk_z, & z \leq z' \end{cases} \tag{2.57}$$

where the contour integral around $C_u^{\rightarrow}$ is traversed in a counter–clockwise direction, (denoted by the right arrow) while the contour integral around $C_l^{\leftarrow}$ is traversed in a clockwise direction (denoted by the left arrow).

To now solve equation (2.57) we simply apply the Cauchy residue theorem [Trim1], which states that the contour integral is proportional to the sum of the residues of the integrand at the enclosed poles, or more exactly,

$$\oint_{C^{\rightarrow}} f(z)dz = -\oint_{C^{\leftarrow}} f(z)dz = 2\pi j \sum Res[f(z), z_j] \quad . \tag{2.58}$$

Therefore, for contour $C_u^{\rightarrow}$ which only encircles the pole $+ju_d$, we must find the residue of the integrand at this pole and similarly for contour $C_l^{\leftarrow}$ which encircles the pole $-ju_d$, we must find the residue of the integrand at that pole. These residues are trivial to calculate,

see [Trim1], and therefore are simply stated below.

$$a) \quad Res\left[\frac{e^{jk_z(z-z')}}{(k_z+ju_d)(k_z-ju_d)}, ju_d\right] = \frac{e^{-u_d(z-z')}}{2ju_d} \tag{2.59}$$

$$b) \quad Res\left[\frac{e^{jk_z(z-z')}}{(k_z+ju_d)(k_z-ju_d)}, -ju_d\right] = -\frac{e^{-u_d(z'-z)}}{2ju_d}$$

Now, using these residues we can finally write our desired solution to equation (2.51) as,

$$G^{(z)}_{A_{dpz}} = \frac{E_d}{2\pi}\int_{-\infty}^{\infty}\frac{e^{+jk_z(z-z')}}{\left(k_z^2+u_d^2\right)}dk_z = E_d\begin{cases}\dfrac{e^{-u_d(z-z')}}{2u_d}, & z \geq z' \\ \dfrac{e^{-u_d(z'-z)}}{2u_d}, & z \leq z'\end{cases} = E_d\frac{e^{-u_d|z-z'|}}{2u_d} \tag{2.60}$$

where, due to the equality of the two solutions when $z = z'$, we have used the absolute value of $z-z'$ within the exponential to allow us to write the upper and lower contour solutions as one result. Note also that this result satisfies the radiation condition as it should. Now that we have the homogeneous solution for $G^{(z)}_{A_{dz}}$ (equation (2.48)) as well as the particular solution (equation (2.60)) we can write the total solution as,

$$G^{(z)}_{A_{dz}} = A_d e^{u_d z} + B_d e^{-u_d z} + E_d\frac{e^{-u_d|z-z'|}}{2u_d} \quad . \tag{2.61}$$

All that still remains to be done to obtain the magnetic vector potential Green function for a z directed source is to match equation (2.47) with equation (2.61) according to the boundary conditions outlined in equation (2.45). To do this we will begin with equation (2.45a) which simply sets the derivative of $G^{(z)}_{A_{dz}}$ equal to zero at $z = -d$. In doing this we can easily see that the relation $z \leq z'$ holds since the source will always be within the dielectric and therefore above or on the ground plane. We therefore write,

$$2u_d\left(A_d e^{-u_d d} - B_d e^{+u_d d}\right) + E_d e^{-u_d(z'+d)} = 0 \tag{2.62}$$

which can be rearranged and reduced to yield,

$$A_d = B_d e^{+2u_d d} - E_d \frac{e^{-u_d z'}}{2u_d} \quad . \tag{2.63}$$

Proceeding to apply condition (2.45b) which enforces the continuity of the derivative of $G_{Az}^{(z)}$ at the air–dielectric interface we note that the source will this time always be below or at the surface of the dielectric so the relation $z \geq z'$ holds, (this will also be true for condition (2.45c)). To then apply condition (2.45b) we equate equations (2.47) and (2.61) as follows,

$$B_0 e^{-u_0 z} = A_d e^{u_d z} + B_d e^{-u_d z} + E_d \frac{e^{-u_d (z-z')}}{2u_d} \tag{2.64}$$

and take the derivative with respect to z, thereafter setting z to zero and including the dielectric constant multiplier, to yield,

$$-u_0 \varepsilon_{rd} B_0 = u_d (A_d - B_d) - E_d \frac{e^{+u_d z'}}{2} \quad . \tag{2.65}$$

Substituting equation (2.63) into the previous equation and rearranging we obtain,

$$B_d = \frac{-\varepsilon_{rd} 2u_0 B_0 + E_d \left(e^{+u_d z'} + e^{-u_d z'} \right)}{2u_d \left(e^{+2u_d d} - 1 \right)} \tag{2.66}$$

which we can quickly substitute back into equation (2.63) to yield,

$$A_d = \frac{-\varepsilon_{rd} 2u_0 B_0 + E_d \left(e^{+u_d z'} + e^{-u_d z'} \right)}{2u_d \left(e^{+2u_d d} - 1 \right)} e^{+2u_d d} - E_d \frac{e^{-u_d z'}}{2u_d} \quad . \tag{2.67}$$

We now have two of the three unknowns in terms of B_0. This leaves us with only one condition left to apply, which enforces the continuity of $G_{Az}^{(z)}$ itself at the air–dielectric interface. The application of this condition simply entails setting z equal to zero in equation (2.64) yielding,

$$B_0 = A_d + B_d + E_d \frac{e^{+u_d z'}}{2u_d} \tag{2.68}$$

into which we can substitute the two previous equations ((2.66) and (2.67)) leaving,

$$B_0 = \frac{-\varepsilon_{rd} 2u_0 B_0 + E_d\left(e^{+u_d z'} + e^{-u_d z'}\right)}{2u_d\left(e^{+2u_d d} - 1\right)}\left(e^{+2u_d d} + 1\right) + E_d \frac{\left(e^{+u_d z'} - e^{-u_d z'}\right)}{2u_d} \quad . \quad (2.69)$$

Examining equation (2.69) we can see hyperbolic functions emerging, so collecting like terms and applying the appropriate hyperbolic definitions [CRC], this equation reduces to,

$$B_0 = \frac{\sinh(u_d z')\tanh(u_d d) + \cosh(u_d z')}{\varepsilon_{rd} u_0 + u_d \tanh(u_d d)} E_d = \frac{N_{v_0}}{D_{TM}} E_d \quad . \quad (2.70)$$

where the numerator function N_{v_0} can be further simplified by expanding the tanh function in terms of sinh and cosh and applying a simple hyperbolic identity as is shown below.

$$N_{v_0} = \frac{\sinh(u_d z')\sinh(u_d d) + \cosh(u_d z')\cosh(u_d d)}{\cosh(u_d d)} = \frac{\cosh\left(u_d(z' + d)\right)}{\cosh(u_d d)} \quad (2.71)$$

Before going on, the denominator function D_{TM} in equation (2.70) demands some discussion. It can be shown that this denominator arises from the magnetic fields transverse to z being supported within the dielectric [Felsen1], which is the reason for the *TM* subscript. It is important since its zeros will be seen to reek havoc in the inverse Fourier transform integration which takes the dyadic magnetic vector potential Green function back into the spatial–frequency domain. Furthermore, it should be mentioned that the poles of the numerator function N_{v_0} can possibly cause problems, similar to those of the D_{TM} function, at frequencies where the wavelength is smaller than the dielectric thickness by a significant degree. This will all be discussed further in section 3.1.2.

Finally, we can substitute equation (2.70) in expanded form into equation (2.66) which can then be substituted into equation (2.63) to solve for the remaining two of the three required unknowns,

$$B_d = \frac{-e^{-u_d d}}{D_{TM}}\left[\frac{\varepsilon_{rd} u_0 \sinh(u_d z') - u_d \cosh(u_d z')}{2u_d \cosh(u_d d)}\right] E_d \quad (2.72)$$

and

$$A_d = \frac{-e^{+u_d d}}{D_{TM}}\left[\frac{\varepsilon_{rd}u_0\sinh(u_d z') - u_d\cosh(u_d z')}{2u_d\cosh(u_d d)}\right]E_d - \frac{e^{-u_d z'}}{2u_d}E_d \quad . \qquad (2.73)$$

At last, we have all the unknowns needed to write the magnetic vector potential Green function due to a vertically directed source. Dealing with this vector Green function in the source–free region first, (which will be of most interest to us in the rest of this document), we find that it can be written by simply substituting equation (2.70) into equation (2.47) and writing the result in vector form, as,

$$\mathbf{G}_{A_0}^{(z)} = \frac{N_{v_0}}{D_{TM}}E_d e^{-u_0 z}\hat{z} \quad . \qquad (2.74)$$

Then for the same Green function in the dielectric region we substitute equations (2.72) and (2.73) into equation (2.61) to obtain,

$$\mathbf{G}_{A_d}^{(z)} = \left(\frac{-\varepsilon_{rd}u_0\sinh(u_d z') + u_d\cosh(u_d z')}{u_d D_{TM}}\frac{\cosh(u_d(z+d))}{\cosh(u_d d)} - \frac{e^{+u_d(z-z')} - e^{-u_d|z-z'|}}{2u_d}\right)E_d\hat{z} \qquad (2.75)$$

which allows us to check the boundary conditions used to arrive at these two magnetic vector potential Green functions.

2.6 The Magnetic Vector Potential Green Function due to Horizontal Electric Sources

In the previous section we derived the magnetic vector potential vector Green function for a vertical electric source, (i.e. the third column of the corresponding dyadic Green function). Now we deal with the remaining two vector Green functions which we need, to completely define the desired dyadic Green function. We are able to find both of these remaining vector Green functions at the same time since the dielectric and ground layers extend infinitely in both the x and the y directions so it is obvious that these directions are interchangeable. This can also be seen from the boundary conditions on the magnetic vector potential Green functions (equations (2.36) to (2.38)), where we find that if we interchange G_{Ax} with G_{Ay} and k_x with k_y we obtain the exact same boundary conditions. We will therefore, write this

section solving for the magnetic vector potential vector Green function for an x–directed electric source and then apply the preceding interchanges to obtain the Green function for a y–directed source.

For an x–directed source we can write similar equations to those written for the z–directed source in the previous section. These equations are as follows.

$$a)\quad \left(\frac{d^2}{dz^2}-u_0^2\right)\mathbf{G}_{A_0}^{(x)}=0 \qquad b)\quad \left(\frac{d^2}{dz^2}-u_d^2\right)\mathbf{G}_{A_d}^{(x)}=-E_d\delta(z-z')\hat{x} \tag{2.76}$$

As before we can split these two equations into component parts yielding three homogeneous equations in the source–free (air) region along with two homogeneous equations and one inhomogeneous equation in the dielectric region. If we also try, as before, to set both components of the Green function transverse to the direction of the source to zero we obtain the following identities,

$$a)\quad G_{A_0y}^{(x)}=G_{A_dy}^{(x)}=0 \qquad b)\quad G_{A_0z}^{(x)}=G_{A_dz}^{(x)}=0 \tag{2.77}$$

and the following equations to be solved.

$$a)\quad \left(\frac{d^2}{dz^2}-u_0^2\right)G_{A_0x}^{(x)}=0 \qquad b)\quad \left(\frac{d^2}{dz^2}-u_d^2\right)G_{A_dx}^{(x)}=0 \tag{2.78}$$

$$c)\quad \left(\frac{d^2}{dz^2}-u_d^2\right)G_{A_dpx}^{(x)}=-E_d\delta(z-z')$$

It is again prudent to check if the $G_{Ax}^{(x)}$ component alone will satisfy all of the required boundary conditions. Therefore, applying equations (2.77) to the boundary conditions in equation (2.36) we simply get,

$$G_{A_dx}^{(x)}\Big|_{z=-d}=0 \tag{2.79}$$

with no difficulties. Similarly from the boundary conditions in equation (2.38) we obtain,

$$\frac{dG_{A_0x}^{(x)}}{dz}\Bigg|_{z=0}=\frac{dG_{A_dx}^{(x)}}{dz}\Bigg|_{z=0} \tag{2.80}$$

with no difficulties either. However problems arise when trying to apply identities (2.77) to the remaining boundary conditions in equation (2.37). In this case equation (2.37a) gives us,

$$G_{A_d x}^{(x)}\Big|_{z=0} = \varepsilon_{rd}\left(\frac{k_0^2 - k_x^2}{k_d^2 - k_x^2}\right) G_{A_0 x}^{(x)}\Big|_{z=0} \tag{2.81}$$

while equation (2.37b) gives us,

$$G_{A_d x}^{(x)}\Big|_{z=0} = \varepsilon_{rd} G_{A_0 x}^{(x)}\Big|_{z=0} \quad . \tag{2.82}$$

Remembering that $k = \omega\sqrt{\mu\varepsilon}$ and that within this wave number only ε changes between the two regions by the amount ε_{rd} we can easily write $k_d = \sqrt{\varepsilon_{rd}}\,k_0$. Because of this, these two equations obviously contradict each other since the only way both of them could be satisfied is if $k_d = k_0$, or in other words if $\varepsilon_{rd} = 1$. Since restricting a dielectric to having a dielectric constant of 1 is basically useless, we can see that using only one component of this vector Green function does not allow us to satisfy the required boundary conditions. From our earlier postulate however, we know that we need at most two components of the magnetic vector potential Green function, in both regions, to properly satisfy all their boundary conditions. We therefore need to choose another component to help satisfy all of the boundary conditions, where obviously, it would be useful to use the one that yields the simplest boundary conditions, if that particular choice allows the boundary conditions on the fields to be properly satisfied. It can easily be shown that for this case the easier boundary conditions come from using the z component along with the x, and so we proceed by applying only equation (2.77a) to equations (2.36) to (2.38). Doing this we end up with the following reduced set of boundary conditions.

$$a) \quad \left[\left(k_d^2 - k_x^2\right) G_{A_d x}^{(x)} + jk_x \frac{dG_{A_d z}^{(x)}}{dz}\right]_{z=-d} = 0 \tag{2.83}$$

$$b) \quad \left[-k_x k_y G_{A_d x}^{(x)} + jk_y \frac{dG_{A_d z}^{(x)}}{dz}\right]_{z=-d} = 0$$

$$a)\quad \varepsilon_{rd}\left[\left(k_0^2-k_x^2\right)G_{A_0x}^{(x)}+jk_x\frac{dG_{A_0z}^{(x)}}{dz}\right]_{z=0}=\left[\left(k_d^2-k_x^2\right)G_{A_dx}^{(x)}+jk_x\frac{dG_{A_dz}^{(x)}}{dz}\right]_{z=0} \tag{2.84}$$

$$b)\quad \varepsilon_{rd}\left[-k_xk_yG_{A_0x}^{(x)}+jk_y\frac{dG_{A_0z}^{(x)}}{dz}\right]_{z=0}=\left[-k_xk_yG_{A_dx}^{(x)}+jk_y\frac{dG_{A_dz}^{(x)}}{dz}\right]_{z=0}$$

$$a)\quad jk_yG_{A_0z}^{(x)}\Big|_{z=0}=jk_yG_{A_dz}^{(x)}\Big|_{z=0} \tag{2.85}$$

$$b)\quad \left[jk_xG_{A_0z}^{(x)}-\frac{dG_{A_0x}^{(x)}}{dz}\right]_{z=0}=\left[jk_xG_{A_dz}^{(x)}-\frac{dG_{A_dx}^{(x)}}{dz}\right]_{z=0}$$

Before we proceed with calculating the Green functions, we find that it is possible to simplify boundary conditions (2.83) by rewriting equation (2.83b) as follows,

$$\left[\frac{dG_{A_dz}^{(x)}}{dz}=-jk_xG_{A_dx}^{(x)}\right]_{z=-d} \tag{2.86}$$

and substituting this equation into equation (2.83a) to directly obtain a reduced boundary condition on $G_{A_dx}^{(x)}$ as,

$$G_{A_dx}^{(x)}\Big|_{z=-d}=0\quad . \tag{2.87}$$

If we then substitute this boundary condition back into equation (2.83b) we obtain a reduced boundary conditions on $G_{A_dz}^{(x)}$ as,

$$\frac{dG_{A_dz}^{(x)}}{dz}\Big|_{z=-d}=0\quad . \tag{2.88}$$

Moving on to equations (2.84), collecting like terms and using the relation $k_d=\sqrt{\varepsilon_{rd}}k_0$ we can write,

$$a)\quad \left[\varepsilon_{rd}\frac{dG_{A_0z}^{(x)}}{dz}-\frac{dG_{A_dz}^{(x)}}{dz}\right]_{z=0}=\frac{\varepsilon_{rd}k_0^2}{jk_x}\left(G_{A_dx}^{(x)}-G_{A_0x}^{(x)}\right)-jk_x\left(\varepsilon_{rd}G_{A_0x}^{(x)}-G_{A_dx}^{(x)}\right)\Big|_{z=0} \tag{2.89}$$

$$b)\quad \left[\varepsilon_{rd}\frac{dG_{A_0z}^{(x)}}{dz}-\frac{dG_{A_dz}^{(x)}}{dz}\right]_{z=0}=-jk_x\left(\varepsilon_{rd}G_{A_0x}^{(x)}-G_{A_dx}^{(x)}\right)\Big|_{z=0}$$

from which we immediately see some obvious similarities between these two equations. Therefore, we can substitute equation (2.89b) into (2.89a) to obtain another boundary condition on $G_{Ax}^{(x)}$, namely,

$$G_{A_0x}^{(x)}\Big|_{z=0} = G_{A_dx}^{(x)}\Big|_{z=0} \tag{2.90}$$

which we can substitute into (2.89b) to obtain a second condition on $G_{Az}^{(x)}$, as,

$$\frac{dG_{A_dz}^{(x)}}{dz}\bigg|_{z=0} = \left[\varepsilon_{rd}\frac{dG_{A_0z}^{(x)}}{dz} + jk_x(\varepsilon_{rd}-1)G_{A_0x}^{(x)}\right]_{z=0} \quad . \tag{2.91}$$

Now that we have obtained reduced boundary conditions from equations (2.83) and (2.84) we need only to do the same with equations (2.85). The last condition on $G_{Az}^{(x)}$ can be seen immediately upon examining equation (2.85a), namely,

$$G_{A_0z}^{(x)}\Big|_{z=0} = G_{A_dz}^{(x)}\Big|_{z=0} \tag{2.92}$$

which when substituted into equation (2.85b) yields the last remaining boundary condition on $G_{Ax}^{(x)}$, as,

$$\frac{dG_{A_0x}^{(x)}}{dz}\bigg|_{z=0} = \frac{dG_{A_dx}^{(x)}}{dz}\bigg|_{z=0} \quad . \tag{2.93}$$

Equations (2.87), (2.90) and (2.93) now define three boundary conditions on $G_{Ax}^{(x)}$, while equations (2.88), (2.91) and (2.92) define three boundary conditions on $G_{Az}^{(x)}$. Writing these conditions together with the appropriate differential equations to be solved we obtain, for the Green function $G_{Ax}^{(x)}$, the equations,

$$a)\quad \left(\frac{d^2}{dz^2} - u_0^2\right)G_{A_0x}^{(x)} = 0 \qquad b)\quad \left(\frac{d^2}{dz^2} - u_d^2\right)\mathbf{G}_{A_dx}^{(x)} = -E_d\delta(z-z') \tag{2.94}$$

along with the boundary conditions,

$$a)\quad G_{A_dx}^{(x)}\Big|_{z=-d} = 0 \qquad b)\quad \frac{dG_{A_0x}^{(x)}}{dz}\bigg|_{z=0} = \frac{dG_{A_dx}^{(x)}}{dz}\bigg|_{z=0} \qquad c)\quad G_{A_0x}^{(x)}\Big|_{z=0} = G_{A_dx}^{(x)}\Big|_{z=0} \quad . \tag{2.95}$$

Similarly, for the Green function $G_{Az}^{(x)}$ we find the equations to be,

$$a)\quad \left(\frac{d^2}{dz^2}-u_0^2\right)G_{A_0z}^{(x)}=0 \qquad b)\quad \left(\frac{d^2}{dz^2}-u_d^2\right)G_{A_dz}^{(x)}=0 \tag{2.96}$$

while the boundary conditions are,

$$a)\quad \left.\frac{dG_{A_dz}^{(x)}}{dz}\right|_{z=-d}=0 \qquad b)\quad G_{A_0z}^{(x)}\Big|_{z=0}=G_{A_dz}^{(x)}\Big|_{z=0} \tag{2.97}$$

$$c)\quad \left.\frac{dG_{A_dz}^{(x)}}{dz}\right|_{z=0}=\left[\varepsilon_{rd}\frac{dG_{A_0z}^{(x)}}{dz}+jk_x\left(\varepsilon_{rd}-1\right)G_{A_0x}^{(x)}\right]_{z=0} \quad .$$

We will now proceed to solve for the Green function $G_{Ax}^{(x)}$. In so doing we can write the solutions to equation (2.94) directly from equations (2.47) and (2.61). This is because the equations to be solved for $G_{Ax}^{(x)}$ (equations (2.94)) are the same as the ones used to solve for $G_{Az}^{(z)}$ in the previous section (equations (2.43)) and so we have,

$$a)\quad G_{A_0x}^{(x)}=B_0e^{-u_0z} \qquad b)\quad G_{A_dx}^{(x)}=A_de^{u_dz}+B_de^{-u_dz}+E_d\frac{e^{-u_d|z-z'|}}{2u_d} \quad . \tag{2.98}$$

Beginning the matching of the boundary conditions with condition (2.95a) and noting that the relation $z \le z'$ holds in this case we can write,

$$2u_d\left(A_de^{-u_dd}+B_de^{+u_dd}\right)+E_de^{-u_d(z'+d)}=0 \tag{2.99}$$

which can be rearranged and reduced to yield,

$$A_d=-B_de^{+2u_dd}-E_d\frac{e^{-u_dz'}}{2u_d} \quad . \tag{2.100}$$

Then, in order to apply condition (2.95b), where the relation $z \ge z'$ holds, we note that this condition is identical to condition (2.45b) on $G_{Az}^{(z)}$ save for a permittivity multiplier. Therefore, since the equations to be matched are the same and the matching condition is almost identical, we can directly write, by inspection, the solution from equation (2.65) as,

$$-u_0B_0=u_d\left(A_d-B_d\right)-E_d\frac{e^{+u_dz'}}{2} \tag{2.101}$$

which, upon substitution of equation (2.100) then yields the following equation for B_d.

$$B_d = \frac{2u_0B_0 - E_d\left(e^{+u_dz'} + e^{-u_dz'}\right)}{2u_d\left(e^{+2u_dd} + 1\right)} \tag{2.102}$$

Thereafter, substituting this equation for B_d back into equation (2.100) gives the following equation for A_d.

$$A_d = \frac{-2u_0B_0 + E_d\left(e^{+u_dz'} + e^{-u_dz'}\right)}{2u_d\left(e^{+2u_dd} + 1\right)}e^{+2u_dd} - E_d\frac{e^{-u_dz'}}{2u_d} \tag{2.103}$$

Now, with one condition remaining, (2.95c), we note that this is exactly the same as condition (2.45c) on $G_{Az}^{(z)}$. Therefore, we can directly write the solution to this condition from equation (2.68) as,

$$B_0 = A_d + B_d + E_d\frac{e^{+u_dz'}}{2u_d} \tag{2.104}$$

which, upon substituting the above equations defining B_d and A_d yields,

$$B_0 = \frac{-2u_0B_0 + E_d\left(e^{+u_dz'} + e^{-u_dz'}\right)}{2u_d\left(e^{+2u_dd} + 1\right)}\left(e^{+2u_dd} - 1\right) + E_d\frac{\left(e^{+u_dz'} - e^{-u_dz'}\right)}{2u_d} \quad . \tag{2.105}$$

Rewriting equation (2.105) using appropriate hyperbolic functions, as was done in the previous section, gives,

$$B_0 = \frac{\sinh(u_dz')\coth(u_dd) + \cosh(u_dz')}{u_0 + u_d\coth(u_dd)}E_d = \frac{N_{h_0}}{D_{TE}}E_d \quad . \tag{2.106}$$

where the numerator function N_{h_0} can be further simplified by expanding the coth function in terms of sinh and cosh and applying a simple hyperbolic identity as is shown below.

$$N_{h_0} = \frac{\sinh(u_dz')\cosh(u_dd) + \cosh(u_dz')\sinh(u_dd)}{\sinh(u_dd)} = \frac{\sinh\left(u_d(z' + d)\right)}{\sinh(u_dd)} \tag{2.107}$$

Before going on, the denominator and numerator functions in equation (2.106) again demand discussion. As in the previous section, the zeros of the denominator function, D_{TE}, and the poles of the numerator function, N_{h_0}, will cause problems in the inverse Fourier

transform integration which takes the dyadic magnetic vector potential Green function back into the spatial–frequency domain. Furthermore, it is worthwhile to note that the equations defining $G_{Ax}^{(x)}$, and its boundary conditions, which we have just solved are identical to those of a vertical magnetic dipole within the substrate [Felsen1]. This can easily be shown by going back to equations (2.14) to (2.16) and setting the electric current and magnetic vector potential to zero, (instead of the magnetic current and the electric vector potential as was done previously), and then repeating the boundary condition calculations and calculating the solution of a vertical magnetic dipole. This is a very important result since it shows that a horizontal electric source within a single dielectric, grounded layer can be represented by using a linear combination of a horizontal electric source and a vertical electric source or a vertical electric source and a vertical magnetic source. Because of this result the D_{TE} function can be seen to be caused by the transverse electric fields existing within the dielectric which is the reason for the TE subscript.

Finally, we can substitute equation (2.106) in expanded form into equations (2.102) and (2.103) and by so doing we can solve for the remaining two of the three required unknowns, yielding,

$$B_d = \frac{e^{-u_d d}}{D_{TE}} \left[\frac{u_0 \sinh(u_d z') - u_d \cosh(u_d z')}{2u_d \sinh(u_d d)} \right] E_d \tag{2.108}$$

$$A_d = \frac{-e^{+u_d d}}{D_{TE}} \left[\frac{u_0 \sinh(u_d z') - u_d \cosh(u_d z')}{2u_d \sinh(u_d d)} \right] E_d - \frac{e^{-u_d z'}}{2u_d} E_d \quad . \tag{2.109}$$

Therefore, we can now write the solution for the x component of the magnetic vector potential Green function for an x directed electric source. In the air region this component can be found by substituting equation (2.106) into equation (2.98a) as,

$$G_{A_0 x}^{(x)} = \frac{N_{h_0}}{D_{TE}} E_d e^{-u_0 z} \tag{2.110}$$

and for the dielectric region this Green function can be found by substituting equations (2.108) and (2.109) into equation (2.98b) to obtain,

$$G_{A_d x}^{(x)} = \left(\frac{-u_0 \sinh(u_d z') + u_d \cosh(u_d z')}{u_d D_{TE}} \frac{\sinh(u_d(z+d))}{\sinh(u_d d)} - \frac{e^{+u_d(z-z')} - e^{-u_d|z-z'|}}{2u_d} \right) E_d \ . \quad (2.111)$$

With one component completely solved for we are only half done with this derivation. To solve for the z component we need to solve equations (2.96) for the conditions (2.97). To begin we can again immediately write the solutions to these equations as,

$$a) \quad G_{A_0 z}^{(x)} = B_0 e^{-u_0 z} \qquad b) \quad G_{A_d z}^{(x)} = A_d e^{u_d z} + B_d e^{-u_d z} \quad (2.112)$$

which are identical to equations (2.98) with no source term present. Applying firstly, condition (2.97a) to equation (2.112b) we obtain,

$$u_d\left(A_d e^{-u_d d} - B_d e^{+u_d d}\right) = 0 \quad (2.113)$$

which can be rearranged to yield,

$$A_d = B_d e^{+2u_d d} \ . \quad (2.114)$$

Then applying condition (2.97b) to equations (2.112) we directly obtain,

$$B_0 = A_d + B_d \quad (2.115)$$

and substituting equation (2.114) we are left with,

$$B_d = \frac{B_0}{\left(e^{+2u_d d} + 1\right)} \quad (2.116)$$

which when substituted back into equation (2.114) yields,

$$A_d = B_0 \frac{e^{+2u_d d}}{\left(e^{+2u_d d} + 1\right)} \ . \quad (2.117)$$

Now, to apply the final condition (2.97c) we take the derivative with respect to z of equations

(2.112) and equate them in the manner demanded by the boundary condition while setting $z = 0$ to obtain,

$$u_d(A_d - B_d) = -\varepsilon_{rd} u_0 B_0 + jk_x(\varepsilon_{rd} - 1)\left[G^{(x)}_{A_0 x}\right]_{z=0} \tag{2.118}$$

which when (2.116) and (2.117) are substituted and the result is rearranged yields,

$$B_0\left(\varepsilon_{rd} u_0 + u_d \tanh(u_d d)\right) = jk_x(\varepsilon_{rd} - 1)\left[G^{(x)}_{A_0 x}\right]_{z=0} \quad . \tag{2.119}$$

Examining equation (2.119) we recognize the denominator D_{TM} from the previous section and so substituting this denominator and equation (2.110) with $z = 0$ for the x component of the magnetic vector potential required we obtain simply,

$$B_0 = \frac{jk_x(\varepsilon_{rd} - 1)N_{h_0}}{D_{TE} D_{TM}} E_d \quad . \tag{2.120}$$

Substituting this result back into equations (2.116) and (2.117) finally yields the other two unknowns as follows,

$$a) \quad B_d = \frac{jk_x(\varepsilon_{rd} - 1)N_{h_0}}{D_{TE} D_{TM}\left(e^{+2u_d d} + 1\right)} E_d \qquad b) \quad A_d = \frac{jk_x(\varepsilon_{rd} - 1)N_{h_0}}{D_{TE} D_{TM}\left(e^{+2u_d d} + 1\right)} e^{+2u_d d} E_d \quad . \tag{2.121}$$

Now, substituting equation (2.120) into (2.112a) we obtain the z component of the magnetic vector potential Green function for the air region as,

$$G^{(x)}_{A_0 z} = \frac{jk_x(\varepsilon_{rd} - 1)N_{h_0}}{D_{TE} D_{TM}} E_d e^{-u_0 z} \tag{2.122}$$

and then, substituting equations (2.121a) and (2.121b) into equation (2.112b) we obtain this Green function component for the dielectric region.

$$G^{(x)}_{A_d z} = \frac{jk_x(\varepsilon_{rd} - 1)N_{h_0}}{D_{TE} D_{TM}} \frac{\cosh u_d(z + d)}{\cosh u_d d} E_d \tag{2.123}$$

Finally, the total magnetic vector potential Green function due to an x–directed electric source can be written as,

$$\mathbf{G}^{(x)}_A = G^{(x)}_{Ax}\hat{x} + G^{(x)}_{Az}\hat{z} \quad . \tag{2.124}$$

For the air region, this is simply a combination of equations (2.110) and (2.122) and is written in vector form as,

$$\mathbf{G}_{A_0}^{(x)} = N_{h_0}\left(\frac{1}{D_{TE}}\hat{x} + \frac{jk_x(\varepsilon_{rd}-1)}{D_{TE}D_{TM}}\hat{z}\right)E_d e^{-u_0 z} \qquad (2.125)$$

while in the dielectric region this becomes a combination of equations (2.111) and (2.123) as,

$$\mathbf{G}_{A_d}^{(x)} = \left(\frac{-u_0\sinh(u_d z') + u_d\cosh(u_d z')}{u_d D_{TE}}\frac{\sinh(u_d(z+d))}{\sinh(u_d d)} - \frac{e^{+u_d(z-z')} - e^{-u_d|z-z'|}}{2u_d}\right)E_d\hat{x}$$

$$+\left(\frac{jk_x(\varepsilon_{rd}-1)N_{h_0}}{D_{TE}D_{TM}}\frac{\cosh u_d(z+d)}{\cosh u_d d}\right)E_d\hat{z} \quad . \qquad (2.126)$$

It is interesting to note before continuing that in the case of a simple horizontal dipole above ground (i.e. $\varepsilon_{rd} = 1$) these functions are only defined in terms of the magnetic vector potential component directed parallel to the source as we would expect.

Now that we have the x–directed magnetic vector potential Green function it is simple to find the y–directed vector potential Green function as we have previously mentioned. To do this the following substitutions must be applyed to equations (2.125) and (2.126), $(x) \rightarrow (y)$, $\hat{x} \rightarrow \hat{y}$, $k_x \rightarrow k_y$. In so doing the resultant y–directed magnetic vector potential Green functions become,

$$\mathbf{G}_{A_0}^{(y)} = N_{h_0}\left(\frac{1}{D_{TE}}\hat{y} + \frac{jk_y(\varepsilon_{rd}-1)}{D_{TE}D_{TM}}\hat{z}\right)E_d e^{-u_0 z} \qquad (2.127)$$

and

$$\mathbf{G}_{A_d}^{(y)} = \left(\frac{-u_0\sinh(u_d z') + u_d\cosh(u_d z')}{u_d D_{TE}}\frac{\sinh(u_d(z+d))}{\sinh(u_d d)} - \frac{e^{+u_d(z-z')} - e^{-u_d|z-z'|}}{2u_d}\right)E_d\hat{y}$$

$$+\left(\frac{jk_y(\varepsilon_{rd}-1)N_{h_0}}{D_{TE}D_{TM}}\frac{\cosh u_d(z+d)}{\cosh u_d d}\right)E_d\hat{z} \quad . \qquad (2.128)$$

Obviously, all the previous results can easily be checked through their application to the appropriate boundary conditions, which must hold.

2.7 An Interesting Result

In sections 2.5 and 2.6 we calculated the magnetic vector potential dyadic Green function in both the air and dielectric regions. Now writing the results for the air region in dyadic form we obtain the following very compact result,

$$\overline{\mathbf{G}}_{A_0} = \begin{bmatrix} \frac{N_{h_0}}{D_{TE}} & 0 & 0 \\ 0 & \frac{N_{h_0}}{D_{TE}} & 0 \\ \frac{jk_x N_{h_0}(\varepsilon_{rd}-1)}{D_{TE}D_{TM}} & \frac{jk_y N_{h_0}(\varepsilon_{rd}-1)}{D_{TE}D_{TM}} & \frac{N_{v_0}}{D_{TM}} \end{bmatrix} E_d e^{-u_0 z} \tag{2.129}$$

which at the air–dielectric interface, (i.e. the surface of the PCB) becomes,

$$\overline{\mathbf{G}}_{A_0}\big|_{z=0} = \begin{bmatrix} \frac{1}{D_{TE}} & 0 & 0 \\ 0 & \frac{1}{D_{TE}} & 0 \\ \frac{jk_x(\varepsilon_{rd}-1)}{D_{TE}D_{TM}} & \frac{jk_y(\varepsilon_{rd}-1)}{D_{TE}D_{TM}} & \frac{1}{D_{TM}} \end{bmatrix} E_d e^{-u_0 z} \quad . \tag{2.130}$$

This result however, is based entirely on the dipole source having been somewhere within the dielectric, so let us regress momentarily and assume that the dipole is hovering above the PCB. To solve this new problem we would simply redo the calculations of sections 2.5 and 2.6 with the source term moved from the defining equation in the dielectric region to the one in the air region, (equation (2.39)). Since this procedure is so similar to that already followed we simply state the result to be,

$$\overline{\mathbf{G}}_{A_0} = \left\{ \begin{bmatrix} \frac{u_0 - u_d \coth u_d d}{2u_0 D_{TE}} & 0 & 0 \\ 0 & \frac{u_0 - u_d \coth u_d d}{2u_0 D_{TE}} & 0 \\ \frac{jk_x(\varepsilon_{rd}-1)}{D_{TE}D_{TM}} & \frac{jk_y(\varepsilon_{rd}-1)}{D_{TE}D_{TM}} & \frac{\varepsilon_{rd}u_0 - u_d \tanh u_d d}{2u_0 D_{TM}} \end{bmatrix} e^{-u_0(z+z')} + \frac{1}{2u_0}\begin{bmatrix} 1 & 0 & 0 \\ 0 & 1 & 0 \\ 0 & 0 & 1 \end{bmatrix} e^{-u_0|z-z'|} \right\} E_d \quad . \tag{2.131}$$

This new dyadic has some similarities to the one in equation (2.129) and at the surface of

the PCB it becomes,

$$\overline{\mathbf{G}}_{A_0} = \begin{bmatrix} \frac{1}{D_{TE}} & 0 & 0 \\ 0 & \frac{1}{D_{TE}} & 0 \\ \frac{jk_x(\varepsilon_{rd}-1)}{D_{TE}D_{TM}} & \frac{jk_y(\varepsilon_{rd}-1)}{D_{TE}D_{TM}} & \frac{\varepsilon_{rd}}{D_{TM}} \end{bmatrix} E_d e^{-u_0 z} \quad . \tag{2.132}$$

Now, comparing equation (2.132) to equation (2.130) we find that these equations are identical except for the single component due to a z–directed dipole. However, since both of these results are complete solutions and the position at which they occur is in both cases at the surface of the PCB we would really expect the solutions to be identical. This seeming contradiction should be examined further to make sure that it actually represents a physical phenomenon. If it is physically correct it has interesting implications in the design of printed circuit boards or integrated circuits. The immediately obvious implication is that since the magnetic vector potential Green function for a vertical electric source is larger for a source slightly above the substrate than a source slightly inside the substrate by an amount identical to the relative permittivity of the substrate, the magnetic vector potential itself and hence the electric and magnetic fields display the same phenomenon. This would indicate that in the design of printed circuits the radiation from these circuits could be significantly reduced by reducing component pin length or burying the pins or even the entire components within the substrate.

CHAPTER 3

CONVERSION FROM THE SPECTRAL–FREQUENCY DOMAIN BACK INTO THE TIME DOMAIN

3.1 Conversion from the Spectral–Frequency Domain into the Frequency Domain

In the last chapter we derived the complete dyadic representation of the magnetic vector potential Green function, $\overline{\mathbf{G}}_A$, in both the dielectric and air regions for an electric source residing within the dielectric. For the remaining part of this paper however, we will just concern ourselves with the dyadic for the source–free air region since for our purposes we are only interested in radiation within this region. We therefore reiterate this spectral–frequency domain dyadic in full below,

$$\overline{\mathbf{G}}_{A_0} = \begin{bmatrix} \dfrac{N_{h_0}}{D_{TE}} & 0 & 0 \\ 0 & \dfrac{N_{h_0}}{D_{TE}} & 0 \\ \dfrac{jk_x N_{h_0}(\varepsilon_{rd}-1)}{D_{TE}D_{TM}} & \dfrac{jk_y N_{h_0}(\varepsilon_{rd}-1)}{D_{TE}D_{TM}} & \dfrac{N_{v_0}}{D_{TM}} \end{bmatrix} e^{-j(k_x x' + k_y y')} e^{-u_0 z} \tag{3.1}$$

and must now continue on to calculate the electric dyadic Green function, $\overline{\mathbf{G}}_{E_0}$, in the frequency domain (and eventually in the time domain). To do this we can either use equation (2.23), remembering that $\overline{\mathbf{G}}_F = 0$, to calculate $\overline{\mathbf{G}}_{E_0}$ before converting back into the frequency domain or we can convert $\overline{\mathbf{G}}_{A_0}$ into the frequency domain directly and then obtain $\overline{\mathbf{G}}_{E_0}$. These two methods can be shown to be identical and so for our purposes we will choose the simpler approach of converting the magnetic vector potential dyadic Green function into the frequency domain first.

3.1.1 The Inverse Fourier Transform Integrals

To proceed in the above manner we simply apply the inverse Fourier transform (equation (2.34b)) to the above dyadic and in so doing write,

$$\overline{\mathbf{G}}_{A_0}(x,y,z) = \frac{1}{4\pi^2} \int_{-\infty}^{\infty} \int_{-\infty}^{\infty} \overline{\mathbf{G}}_{A_0}(k_x,k_y,z) e^{+j[k_x(x-x')+k_y(y-y')]} dk_x dk_y \tag{3.2}$$

which when written as separate equations for each non–zero component of the dyadic yields the following four integrals.

$$G_{A_0x}^{(x)}(x,y) = G_{A_0y}^{(y)}(x,y) = \frac{1}{4\pi^2}\int_{-\infty}^{\infty}\int_{-\infty}^{\infty}\frac{N_{h_0}}{D_{TE}}e^{-u_0z+j[k_x(x-x')+k_y(y-y')]}dk_xdk_y \tag{3.3}$$

$$G_{A_0z}^{(x)}(x,y) = \frac{(\varepsilon_{rd}-1)}{4\pi^2}\int_{-\infty}^{\infty}\int_{-\infty}^{\infty}\frac{jk_xN_{h_0}}{D_{TE}D_{TM}}e^{-u_0z+j[k_x(x-x')+k_y(y-y')]}dk_xdk_y \tag{3.4}$$

$$G_{A_0z}^{(y)}(x,y) = \frac{(\varepsilon_{rd}-1)}{4\pi^2}\int_{-\infty}^{\infty}\int_{-\infty}^{\infty}\frac{jk_yN_{h_0}}{D_{TE}D_{TM}}e^{-u_0z+j[k_x(x-x')+k_y(y-y')]}dk_xdk_y \tag{3.5}$$

$$G_{A_0z}^{(z)}(x,y) = \frac{1}{4\pi^2}\int_{-\infty}^{\infty}\int_{-\infty}^{\infty}\frac{N_{v_0}}{D_{TM}}e^{-u_0z+j[k_x(x-x')+k_y(y-y')]}dk_xdk_y \tag{3.6}$$

Let us now apply the following change of variables to these four equations.

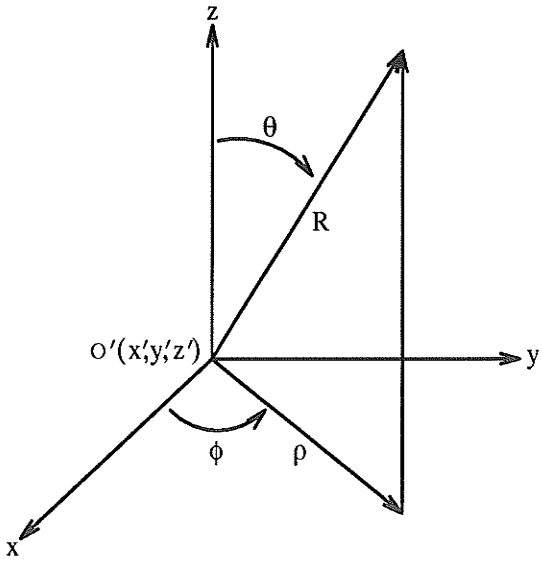

Figure 5: The Spatial Coordinate Relations

$$a)\quad k_x = k_\varrho \sin\psi \quad , \quad k_y = k_\varrho \cos\psi \tag{3.7}$$

$$b)\quad x - x' = \varrho\cos\phi \quad , \quad y - y' = \varrho\sin\phi$$

This change of variables is basically a transformation to polar coordinates in both the spectral, (3.7a), and spatial, (3.7b), domains, with the spatial origin moved to the position of the source, (as shown in Fig. 5). From this we find that $k_x^2 + k_y^2 = k_\varrho^2$, and thereby u_0 and u_d become,

$$a)\quad u_0 = \sqrt{k_\varrho^2 - k_0^2} \qquad b)\quad u_d = \sqrt{k_\varrho^2 - \varepsilon_{rd}k_0^2} \tag{3.8}$$

with which the numerator and denominator functions also change appropriately.

Furthermore, this change of variables also causes part of the common exponent within these integrals to become,

$$k_x(x-x')+k_y(y-y')=k_\varrho\varrho(\sin\psi\cos\phi+\cos\psi\sin\phi)=k_\varrho\varrho\sin(\psi+\phi) \quad . \quad (3.9)$$

Therefore the integrals, which are now integrable over a polar surface, can be written as,

$$G_{A_0x}^{(x)}\left(k_\varrho,\psi\right)=G_{A_0y}^{(y)}\left(k_\varrho,\psi\right)=\frac{1}{4\pi^2}\int_0^\infty\int_{-\pi}^{\pi}\frac{N_{h_0}}{D_{TE}}e^{-u_0z+jk_\varrho\varrho\sin(\psi+\phi)}k_\varrho dk_\varrho d\psi \quad (3.10)$$

$$G_{A_0z}^{(x)}\left(k_\varrho,\psi\right)=\frac{(\varepsilon_{rd}-1)}{4\pi^2}\int_0^\infty\int_{-\pi}^{\pi}\frac{jk_\varrho\sin\psi N_{h_0}}{D_{TE}D_{TM}}e^{-u_0z+jk_\varrho\varrho\sin(\psi+\phi)}k_\varrho dk_\varrho d\psi \quad (3.11)$$

$$G_{A_0z}^{(y)}\left(k_\varrho,\psi\right)=\frac{(\varepsilon_{rd}-1)}{4\pi^2}\int_0^\infty\int_{-\pi}^{\pi}\frac{jk_\varrho\cos\psi N_{h_0}}{D_{TE}D_{TM}}e^{-u_0z+jk_\varrho\varrho\sin(\psi+\phi)}k_\varrho dk_\varrho d\psi \quad (3.12)$$

$$G_{A_0z}^{(z)}\left(k_\varrho,\psi\right)=\frac{1}{4\pi^2}\int_0^\infty\int_{-\pi}^{\pi}\frac{N_{v_0}}{D_{TM}}e^{-u_0z+jk_\varrho\varrho\sin(\psi+\phi)}k_\varrho dk_\varrho d\psi \quad . \quad (3.13)$$

These new integrals can be further simplified through application of the identity [MyintU],

$$J_n\left(k_\varrho\varrho\right)e^{jn\phi}=\frac{1}{2\pi}\int_{-\pi}^{\pi}e^{-jn\psi+jk_\varrho\varrho\sin(\psi+\phi)}d\psi \quad (3.14)$$

where $J_n\left(k_\varrho\varrho\right)$ is the Bessel function of order n. Using this identity, equations (3.10) and (3.13) can immediately be rewritten as follows.

$$G_{A_0x}^{(x)}\left(k_\varrho\right)=G_{A_0y}^{(y)}\left(k_\varrho\right)=\frac{1}{2\pi}\int_0^\infty\frac{N_{h_0}}{D_{TE}}J_0\left(k_\varrho\varrho\right)e^{-u_0z}k_\varrho dk_\varrho \quad (3.15)$$

$$G_{A_0z}^{(z)}\left(k_\varrho\right)=\frac{1}{2\pi}\int_0^\infty\frac{N_{v_0}}{D_{TM}}J_0\left(k_\varrho\varrho\right)e^{-u_0z}k_\varrho dk_\varrho \quad (3.16)$$

The remaining two equations ((3.11) and (3.12)) however, need special consideration due

to the trigonometric functions within their integrals. Therefore, writing equation (3.11) with respect to its ψ integration only, we obtain,

$$G_{A_0z}^{(x)}(\psi) = \frac{1}{2\pi}\int_{-\pi}^{\pi} \sin\psi e^{+jk_\varrho \varrho \sin(\psi+\phi)} d\psi = \frac{-j}{4\pi}\int_{-\pi}^{\pi} \left(e^{j\psi} - e^{-j\psi}\right) e^{+jk_\varrho \varrho \sin(\psi+\phi)} d\psi \qquad (3.17)$$

which, through application of equation (3.14) becomes,

$$G_{A_0z}^{(x)}(\psi) = -\frac{j}{2}\left(e^{-j\phi} J_{-1}\left(k_\varrho \varrho\right) - e^{+j\phi} J_1\left(k_\varrho \varrho\right)\right) \quad . \qquad (3.18)$$

Now, making use of another identity which states, $J_{-1}\left(k_\varrho \varrho\right) = -J_1\left(k_\varrho \varrho\right)$ [CRC], equation (3.18) can be rewritten as,

$$G_{A_0z}^{(x)}(\psi) = j\cos\phi J_1\left(k_\varrho \varrho\right) \qquad (3.19)$$

and consequently equation (3.11) simplifies to the following.

$$G_{A_0z}^{(x)}\left(k_\varrho\right) = -\cos\phi \frac{\left(\varepsilon_{rd}-1\right)}{2\pi}\int_0^{\infty} \frac{N_{h_0} J_1\left(k_\varrho \varrho\right)}{D_{TE} D_{TM}} e^{-u_{0z} k_\varrho^2} dk_\varrho \qquad (3.20)$$

Likewise, in a similar manner equation (3.12) becomes,

$$G_{A_0z}^{(y)}\left(k_\varrho\right) = -\sin\phi \frac{\left(\varepsilon_{rd}-1\right)}{2\pi}\int_0^{\infty} \frac{N_{h_0} J_1\left(k_\varrho \varrho\right)}{D_{TE} D_{TM}} e^{-u_{0z} k_\varrho^2} dk_\varrho \qquad (3.21)$$

to yield the last of the four double integrals in terms of a single integral only.

Now, examining the four Green function integrals which we are now required to solve, (equations (3.15), (3.16), (3.20) and (3.21)) we find that there are actually only three individual integrals which we need to solve for. These are shown in the next three equations along with their relations to the four Green function component integrals just mentioned.

$$a)\ I_1\left(k_\varrho\right) = \frac{1}{2\pi}\int_0^{\infty} \frac{N_{h_0} J_0\left(k_\varrho \varrho\right)}{D_{TE}} e^{-u_{0z} k_\varrho} dk_\varrho \qquad b)\ G_{A_0x}^{(x)}\left(k_\varrho\right) = G_{A_0y}^{(y)}\left(k_\varrho\right) = I_1\left(k_\varrho\right) \qquad (3.22)$$

$$a)\ I_2\left(k_\varrho\right)=\frac{1}{2\pi}\int_0^\infty \frac{N_{v_0}J_0\left(k_\varrho\varrho\right)}{D_{TM}}e^{-u_{0z}z}k_\varrho dk_\varrho \qquad b)\ G_{A_{0z}}^{(z)}\left(k_\varrho\right)=I_2\left(k_\varrho\right) \tag{3.23}$$

$$a)\ I_3\left(k_\varrho\right)=\frac{1}{2\pi}\int_0^\infty \frac{N_{h_0}J_1\left(k_\varrho\varrho\right)}{D_{TE}D_{TM}}e^{-u_{0z}z}k_\varrho^2 dk_\varrho \qquad b)\ G_{A_{0z}}^{(x)}\left(k_\varrho\right)=\begin{cases}\cot\phi G_{A_{0z}}^{(y)}= \\ -\cos\phi\left(\varepsilon_{rd}-1\right)I_3\left(k_\varrho\right)\end{cases} \tag{3.24}$$

To go about solving these integrals it would seem prudent to find a solution strategy through contour integration in the complex k_ϱ plane. This is because, as was mentioned previously, the denominator functions (D_{TE} and D_{TM}) and numerator functions (N_{v_0} and N_{h_0}) yield poles of the integrand and so the infamous Cauchy residue theorem springs to mind again. To proceed in this direction we must first convert the three previous integrals so that they are integrated from $-\infty \rightarrow \infty$. This is accomplished by writing the Bessel functions in terms of Hankel functions, as is shown below [CRC], and following through with the elimination of one or the other of these functions.

$$J_n\left(k_\varrho\varrho\right)=\frac{1}{2}\left[H_n^{(1)}\left(k_\varrho\varrho\right)+H_n^{(2)}\left(k_\varrho\varrho\right)\right] \tag{3.25}$$

Therefore, let us begin this procedure with equation (3.22a) from which the others will follow in a similar manner. Splitting this equation into two parts (each of which contains one of the two Hankel functions) yields,

$$I_1\left(k_\varrho\right)=I_1^{(1)}\left(k_\varrho\right)+I_1^{(2)}\left(k_\varrho\right) \tag{3.26}$$

where,

$$a)\quad I_1^{(1)}\left(k_\varrho\right)=\frac{1}{4\pi}\int_0^\infty \frac{N_{h_0}H_0^{(1)}\left(k_\varrho\varrho\right)}{D_{TE}}e^{-u_{0z}z}k_\varrho dk_\varrho \tag{3.27}$$

$$b)\quad I_1^{(2)}\left(k_\varrho\right)=\frac{1}{4\pi}\int_0^\infty \frac{N_{h_0}H_0^{(2)}\left(k_\varrho\varrho\right)}{D_{TE}}e^{-u_{0z}z}k_\varrho dk_\varrho \quad .$$

Now, making use of another ingenious identity (equation (3.28)), which is a relation between the two Hankel functions [Abramowitz],

$$H_n^{(1)}\left(k_\varrho\varrho e^{j\pi}\right)=-e^{-jn\pi}H_n^{(2)}\left(k_\varrho\varrho\right) \tag{3.28}$$

allows us to interchange the functions in equations (3.27). This allows us to only use one of the Hankel functions were we find that the proper Hankel function to use is that of the second kind, $H_n^{(2)}\left(k_\varrho \varrho\right)$, since it will ensure that the solution we obtain satisfies the radiation condition, a fact which will be proven before the end of this chapter. It therefore behooves us to rewrite equation (3.27a) in terms of $H_n^{(2)}\left(k_\varrho \varrho\right)$, which can be accomplished by applying the following change of variable.

$$k_\varrho = e^{j\pi} k_\varrho' = -k_\varrho' \quad , \quad k_\varrho dk_\varrho = e^{j2\pi} k_\varrho' dk_\varrho' = k_\varrho' dk_\varrho' \tag{3.29}$$

The limits of integration now become negative along with the argument of the Hankel function but since the definitions of the D_{TE} denominator function and the N_{h_0} numerator function only contain k_ϱ^2 the previous change of variable has no effect on them. Hence equation (3.27a) can be written in terms of the new variable of integration k_ϱ' as,

$$I_1^{(1)}\left(k_\varrho'\right) = \frac{1}{4\pi} \int_{-\infty}^{0} \frac{N_{h_0} H_0^{(2)}\left(k_\varrho' \varrho\right)}{D_{TE}} e^{-u_0 z} k_\varrho' dk_\varrho' \tag{3.30}$$

and when it is again combined with its counterpart through equation (3.26) the desired integral finally becomes,

$$I_1\left(k_\varrho\right) = \frac{1}{4\pi} \int_{-\infty}^{\infty} \frac{N_{h_0} H_0^{(2)}\left(k_\varrho \varrho\right)}{D_{TE}} e^{-u_0 z} k_\varrho dk_\varrho \quad . \tag{3.31}$$

Similarly then, integrals (3.23a) and (3.24a) become,

$$I_2\left(k_\varrho\right) = \frac{1}{4\pi} \int_{-\infty}^{\infty} \frac{N_{v_0} H_0^{(2)}\left(k_\varrho \varrho\right)}{D_{TM}} e^{-u_0 z} k_\varrho dk_\varrho \tag{3.32}$$

and

$$I_3\left(k_\varrho\right) = \frac{1}{4\pi} \int_{-\infty}^{\infty} \frac{N_{h_0} H_1^{(2)}\left(k_\varrho \varrho\right)}{D_{TE} D_{TM}} e^{-u_0 z} k_\varrho^2 dk_\varrho \tag{3.33}$$

respectively.

3.1.2 The Relevant Poles of the Inverse Fourier Transform Integrands

Before moving on into the complex plane let us examine equations (3.31) to (3.33) a little more carefully. As was discussed in the previous chapter the two denominator functions, D_{TE} and D_{TM}, as well as the two numerator functions, N_{v_0} and N_{h_0}, contain singularities which must somehow be overcome in these integrations. To do this however, we must have some idea as to where and why these singularities occur. Beginning therefore, with the numerator functions which are reiterated below,

$$a)\quad N_{v_0} = \frac{\cosh\left(u_d(z'+d)\right)}{\cosh(u_d d)} \qquad b)\quad N_{h_0} = \frac{\sinh\left(u_d(z'+d)\right)}{\sinh(u_d d)} \tag{3.34}$$

we find that singularities of N_{v_0} occur when $\cosh(u_d d)$ becomes zero unless the zeros of $\cosh\left(u_d(z'+d)\right)$, which are of the same order, coincide to cancel them. This cancellation of singularities is contained between two special cases of N_{v_0}, which are shown below and are dependent on the position of the source within the dielectric,

$$N_{v_0} = \begin{cases} 1, & z' = 0 \\ \dfrac{1}{\cosh(u_d d)}, & z' = -d \end{cases} \tag{3.35}$$

where in the first of the two cases, N_{v_0} has no poles at all and in the second case it has many. Let us now find an equation defining the locations of all the poles of N_{v_0}. To do so we allow u_d to be complex, as $u_d = \alpha + j\beta$, and substitute this into $\cosh(u_d d) = 0$ to obtain,

$$\cosh(u_d d) = \cosh\left[(\alpha + j\beta)d\right] = 0 \tag{3.36}$$

which can be rewritten using a complex hyperbolic–trigonometric identity [CRC], as,

$$\cosh\left[(\alpha + j\beta)d\right] = \cosh(\alpha d)\cos(\beta d) + j\sinh(\alpha d)\sin(\beta d) = 0 \quad . \tag{3.37}$$

Collecting the real and imaginary parts of this equation we obtain two equations which define the desired possible poles, where $n_p = 0, 1, 2, \ldots$ and we note that negative values

of n_p have not been included, in order to eliminate redundancy. These are,

$$a)\quad \cosh(\alpha d)\cos(\beta d)\quad \begin{cases} = 0, & \beta_{n_p} = (2n_p+1)\dfrac{\pi}{2d} \\ \neq 0, & otherwise \end{cases} \tag{3.38}$$

$$b)\quad \sinh(\alpha d)\sin(\beta d)\quad \begin{cases} = 0, & \alpha = 0 \ \ or \ \ \beta_{n_p} = \dfrac{n_p\pi}{d} \\ \neq 0, & otherwise \end{cases} . \tag{3.39}$$

For both of these equations to be zero simultaneously we must obviously choose $\alpha = 0$ and $\beta_{n_p} = (2n_p+1)\dfrac{\pi}{2d}$. Thus $u_d = j\beta_{n_p} = j(2n_p+1)\dfrac{\pi}{2d}$ at the possible poles of N_{v_0}. Equating this result to the actual definition of u_d as follows,

$$u_d = \sqrt{k_{\varrho n_p}^2 - \varepsilon_{rd}k_0^2} = j(2n_p+1)\frac{\pi}{2d} \tag{3.40}$$

we can obtain the values of k_ϱ at which the poles of N_{v_0} occur ($k_{\varrho n_p}$), namely,

$$k_{\varrho n_p} = \pm\sqrt{\varepsilon_{rd}k_0^2 - \left[(2n_p+1)\frac{\pi}{2d}\right]^2} . \tag{3.41}$$

Now, the zeros of N_{v_0} are defined by a similar equation which is obtained simply by substituting $z'+d$ for d in equation (3.41) yielding,

$$k_{\varrho n_z} = \pm\sqrt{\varepsilon_{rd}k_0^2 - \left[(2n_z+1)\frac{\pi}{2(z'+d)}\right]^2} . \tag{3.42}$$

The cancellation of singularities, which was mentioned previously, occurs when the values of $k_{\varrho n_p}$ and $k_{\varrho n_z}$ are identical. The criterion for this occurrence can easily be deduced from the above two equations and is simply,

$$\frac{z'+d}{d} = \pm\frac{2n_z+1}{2n_p+1} = \frac{2n_z+1}{2n_p+1} \quad , \quad n_z \le n_p \tag{3.43}$$

where the positive sign has been chosen since the ratio of $z'+d$ to d must be positive and both n_z and n_p have been chosen to be positive. Furthermore, we also know that n_z must

be smaller than or equal to n_p since $-d \leq z' \leq 0$ and therefore $0 \leq z'+d \leq d$. Let us now give an example to clarify this singularity cancellation relation. If we let $n_z = 0$ and $n_p = 1$ the above result yields $z'+d = d/3$ or $z' = -2d/3$ for which we obtain,

$$k_{\varrho n_p} = k_{\varrho n_z} = \pm \sqrt{\varepsilon_{rd} k_0^2 - \left(\frac{3\pi}{2d}\right)^2} \tag{3.44}$$

where it should be obvious that this is the first non–trivial singularity cancellation encountered, (i.e. the cancellation occurring at the largest value of k_ϱ (when k_ϱ is real) other than the one which occurs at $z' = 0$ where no poles occur anyway according to equation (3.35)). Furthermore, this value of k_ϱ corresponds to the second occurring pole, (which can be seen from equation (3.41)), so if the source resides at a depth of $z' = -2d/3$ within the substrate the second singularity will be cancelled.

Now, for $\varepsilon_{rd} k_0^2$ real, we can see that all possible poles will occur either on the real k_ϱ axis in the range $-\sqrt{\varepsilon_{rd}}\,k_0 \leq k_\varrho \leq \sqrt{\varepsilon_{rd}}\,k_0$ or somewhere on the imaginary k_ϱ axis. At this time however, it is the ones which occur on the real k_ϱ axis which are of particular concern to us since they lie directly on the integration path for equations (3.31) to (3.33). Consequently, from equation (3.41) we can see that $k_{\varrho n_p}$ will be real if,

$$\sqrt{\varepsilon_{rd}}\,k_0 \geq \left(2n_p + 1\right)\frac{\pi}{2d} \tag{3.45}$$

and that increasing ε_{rd}, k_0 or d will allow more values of n_p to satisfy this relation, hence allowing more poles to occur on the real k_ϱ axis. Of interest then, is a ratio of thickness to wavelength below which no poles can occur on the real axis. This ratio can be found from the previous equation by letting $n_p = 0$ and $k_0 = 2\pi/\lambda$, (where λ is the wavelength of the frequency corresponding to k_0), and then solving for d/λ as below,

$$\frac{d}{\lambda} = \frac{1}{4\sqrt{\varepsilon_{rd}}} \quad . \tag{3.46}$$

From this we can see that if d becomes too large or λ too small, poles of N_{v_0} could reside on the real k_ϱ axis unless singularity cancellation happens to occur. This is obviously a useful relation to know for any future numerical analysis of our Green functions.

Proceeding to the other numerator function, N_{h_0}, we find that it has very similar properties to N_{v_0} and so we will just give corresponding conclusions to the ones made previously. For this numerator function, two special cases dependent on the position of the source within the dielectric are again evident and occur for the same values of z' as before. These are shown below.

$$N_{h_0} = \begin{cases} 1, & z' = 0 \\ 0, & z' = -d \end{cases} \tag{3.47}$$

In this case however, no poles occur for either of the two extremes of N_{h_0} but as before poles do occur for other possible values of z'. This time we find $u_d = j\frac{n_p\pi}{d}$ at the poles of N_{h_0}, where $n_p = 0, 1, 2, \ldots$ as previously, and the equation defining $k_{\varrho n_p}$ is,

$$k_{\varrho n_p} = \pm \sqrt{\varepsilon_{rd}k_0^2 - \left(\frac{n_p\pi}{d}\right)^2} \tag{3.48}$$

while the equation defining $k_{\varrho n_z}$ is,

$$k_{\varrho n_z} = \pm \sqrt{\varepsilon_{rd}k_0^2 - \left(\frac{n_z\pi}{(z'+d)}\right)^2} \tag{3.49}$$

and the criterion for singularity cancellation is,

$$\frac{z'+d}{d} = \frac{n_z}{n_p} \quad , \quad n_z \leq n_p \quad . \tag{3.50}$$

One major difference between the results for N_{h_0} and N_{v_0} is that for N_{h_0} we get an added cancellation which occurs for all values of z' when $n_p = n_z = 0$ due to the fact that in this case u_d becomes zero and hence both the numerator and the denominator of N_{h_0} become zero simultaneously. Because of this we can ignore $n_p = n_z = 0$ in equations (3.48) and

(3.49) and consider them valid for $n_p = n_z = 1, 2, \ldots$. With this in mind we can again find a ratio of thickness to wavelength below which no poles can occur on the real k_ϱ axis as,

$$\frac{d}{\lambda} = \frac{1}{2\sqrt{\varepsilon_{rd}}} \tag{3.51}$$

whose value is obviously twice that of the same ratio for N_{v_0}. This tells us that if the thickness of the substrate or the wavelength for a given frequency is such that, N_{v_0} has no poles on the real axis, N_{h_0} will also have no poles on the real axis.

Finally, one remaining question should come to mind regarding the numerator functions. This pertains to the values that these functions take on when singularity cancellation occurs. These can be found very simply by taking the limit of N_{v_0} and N_{h_0} as k_ϱ approaches a $k_{\varrho n_p}$ at which such cancellation occurs. Making use of l'Hopitals rule [Trim1], we find that for both numerator functions this value is simply,

$$(-1)^{n_z - n_p} \frac{z' + d}{d} \quad . \tag{3.52}$$

Now that we have examined both numerator functions to our satisfaction let us move on to the denominator functions, D_{TE} and D_{TM}. Rehashing the definitions of these functions as,

$$a)\ D_{TE} = u_0 + u_d \coth(u_d d) \quad b)\ D_{TM} = \varepsilon_{rd} u_0 + u_d \tanh(u_d d) \tag{3.53}$$

$$c)\ u_0 = \sqrt{k_\varrho^2 - k_0^2} \qquad d)\ u_d = \sqrt{k_\varrho^2 - \varepsilon_{rd} k_0^2}$$

we can see that, for all quantities real, u_0 must be imaginary for $-k_0 < k_\varrho < k_0$ and real for the rest of the range of k_ϱ with its only zeros being at $\pm k_0$. Similarly then, u_d is imaginary for $-\sqrt{\varepsilon_{rd}} k_0 < k_\varrho < \sqrt{\varepsilon_{rd}} k_0$ and real for the rest of the range of k_ϱ with its only zeros being at $\pm \sqrt{\varepsilon_{rd}} k_0$. From this we can immediately see that since both u_0 and u_d are real, positive and monotonically increasing in the range $|k_\varrho| \geq \sqrt{\varepsilon_{rd}} k_0$ and the hyperbolic tangents are

therefore also real, positive and both approach a value of one as their arguments approach infinity, neither D_{TE} nor D_{TM} can be zero in this range. Now, in the range $-\sqrt{\varepsilon_{rd}}k_0 < k_\varrho < \sqrt{\varepsilon_{rd}}k_0$, u_d becomes,

$$u_d = \pm\, j\sqrt{\varepsilon_{rd}k_0^2 - k_\varrho^2} = \pm\, ju'_d \tag{3.54}$$

and so the hyperbolic terms in D_{TE} and D_{TM} become,

$$a)\quad u_d \coth(u_d d) = u'_d \cot(u'_d d) \qquad b)\quad u_d \tanh(u_d d) = -u'_d \tan(u'_d d) \tag{3.55}$$

which are both real. What this means then is that within the range $-k_0 \le k_\varrho \le k_0$ neither D_{TE} nor D_{TM} can possibly be zero since u_0 is imaginary and therefore no cancellation can occur. Examining the remaining range of the real k_ϱ axis between $\pm\, k_0$ and $\pm\, \sqrt{\varepsilon_{rd}}k_0$ we can see that both D_{TE} and D_{TM} are real functions and although u_0 is monotonically increasing the trigonometric terms can have both roots and poles of varying sign within this range. We can therefore conclusively state that all poles occurring along the real k_ϱ axis given a real wave–number and relative permittivity must occur within the ranges $k_0 < |k_\varrho| < \sqrt{\varepsilon_{rd}}k_0$. The question then is where are they, how many will there be and is there a ratio of substrate thickness to wavelength below which no poles can occur.

Considering where these poles occur, we can see that since both $D_{TE} = 0$ and $D_{TM} = 0$ are transcendental equations no direct formula for $k_{\varrho p}$ can be found. Their positions can be found graphically or numerically however, for given values of frequency, substrate thickness and dielectric constant. Now, although we can not find their exact positions with an equation as we did with the numerator poles, it is possible to find out how many poles can occur by noting that both the tangent and cotangent functions have values ranging from $-\infty$ to ∞ for every multiple of π that their arguments subtend. This means that for both D_{TE} and D_{TM} we will have at most $n_r + 1$ poles for n_r full multiples of π

occurring in between $\pm k_0$ and $\pm \sqrt{\varepsilon_{rd}} k_0$. Let us then, calculate the value of n_r for arbitrary values of ε_{rd}, k_0 or d. To do so we note that since $k_0 \sqrt{\varepsilon_{rd} - 1} \leq u'_d \leq 0$ as k_ϱ ranges between $\pm k_0$ and $\pm \sqrt{\varepsilon_{rd}} k_0$, the maximum range of the trigonometric function arguments is $k_0 d \sqrt{\varepsilon_{rd} - 1}$. Setting this equal to $n_r \pi$, letting $k_0 = \frac{2\pi}{\lambda}$, and solving for n_r we obtain,

$$n_r = \frac{2d}{\lambda} \sqrt{\varepsilon_{rd} - 1} \tag{3.56}$$

where, since n_r must be an integer, the value is rounded down. Finally, setting $n_r = 1$ we can solve for the ratio of substrate thickness to wavelength below which only one pole can occur in the range of both D_{TE} and D_{TM} yielding,

$$\frac{d}{\lambda} = \frac{1}{2\sqrt{\varepsilon_{rd} - 1}} \quad . \tag{3.57}$$

This has considerable similarity with the ratios calculated for the numerator functions, (equations (3.46) and (3.51)). Such a ratio however, below which *no* poles can occur, can only be found for the function D_{TE} since this function can become zero only if the cotangent function is negative which occurs for arguments greater than $\pi/2$. Therefore setting $k_0 d \sqrt{\varepsilon_{rd} - 1}$ equal to $\pi/2$ it can be found that D_{TE} can have no poles below,

$$\frac{d}{\lambda} = \frac{1}{4\sqrt{\varepsilon_{rd} - 1}} \quad . \tag{3.58}$$

For D_{TM} though, a value such as this can only be found by finding the location of the first pole which will occur for some argument of the tangent function less than $\pi/2$. The locations of the preceding denominator poles was discussed briefly by Marin et al [Marin2].

3.1.3 The Inverse Fourier Transform Integrals in the Complex k_ϱ Plane

Now that we know a bit about the poles of the numerator and denominator functions we can move into the complex k_ϱ plane with more confidence. It is appropriate however, to first

make a few remarks on convergence and propagation, remembering that the radiation condition requires a decaying and outward propagating wave at infinity [Tai]. Looking at the exponential $e^{-u_0 z}$ within the integrations which we wish to perform (equations (3.31) to (3.33)), and remembering from section 2.1 that we are using an $e^{+j\omega t}$ time dependance we know that each wave in space and time for any individual frequency will be characterized by the following phase relation, where we have let $u_0 = \alpha + j\beta$.

$$e^{-u_0 z} e^{+j\omega t} = e^{-(\alpha+j\beta)z} e^{+j\omega t} = e^{-\alpha z} e^{-j(\beta z - \omega t)} \tag{3.59}$$

From this it is immediately evident that the first exponential relation, $e^{-\alpha z}$, describes a wave that decays with increasing positive z, only if $\alpha > 0$ and that the second exponential, $e^{-j(\beta z - \omega t)}$, describes a wave propagating outward from the origin along positive z, if $\beta > 0$. These then, are the conditions which must then be met in defining our integration path in the complex k_ρ plane. To meet the above conditions, ($\mathrm{Re}\{u_0\} > 0$ and $\mathrm{Im}\{u_0\} > 0$), we require a closer look at u_0. Note first of all, that this is a square root function and therefore is double–valued for complex arguments [Trim1]. This can be seen by examining the function $w^{1/2}$, which is written below in terms of the magnitude and phase of w where $Arg(w)$ has been defined between $-\pi$ and π.

$$w^{\frac{1}{2}} = \sqrt{|w|}\, e^{\frac{j}{2}\arg w} = \sqrt{|w|}\, e^{\frac{j}{2}(Arg w + 2n\pi)} = \pm \sqrt{|w|}\, e^{\frac{j}{2} Arg w} \tag{3.60}$$

If $Arg(w)$ is restricted to this range we know from the phase of $w^{1/2}$ that whichever sign is chosen to represent $\sqrt{w}$, this choice will remain constant for any w whose phase is within this range. Restriction of the range of $Arg(w)$ in this way means however that we are not allowed to step on the negative, real w axis since this is where the sign of $\sqrt{w}$ must change. Therefore, to keep us off this axis we will draw a line called a branch cut along it. This branch cut emanates from a branch point at $w = 0$ and is simply the 'dividing' line between two w planes (commonly called Riemann sheets [Felsen1]) which yield opposite signs for

$\mathrm{Re}\left\{\sqrt{w}\right\}$. Now, in the case of u_0, if we choose the positive sign of the square root we can immediately see one of the two conditions specified earlier being satisfied. This is evident from equation (3.60) since the real part of the phase of $\sqrt{w}$, ($\cos\left(Arg(w)/2\right)$) will always be positive in the above specified argument range. In the k_ϱ plane we find however, two branch points of u_0, defined at $k_\varrho = \pm\ k_0$, and the branch cuts reside along the lines where $\mathrm{Re}\left\{k_\varrho^2 - k_0^2\right\} \leq 0$ and $\mathrm{Im}\left\{k_\varrho^2 - k_0^2\right\} = 0$. If k_0 is real, these lines are evident by direct inspection of $k_\varrho^2 - k_0^2$ since the above conditions will hold for k_ϱ real and less than $|k_0|$ as well as for k_ϱ imaginary. Now, to enforce the other required condition, $\mathrm{Im}\{u_0\} > 0$, we can let $k_\varrho = \gamma + j\delta$ and k_0 be real to write the argument of u_0 as,

$$k_\varrho^2 - k_0^2 = \left(\gamma^2 - \delta^2 - k_0^2\right) + 2j\gamma\delta \quad . \tag{3.61}$$

Then, since we know from the phase of equation (3.60) that $\mathrm{Im}\{u_0\} > 0$ when $\mathrm{Im}\left\{k_\varrho^2 - k_0^2\right\} > 0$, the real and imaginary parts of k_ϱ must be of the same sign thereby requiring k_ϱ to be in the first or third quadrants of the k_ϱ plane [Felsen1].

These above defined criteria will affect the integration contour in the k_ϱ plane and so the aforementioned branch cuts along with the path of integration which satisfies the radiation condition requirements are shown in Fig. 6 along with some poles due to D_{TE} and D_{TM}. Note that the branch points and poles are positioned off the real axis since in an actual situation k_0 will have some loss. The sign of

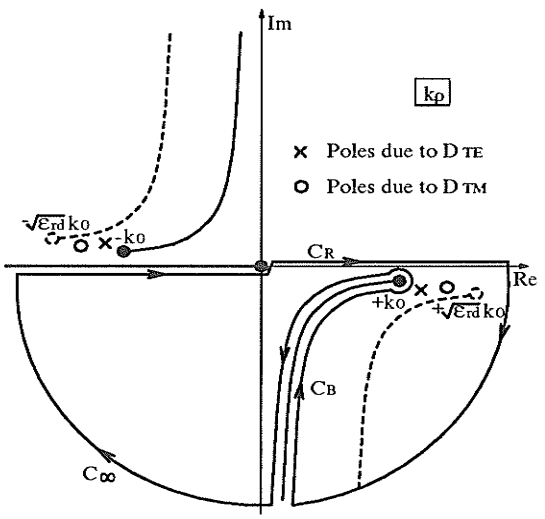

Figure 6: The Contour Integration in the k_ϱ Plane for the Inverse Fourier Transform

this loss determines the quadrant in which the poles or branch points occur and has been found by specifying a conductivity in the Maxwell equations and solving for k_0 in a similar way to that done in section 2.1. Note also that the path of integration has been drawn to explicitly show its course through the quadrants giving proper convergence and that the branch cut residing within the region, encircled by the contour, is never crossed since the contour is deformed around the branch. The fact that the path passes through the fourth quadrant where waves are inward propagating does not cause a discrepancy in our result since at infinity the waves are attenuated. Figure 6 also shows several other branch cuts, one of which runs along the negative k_ϱ axis and is due to the multi–valued logarithm function inherent in the Hankel function present in all three of the integrals. This branch will cause no problems for our integration since it is completely outside of the integration contour. There are also two other branch cuts (represented by dotted lines in this figure) emanating from the branch points $\pm \sqrt{\varepsilon_{rd}}k_0$. These come from the other square root function, u_d, contained in all of our integrands via the numerator and denominator functions. They are dotted since they essentially have no effect on our results due to the fact that a change of sign of u_d will always be offset by a corresponding sign change from the hyperbolic functions, making their effect single valued and therefore an integration around this branch would not contribute to the integral. Note that if the dielectric slab was not grounded, an integration around this branch would contribute, from which we see that the contribution would then have to be a downward propagating space wave.

We can now take equations (3.31) to (3.33) and evaluate them using contour integration along the path specified in Fig. 6. The result of this integration is, as we know, proportional to the sum of the residues at the poles contained within the contour and can be written as,

$$I_C\left(k_\varrho\right) = I_{C_R}\left(k_\varrho\right) + I_{C_B}\left(k_\varrho\right) + I_{C_\infty}\left(k_\varrho\right) = -2\pi j \sum_{i=1}^{N} Res\left[I_C\left(k_\varrho\right), k_{\varrho i}\right] \qquad (3.62)$$

where the integral which follows the real k_ϱ axis (I_{C_R}) is the desired result. Rewriting the

previous equation with this in mind we obtain,

$$I_{C_R}\left(k_\varrho\right) = -2\pi j \sum_{i=1}^{N} Res\left[I_C\left(k_\varrho\right), k_{\varrho i}\right] - I_{C_B}\left(k_\varrho\right) - I_{C_\infty}\left(k_\varrho\right) \tag{3.63}$$

where the integral along I_{C_∞} is zero due to the radiation condition which we enforced previously. It is useful to note from the form of this equation, that the integration around the branch cut yields an upward propagating space wave while the residues of the contained poles contribute to the surface waves supported by the structure. We are now left with two options as to how we can obtain the result which we desire (I_{C_R}). The first of these is just to integrate along C_R while the other requires integration along C_B as well as inclusion of the residues ([Marin1], [Barkeshli]). As it turns out the first option is usually the better choice since the exact positions of the poles are defined by transcendental equations and the integration around the branch is at least as difficult as the integration along the real axis. Because of this, the next two sections of this chapter will deal with the solution of integrals (3.31) to (3.33) along the contour C_R which must generally be solved numerically to obtain correct answers in the near field region. For a far field solution however, we can use an asymptotic approximation to these integrals to obtain reasonable results [Felsen1]. This approach is the one we will apply since it is the more interesting of the two in that it yields a closed form solution of the integrals which gives surprisingly accurate results. The method of asymptotic approximation which we will use here is known as the method of steepest descents through which the contour C_R will be deformed to yield a contour along which the imaginary part of the exponent within the integrand is constant and the real part varies to the greatest degree [Collin]. The advantage of this new path of integration is that the major contribution to the result will occur in a very small section of the deformed integration path allowing us to approximate the result analytically. It should be noted however, that full integration along this contour will yield results identical to the original contour as long as no poles are crossed in the contour deformation.

Before deforming the path of integration along C_R into the steepest descent path we

note first of all that, since we are using an asymptotic approximation to the required integrals we can immediately substitute the asymptotic form of the appropriate Hankel functions, (all of which are defined by the following equation),

$$\lim_{k_\varrho \varrho \to \infty} H_n^{(2)}\left(k_\varrho \varrho\right) = \sqrt{\frac{2}{\pi k_\varrho \varrho}} e^{-j\left(k_\varrho \varrho - n\frac{\pi}{2} - \frac{\pi}{4}\right)} = \sqrt{\frac{2j}{\pi k_\varrho \varrho}} e^{-jk_\varrho \varrho} j^n \tag{3.64}$$

into integrals (3.31) to (3.33) [Kong]. Writing these integrals as contour integrals we obtain,

$$I_1\left(k_\varrho\right) = \frac{1}{4\pi}\sqrt{\frac{2j}{\pi\varrho}} \int_{C_R} \frac{N_{h_0}}{D_{TE}} e^{-u_0 z - jk_\varrho \varrho} \sqrt{k_\varrho}\, dk_\varrho \tag{3.65}$$

$$I_2\left(k_\varrho\right) = \frac{1}{4\pi}\sqrt{\frac{2j}{\pi\varrho}} \int_{C_R} \frac{N_{v_0}}{D_{TM}} e^{-u_0 z - jk_\varrho \varrho} \sqrt{k_\varrho}\, dk_\varrho \tag{3.66}$$

and

$$I_3\left(k_\varrho\right) = \frac{j}{4\pi}\sqrt{\frac{2j}{\pi\varrho}} \int_{C_R} \frac{N_{h_0}}{D_{TE} D_{TM}} e^{-u_0 z - jk_\varrho \varrho} \sqrt{k_\varrho}\, k_\varrho dk_\varrho \tag{3.67}$$

from which we can explicitly see the source of the Hankel function branch cut of Fig. 6, (i.e. the square root of k_ϱ function contained in all three of the integrals).

3.1.4 Solution of the Inverse Fourier Transform Integrals in the Complex Ψ Plane

To solve the three contour integrals of equations (3.65) to (3.67) we first convert the spatial variables from the cylindrical coordinate system into the spherical coordinate system by applying the following transformations, $z = r\cos\theta, \varrho = r\sin\theta$ and simultaneously change the variable of integration using the transformation, $k_\varrho = k_0 \sin\Psi$. This change of variable modifies the following parameters as well as the numerator and denominator functions,

$$a)\quad dk_\varrho = k_0 \cos\Psi d\Psi \qquad b)\quad u_0 = k_0\sqrt{\sin^2\Psi - 1} = jk_0\cos\Psi \tag{3.68}$$

$$c)\quad u_d = k_0\sqrt{\sin^2\Psi - \varepsilon_{rd}} = jk_0\sqrt{\varepsilon_{rd} - \sin^2\Psi} = j\frac{\omega}{c}\sqrt{\varepsilon_{rd} - \sin^2\Psi}$$

and yields the next three integrals.

$$I_1(\Psi) = \frac{1}{4\pi}\sqrt{\frac{2j}{\pi r \sin\theta}}\int_{C_{R_\Psi}} \frac{N_{h_0}}{D_{TE}} e^{-jk_0 r\cos(\Psi-\theta)}\sqrt{k_0 \sin\Psi}\, k_0 \cos\Psi d\Psi \qquad (3.69)$$

$$I_2(\Psi) = \frac{1}{4\pi}\sqrt{\frac{2j}{\pi r \sin\theta}}\int_{C_{R_\Psi}} \frac{N_{v_0}}{D_{TM}} e^{-jk_0 r\cos(\Psi-\theta)}\sqrt{k_0 \sin\Psi}\, k_0 \cos\Psi d\Psi \qquad (3.70)$$

$$I_3(\Psi) = \frac{j}{4\pi}\sqrt{\frac{2j}{\pi r \sin\theta}}\int_{C_{R_\Psi}} \frac{N_{h_0}}{D_{TE}D_{TM}} e^{-jk_0 r\cos(\Psi-\theta)}\sqrt{k_0 \sin\Psi}\, k_0^2 \sin\Psi \cos\Psi d\Psi \qquad (3.71)$$

Note that, in these integrals the cos term in the exponential was arrived at by using a simple trigonometric identity [CRC]. These integrals also indicate that the choice of the Hankel function of the second kind was the proper one, since the exponential within these three integrals represents an outward propagating and decaying wave for an $e^{+j\omega t}$ time dependence.

Let us now examine the new Ψ plane in some detail. Notice first of all from equation (3.68b) that u_0 no longer contains a square root and therefore looks single valued. This does not mean, however, that we have lost any information, since what has actually happened is that the two Riemann sheets discussed earlier have been unfolded and now lie together in the Ψ plane [Felsen1]. This is evident when we graphically convert Fig. 6 into the Ψ plane as is shown in Fig. 7. The proper Riemann sheet, which has $\mathrm{Re}\{u_0\} > 0$, is shown as the shaded area and the quadrants corresponding to those in the k_ρ plane are labeled, P_1, P_2, P_3 and P_4. The improper sheet is correspondingly unshaded and the quadrants corresponding to those in the k_ρ plane are labeled I_1, I_2, I_3 and I_4. Note that the arrangement of the quadrants

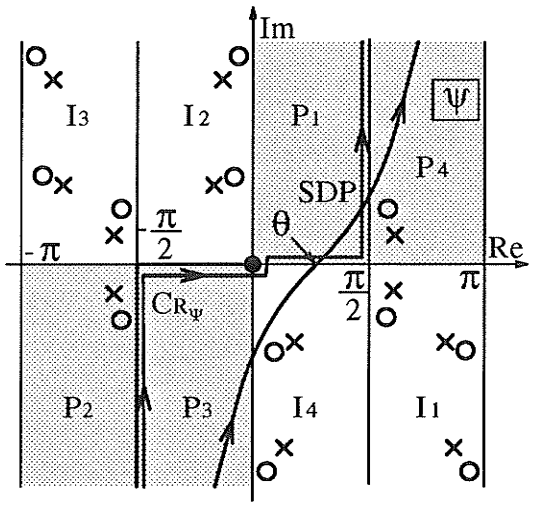

Figure 7: The Contour Integration in the Ψ Plane for the Inverse Fourier Transform

on both sheets is determined from the sign of the exponential decay and direction of propagation in those quadrants [Kong].

Now, with the change of variables which takes us into the Ψ plane we find that $k_\varrho = \pm\, k_0$ corresponds to $\Psi = \pm\, \pi/2$ and, if k_0 is real, the section of the real k_ϱ axis between $\pm\, k_0$ corresponds to the real Ψ axis between $\pm\, \pi/2$. Furthermore the remainder of the real k_ϱ axis maps onto the vertical lines passing through $\Psi = \pm\, \pi/2$ and the imaginary axis maps onto the vertical line passing through $\Psi = 0$. On the proper sheet then we can see the poles of D_{TE} and D_{TM}, which correspond to those in Fig. 6, residing in quadrants 2 and 4 and occurring between $\Psi = \pm\, \pi/2$ and $\Psi = \pm\, \pi/2 \pm j \sin^{-1}\left(\sqrt{\varepsilon_{rd}}\right)$ with the same added loss. At this time it is worthwhile to note that no other poles, besides those due to the numerator functions, occur on the proper sheet of the Riemann surface. This can be proven numerically as well as through mathematical manipulation of the denominator functions [Collin]. There are however an infinite number of poles occurring on the improper sheet which do not effect the normal integration along C_{R_Ψ} but may effect the saddle point integration. As for the numerator poles, it can be shown that they occur along the branch cuts and so would not effect the original integral but may contribute to an integration along the deformed path. It should be stated here, concerning these numerator poles, that only the locations of these poles have been studied in this thesis, and no explanation of their physical meaning or their exact effect have been found.

Now, as mentioned previously the steepest descent path resides along a contour along which the imaginary part of the exponent within the integrand is constant and the real part varies to the greatest degree. To see what this means we firstly observe the three integrals (3.69) to (3.71) and find that they all contain a complex exponential which we know is an oscillatory function and whose exponent can be represented as,

$$f(\Psi) = -jk_0 r \cos(\Psi - \theta) \quad . \tag{3.72}$$

Saddle points of this exponent occur where $\frac{\partial f(\Psi)}{\partial \Psi} = 0$ and are so called since complex functions such as the one in question have no maxima or minima as a whole but rather, the real and imaginary parts themselves have maxima and minima. When they occur simultaneously they form a saddle point (i.e. a graph of the function around a saddle point takes on the shape of a saddle). Therefore, calculating the previous derivative we obtain,

$$\frac{\partial f(\Psi)}{\partial \Psi} = jk_0 r \sin(\Psi - \theta) \tag{3.73}$$

from which we can immediately see one saddle point occurring when $\Psi = \theta$. The steepest descent path which passes through this point is then defined by the condition,

$$\mathrm{Im}\{f(\Psi) - f(\theta)\} = 0 \tag{3.74}$$

which simply enforces the imaginary part of the complex exponent to be equal to its value at the saddle point. From this we can obtain an equation defining the steepest descent path by letting $\Psi = \alpha + j\beta$ in the above condition and writing,

$$\mathrm{Im}\{-jk_0 r\cos(\alpha - \theta + j\beta) + jk_0 r\} = k_0 r[1 - \cos(\alpha - \theta)\cosh(\beta)] = 0 \tag{3.75}$$

or,

$$\cos(\alpha - \theta)\cosh(\beta) = 1 \quad . \tag{3.76}$$

Along this path then, $f(\Psi)$ becomes,

$$\begin{aligned} f_{sdp}(\Psi) &= -jk_0 r\cos(\Psi - \theta)\big|_{sdp} = -jk_0 r\cos(\alpha - \theta + j\beta)\big|_{sdp} \\ &= -jk_0 r[\cos(\alpha - \theta)\cosh(\beta) - j\sin(\alpha - \theta)\sinh(\beta)]_{sdp} \\ &= -jk_0 r - k_0 r\sin(\alpha - \theta)\sinh(\beta) \end{aligned} \tag{3.77}$$

which we can see causes the exponential to decay rapidly with r as well as with $\sinh(\beta)$. Because of this we can state that the major contribution to the integral comes from the immediate vicinity of the saddle point. This statement is not altogether true if any poles lie near the saddle point or steepest descent path or more importantly are crossed when deforming the original path of integration to the steepest descent path. In this case the

solution is much more difficult since the contribution from each of these poles must be taken into account individually. For this reason we will assume for the moment that all poles are far from the steepest descent path and that none are crossed in the deformation of the path. The error caused by this assumption will be assessed later in the numerical results of Chapter 4, using the positions of the poles which we took such pains to find in section 3.1.2 as accuracy indicators. Having made this clarification and assumption we can proceed by representing all three of integrals (3.69) to (3.71) as follows,

$$I_n(\Psi) = A_n \int_{C_{sdp}} F_n(\Psi) e^{f_{sdp}(\Psi)} d\Psi \tag{3.78}$$

and expand $F_n(\Psi)$ in a Taylor series about the saddle point. Doing so yields,

$$F_n(\Psi) = \sum_{m=0}^{\infty} \frac{(\Psi-\theta)^m}{m!} F_n^{(m)}(\theta) \tag{3.79}$$

which upon substitution into equation (3.78) and interchange of the order of integration and summation leaves,

$$I_n(\Psi) = A_n \sum_{m=0}^{\infty} \left\{ \frac{F_n^{(m)}(\theta)}{m!} \int_{C_{sdp}} (\Psi-\theta)^m e^{f_{sdp}(\Psi)} d\Psi \right\} . \tag{3.80}$$

Of course, the exponent $f_{sdp}(\Psi)$ can also be expanded in the same way but since $f_{sdp}'(\Psi)$ (and for that matter all the odd order derivatives) are equal to zero at the saddle point this becomes,

$$f_{sdp}(\Psi) = f(\theta) + f^{(2)}(\theta)\frac{(\Psi-\theta)^2}{2} + f^{(4)}(\theta)\frac{(\Psi-\theta)^4}{24} \ldots \tag{3.81}$$

Taking only the first two terms of this expansion and substituting them into equation (3.80) we obtain,

$$I_n(\Psi) = A_n e^{f(\theta)} \sum_{m=0}^{\infty} \left\{ \frac{F_n^{(m)}(\theta)}{m!} \int_{C_{sdp}} (\Psi-\theta)^m e^{f^{(2)}(\theta)(\Psi-\theta)^2/2} d\Psi \right\} \tag{3.82}$$

which, upon substitution of the transformation $f^{(2)}(\theta)(\Psi-\theta)^2 = -t^2$ becomes,

$$I_n(\Psi) = A_n e^{f(\theta)} \sum_{m=0}^{\infty} \left\{ \frac{F_n^{(m)}(\theta)}{m!} \left[-f^{(2)}(\theta)\right]^{-\frac{(m+1)}{2}} \int_{-\infty}^{\infty} t^m e^{-\frac{t^2}{2}} dt \right\} . \tag{3.83}$$

This equation can easily be solved using Gamma functions [Collin], and so we are now trivially able to solve integrals of the type described by equation (3.78). Assuming furthermore that the first term of equation (3.83) is dominant we can write solutions to equations of the form given in equation (3.78) in a trivial manner as [Kong],

$$I_n(\Psi) = A_n \int_{C_{sdp}} F_n(\Psi) e^{f_{sdp}(\Psi)} d\Psi = A_n \sqrt{\frac{2\pi}{-f''(\theta)}} F_n(\theta) e^{f(\theta)} \tag{3.84}$$

where for our purposes $f(\theta) = -jk_0 r$ and $f''(\theta) = jk_0 r$. The solutions of the three integrals which we desired to solve with the method of steepest descents can now be simply written by inspection of equations (3.69) to (3.71) and equation (3.84). In so doing we obtain,

$$I_1(\Psi) = j\frac{e^{-jk_0 r}}{2\pi r}\frac{N_{h_0}}{D_{TE}} k_0 \cos\theta \tag{3.85}$$

$$I_2(\Psi) = j\frac{e^{-jk_0 r}}{2\pi r}\frac{N_{v_0}}{D_{TM}} k_0 \cos\theta \tag{3.86}$$

$$I_3(\Psi) = -\frac{e^{-jk_0 r}}{2\pi r}\frac{N_{h_0}}{D_{TE} D_{TM}} k_0^2 \cos\theta \sin\theta \tag{3.87}$$

which when applied to the equations defining the Green functions (equations (3.22b), (3.23b) and (3.24b)) yields,

$$G_{A_0x}^{(x)}(\Psi) = G_{A_0y}^{(y)}(\Psi) = I_1(\theta) = j\frac{e^{-jk_0 r}}{2\pi r}\frac{N_{h_0}}{D_{TE}} k_0 \cos\theta \tag{3.88}$$

$$G_{A_0z}^{(z)}(\Psi) = I_2(\theta) = j\frac{e^{-jk_0 r}}{2\pi r}\frac{N_{v_0}}{D_{TM}} k_0 \cos\theta \tag{3.89}$$

$$G_{A_0z}^{(x)}(\Psi) = -\cos\phi(\varepsilon_{rd} - 1) I_3(\theta) = \frac{e^{-jk_0 r}}{2\pi r}\frac{(\varepsilon_{rd} - 1) N_{h_0}}{D_{TE} D_{TM}} k_0^2 \cos\theta \sin\theta \cos\phi \tag{3.90}$$

$$G_{A_0z}^{(y)}(\Psi) = -\sin\phi(\varepsilon_{rd} - 1) I_3(\theta) = \frac{e^{-jk_0 r}}{2\pi r}\frac{(\varepsilon_{rd} - 1) N_{h_0}}{D_{TE} D_{TM}} k_0^2 \cos\theta \sin\theta \sin\phi \quad . \tag{3.91}$$

3.1.5 The Closed–Form Results of the Electric Field Dyadic Green Function

Given the above results for the magnetic vector potential dyadic Green function in the spatial–frequency domain we can use equation (2.23) with $\overline{\mathbf{G}}_F = 0$, (which is repeated

below in spherical coordinates) to obtain the electric field dyadic Green function in the spatial–frequency domain.

$$\overline{\mathbf{G}}_E(r,\theta,\phi) = \frac{1}{j\omega\varepsilon}\left(\nabla\nabla\cdot + k^2\right)\overline{\mathbf{G}}_A(r,\theta,\phi) \tag{3.92}$$

Before applying this equation however, we must first convert equations (3.88) to (3.91) into spherical coordinates and thereby obtain, for an x–directed dipole source,

$$\begin{aligned} G^{(x)}_{A_0 r} &= G^{(x)}_{A_0 x}\sin\theta\cos\phi + G^{(x)}_{A_0 y}\sin\theta\sin\phi + G^{(x)}_{A_0 z}\cos\theta \\ &= \frac{e^{-jk_0 r}}{2\pi r}N_{h_0}\left(\frac{jk_0\cos\theta}{D_{TE}} + \frac{k_0^2(\varepsilon_{rd}-1)}{D_{TE}D_{TM}}\cos^2\theta\right)\sin\theta\cos\phi \end{aligned} \tag{3.93}$$

$$\begin{aligned} G^{(x)}_{A_0\theta} &= G^{(x)}_{A_0 x}\cos\theta\cos\phi + G^{(x)}_{A_0 y}\cos\theta\sin\phi - G^{(x)}_{A_0 z}\sin\theta \\ &= \frac{e^{-jk_0 r}}{2\pi r}N_{h_0}\left(\frac{jk_0\cos\theta}{D_{TE}} - \frac{k_0^2(\varepsilon_{rd}-1)}{D_{TE}D_{TM}}\sin^2\theta\right)\cos\theta\cos\phi \end{aligned} \tag{3.94}$$

and

$$G^{(x)}_{A_0\phi} = -G^{(x)}_{A_0 x}\sin\phi + G^{(x)}_{A_0 y}\cos\phi = \frac{e^{-jk_0 r}}{2\pi r}N_{h_0}\left(\frac{-jk_0\cos\theta}{D_{TE}}\right)\sin\phi \quad . \tag{3.95}$$

Then, since the results for a y–directed dipole source are very similar we can simply write them in terms of the x–directed results by inspection of the magnetic vector potential Green functions and the relations for conversion to spherical coordinates given in the previous three equations, namely,

$$a)\quad G^{(y)}_{A_0 r} = \tan\phi\, G^{(x)}_{A_0 r} \qquad b)\quad G^{(y)}_{A_0\theta} = \tan\phi\, G^{(x)}_{A_0\theta} \qquad c)\quad G^{(y)}_{A_0\phi} = -\cot\phi\, G^{(x)}_{A_0\phi} \quad . \tag{3.96}$$

Finally, the z–directed results are found by again using the same conversion relations to spherical coordinates as above, giving,

$$a)\quad G^{(z)}_{A_0 r} = \frac{e^{-jk_0 r}}{2\pi r}N_{v_0}\left(\frac{jk_0\cos\theta}{D_{TM}}\right)\cos\theta \qquad b)\quad G^{(z)}_{A_0\theta} = -\tan\theta\, G^{(z)}_{A_0 r} \qquad c)\quad G^{(z)}_{A_0\phi} = 0 \; . \tag{3.97}$$

It is interesting to note that all of the preceding equations are proportional to one half of the free space radiation from an electric dipole source [Balanis], and so can be considered as the

free space solution multiplied by a geometry factor which takes into account the effect of the grounded dielectric substrate.

Now that the magnetic vector potential Green function has been completely converted into spherical coordinates we can proceed to solve equation (3.92). To do this it is first worthwhile to note that all the components of the preceding dyadic can be written as follows,

$$G_{A_0 v}^{(u)} = \frac{e^{-jk_0 r}}{r} f_v(\theta,\phi) \tag{3.98}$$

where $f(\theta,\phi)$ is some function of θ and ϕ and the superscript u refers to any of the three dipole directions while the subscript v refers to any of the three spherical components. Writing the above dyadic components in this way is important as far as we are concerned since we wish to deal with far field results only, (as was indicated by the use of the steepest descent method). As a result of this, any components which have terms varying with inverse powers of r greater than unity can be ignored. Let us now expand equation (3.92) in terms of equation (3.98) for one direction of source. Note that the particular source direction is irrelevant in this case and so no superscripts will be shown in the following expansion. Therefore, beginning with the divergence term we can write,

$$\nabla\cdot\mathbf{G}_{A_0} = \frac{f_r(\theta,\phi)}{r^2}\frac{\partial}{\partial r}\left(re^{-jk_0 r}\right) + \frac{e^{-jk_0 r}}{r^2\sin\theta}\left[\frac{\partial}{\partial\theta}\left(\sin\theta f_\theta(\theta,\phi)\right) + \frac{\partial}{\partial\phi}f_\phi(\theta,\phi)\right] \tag{3.99}$$

where the second term of the expanded divergence can be seen to vary with the inverse square of r. Neglecting this term from here on in and simply performing the derivative within the first term gives,

$$\nabla\cdot\mathbf{G}_{A_0} \approx \frac{f_r(\theta,\phi)}{r^2}\frac{\partial}{\partial r}\left(re^{-jk_0 r}\right) = f_r(\theta,\phi)\frac{e^{-jk_0 r}}{r^2}\left(1-jk_0 r\right) \approx -jk_0\frac{e^{-jk_0 r}}{r}f_r(\theta,\phi) \tag{3.100}$$

where one term resulting from the derivative has also been thrown away for the same reason as above. Now that we have the proper divergence let us proceed with the gradient. Applying

the gradient operator to the result of equation (3.100) we obtain,

$$\nabla\nabla\cdot\mathbf{G}_{A_0} = -jk_0\left\{f_r(\theta,\phi)\frac{\partial}{\partial r}\left(\frac{e^{-jk_0r}}{r}\right)\hat{r}\right. \tag{3.101}$$

$$\left. + \frac{e^{-jk_0r}}{r^2}\left[\frac{\partial}{\partial\theta}\left(f_r(\theta,\phi)\right)\hat{\theta} + \frac{1}{\sin\theta}\frac{\partial}{\partial\phi}\left(f_r(\theta,\phi)\right)\hat{\phi}\right]\right\} \tag{3.102}$$

where we can again neglect the second term for the same reasons as previously, giving,

$$\nabla\nabla\cdot\mathbf{G}_{A_0} \approx -jk_0 f_r(\theta,\phi)\frac{\partial}{\partial r}\left(\frac{e^{-jk_0r}}{r}\right)\hat{r}$$

$$= -jk_0 f_r(\theta,\phi)\frac{e^{-jk_0r}}{r^2}\left(-jk_0r-1\right)\hat{r} \approx -k_0^2\frac{e^{-jk_0r}}{r}f_r(\theta,\phi)\hat{r} \tag{3.103}$$

within which another term was again neglected due to expansion of the derivative. The dyadic produced by this operator is then obviously,

$$\nabla\nabla\cdot\overline{\mathbf{G}}_{A_0} = -k_0^2\frac{e^{-jk_0r}}{r}\begin{bmatrix} f_r^{(x)}(\theta,\phi) & f_r^{(y)}(\theta,\phi) & f_r^{(z)}(\theta,\phi) \\ 0 & 0 & 0 \\ 0 & 0 & 0 \end{bmatrix} \tag{3.104}$$

while the remaining dyadic within equation (3.92) is,

$$k_0^2\overline{\mathbf{G}}_{A_0} = k_0^2\frac{e^{-jk_0r}}{r}\begin{bmatrix} f_r^{(x)}(\theta,\phi) & f_r^{(y)}(\theta,\phi) & f_r^{(z)}(\theta,\phi) \\ f_\theta^{(x)}(\theta,\phi) & f_\theta^{(y)}(\theta,\phi) & f_\theta^{(z)}(\theta,\phi) \\ f_\phi^{(x)}(\theta,\phi) & f_\phi^{(y)}(\theta,\phi) & f_\phi^{(z)}(\theta,\phi) \end{bmatrix} \tag{3.105}$$

where relation (3.98) was again used. Finally then, combining the above two dyadics as in equation (3.92) we obtain the electric field dyadic Green function, as displayed below.

$$\overline{\mathbf{G}}_{E_0} = -j\omega\mu\frac{e^{-jk_0r}}{r}\begin{bmatrix} 0 & 0 & 0 \\ f_\theta^{(x)}(\theta,\phi) & f_\theta^{(y)}(\theta,\phi) & f_\theta^{(z)}(\theta,\phi) \\ f_\phi^{(x)}(\theta,\phi) & f_\phi^{(y)}(\theta,\phi) & f_\phi^{(z)}(\theta,\phi) \end{bmatrix} \tag{3.106}$$

From this result we can immediately see that there is no radial component of field in this result, which is expected due to its far field nature.

Now that we have the electric field dyadic Green function let us write out its individual components. To do this let us first expand the numerator and denominator functions using equations (3.68b) to (3.68c) and let $k_0 = \omega/c$, $h = 1 + (z'/d)$ and $u_d d = j\omega\tau_\theta$ where,

$$\tau_\theta = \sqrt{\varepsilon_{rd} - \sin^2\theta}\,(d/c) \tag{3.107}$$

and c is the wave velocity in the air region. Using these substitutions the numerator functions become,

$$a)\quad N_{h_0} = \frac{\sinh\left(u_d(z'+d)\right)}{\sinh(u_d d)} = \frac{\sin(\omega\tau_\theta h)}{\sin(\omega\tau_\theta)} \qquad b)\quad N_{v_0} = \frac{\cosh\left(u_d(z'+d)\right)}{\cosh(u_d d)} = \frac{\cos(\omega\tau_\theta h)}{\cos(\omega\tau_\theta)} \tag{3.108}$$

while the denominator functions become,

$$a)\quad D_{TE} = u_0 + u_d\coth(u_d d) = k_0\left(j\cos\theta + \tau_\theta\frac{c}{d}\cot(\omega\tau_\theta)\right) \tag{3.109}$$

$$b)\quad D_{TM} = \varepsilon_{rd}u_0 + u_d\tanh(u_d d) = k_0\left(j\varepsilon_{rd}\cos\theta - \tau_\theta\frac{c}{d}\tan(\omega\tau_\theta)\right)\ .$$

It is also useful to write out the multiplication of the denominator functions and rearrange them slightly for future use as follows.

$$\begin{aligned} D_{TE}D_{TM} &= k_0^2\left(j\cos\theta + \tau_\theta\frac{c}{d}\cot(\omega\tau_\theta)\right)\left(j\varepsilon_{rd}\cos\theta - \tau_\theta\frac{c}{d}\tan(\omega\tau_\theta)\right) \\ &= k_0^2\left(-\varepsilon_{rd}\cos^2\theta - j\cos\theta\tau_\theta\frac{c}{d}\left(\tan(\omega\tau_\theta) - \varepsilon_{rd}\cot(\omega\tau_\theta)\right) - \left(\tau_\theta\frac{c}{d}\right)^2\right) \\ &= k_0^2\left(j\tau_\theta\frac{c}{d} - \cos\theta\tan(\omega\tau_\theta)\right)\left(j\tau_\theta\frac{c}{d} + \varepsilon_{rd}\cos\theta\cot(\omega\tau_\theta)\right) \end{aligned} \tag{3.110}$$

Now, using equation (3.106) and a slightly modified version of equation (3.94) the Green function $G^{(x)}_{E_0\theta}$ can be written as,

$$G^{(x)}_{E_0\theta} = -j\omega\mu\frac{e^{-jk_0 r}}{2\pi r}\frac{\sin(\omega\tau_\theta h)}{\sin(\omega\tau_\theta)}\left(\frac{jk_0\cos\theta D_{TM} - k_0^2(\varepsilon_{rd}-1)\sin^2\theta}{D_{TE}D_{TM}}\right)\cos\theta\cos\phi \tag{3.111}$$

where if we expand the numerator within the brackets of this equation using equation

(3.109b) and rearrange slightly we obtain,

$$G_{E_0\theta}^{(x)} = -j\omega\mu \frac{e^{-jk_0 r}}{2\pi r} \frac{\sin(\omega\tau_\theta h)}{\sin(\omega\tau_\theta)} \left[\frac{jk_0^2 \tau_\theta \frac{c}{d}\left(j\tau_\theta \frac{c}{d} - \cos\theta \tan(\omega\tau_\theta)\right)}{D_{TE} D_{TM}} \right] \cos\theta \cos\phi \quad . \quad (3.112)$$

Within this equation then, we can immediately see that most of the new numerator within the brackets of the above equation can be cancelled by the modified form of $D_{TE}D_{TM}$ given in equation (3.110). Therefore, our final result for this component is,

$$G_{E_0\theta}^{(x)} = -j\omega\mu \frac{e^{-jk_0 r}}{2\pi r} \tau_\theta \frac{c}{d} \left[\frac{\sin(\omega\tau_\theta h)}{\tau_\theta \frac{c}{d} \sin(\omega\tau_\theta) - j\varepsilon_{rd} \cos\theta \cos(\omega\tau_\theta)} \right] \cos\theta \cos\phi \quad (3.113)$$

and the corresponding result for a y–directed source is simply found by applying this component to equation (3.96b). Moving on to $G_{E_0\phi}^{(x)}$ we can write, by inspection of equations (3.106) and (3.95) and use of the previous substitutions,

$$G_{E_0\phi}^{(x)} = -j\omega\mu \frac{e^{-jk_0 r}}{2\pi r} \frac{\sin(\omega\tau_\theta h)}{\sin(\omega\tau_\theta)} \left[\frac{-jk_0 \cos\theta}{k_0\left(j\cos\theta + \tau_\theta \frac{c}{d} \cot(\omega\tau_\theta)\right)} \right] \sin\phi \quad (3.114)$$

which simply becomes,

$$G_{E_0\phi}^{(x)} = -j\omega\mu \frac{e^{-jk_0 r}}{2\pi r} \left[\frac{\sin(\omega\tau_\theta h)}{\left(j\tau_\theta \frac{c}{d} \cos(\omega\tau_\theta) - \cos\theta \sin(\omega\tau_\theta)\right)} \right] \cos\theta \sin\phi \quad . \quad (3.115)$$

The corresponding result for a y–directed source is then found by applying this component to equation (3.96c). With only the vertical source components remaining we can again write, by inspection of equations (3.106) and (3.97b) and use of the previous substitutions,

$$G_{E_0\theta}^{(z)} = -j\omega\mu \frac{e^{-jk_0 r}}{2\pi r} \frac{\cos(\omega\tau_\theta h)}{\cos(\omega\tau_\theta)} \left[\frac{-jk_0 \cos\theta}{k_0\left(j\varepsilon_{rd} \cos\theta - \tau_\theta \frac{c}{d} \tan(\omega\tau_\theta)\right)} \right] \sin\theta \quad (3.116)$$

which becomes,

$$G_{E_0\theta}^{(z)} = j\omega\mu \frac{e^{-jk_0 r}}{2\pi r} \left[\frac{\cos(\omega\tau_\theta h)}{\left(\varepsilon_{rd} \cos\theta \cos(\omega\tau_\theta) + j\tau_\theta \frac{c}{d} \sin(\omega\tau_\theta)\right)} \right] \cos\theta \sin\theta \quad . \quad (3.117)$$

Now, since we already know through equation (3.97c) that the last remaining component,

$G^{(z)}_{E_0\phi}$, is simply equal to zero, we know all nine components of the electric dyadic Green function in the far field. These compare exactly with previously documented results [Vegni].

3.2 Conversion From the Frequency Domain into the Time Domain

In the preceding section we derived the frequency domain representation of the electric field dyadic Green function, however, in this thesis we wish to work with time domain fields. We can therefore obtain these desired fields for any particular single dielectric, printed circuit, problem by one of two ways. The first is to obtain the spectrum of the electric field for a particular problem numerically at a given point in space and then convert to the time domain (probably through employing an FFT). The other way is to analytically convert the frequency domain field representation into the time domain, and then proceed to obtain the time domain results numerically through a new time domain electric field dyadic Green function. The latter is the approach that we will use in this document, and its derivation is accomplished in this, the last, section of this chapter.

Before performing the inverse Fourier transform on the electric dyadic Green function we should take a closer look at the dipole source which we used in section 2.1 to excite the magnetic vector potential Green function defining equation. The reason for this is that in the previous case the dipole source was simply a three dimensional unit impulse occurring at some point in space and at time zero. However, if the source does not occur at time zero but at some initial time, another unit impulse would be needed as defined in the following current density representation,

$$J(t) = \delta(t - t')\delta(\bar{r} - \bar{r}') \quad . \tag{3.118}$$

This in turn would require another integral similar to the volume integral in equation (2.25a), (or in equation (2.26a) with no magnetic sources present), which would then be responsible for summing up all the contributions to the field from each point in time just as the volume integral is responsible for summing up the contributions from each point in space. The

combination of these two integrals is shown in equation (3.119),

$$\mathbf{E}(\mathbf{r},t) = \int\int\int_{V}\int_{-\infty}^{t} \overline{\mathbf{G}}_E(\mathbf{r},t \mid \mathbf{r}',t-t')\cdot\mathbf{J}(\mathbf{r}',t')dt'dV \tag{3.119}$$

where we can see that the the added time integral only adds contributions up to the present time t. This is a reasonable result since currents occurring at future times cannot be expected to affect currents at the present time or past times.

To now find the time domain electric dyadic Green function shown in equation (3.119) we proceed to convert the new current density representation of equation (3.118) into the frequency domain as follows,

$$J(\omega) = e^{-j\omega t'}\delta(\bar{r}-\bar{r}') \tag{3.120}$$

and therefore include the factor $e^{-j\omega t'}$ in all of the components of the electric field dyadic Green function derived in the previous section. Now, the Fourier transform pair which allows us to move between the time domain and the frequency domain was given in section 2.1, (equation (2.3)). In this case however, we only require the inverse Fourier transform, which we have reiterated below.

$$f(t) = \frac{1}{2\pi}\int_{-\infty}^{\infty} F(\omega)e^{+j\omega t}d\omega \tag{3.121}$$

Before applying this transform however we find, observing the results obtained in the preceding section, that all of these results can be written in the form,

$$G_{E_0v}^{(u)}(\omega) = j\omega e^{-jk_0 r}F_v^{(u)}(\omega) = j\omega e^{-j\omega\frac{r}{c}}F_v^{(u)}(\omega) \quad . \tag{3.122}$$

Therefore, substituting this and the time shift factor into the inverse Fourier transform we immediately obtain,

$$G_{E_0v}^{(u)}(t) = \frac{1}{2\pi}\int_{-\infty}^{\infty} j\omega F_v^{(u)}(\omega)e^{+j\omega\left(t-\frac{r}{c}-t'\right)}d\omega \quad . \tag{3.123}$$

This can then be simplified by using the following two relations [MyintU],

$$a)\quad \frac{d}{dt}f(t) \Leftrightarrow j\omega F(\omega) \qquad b)\quad f(t-t') \Leftrightarrow e^{-j\omega t'}F(\omega) \tag{3.124}$$

in equation (3.123) to obtain,

$$G_{E_0v}^{(u)}\left(t-\frac{r}{c}-t'\right)=G_{E_0v}^{(u)}(\tau)=\frac{d}{d\tau}\left[\frac{1}{2\pi}\int_{-\infty}^{\infty}F_v^{(u)}(\omega)e^{+j\omega\tau}d\omega\right] \tag{3.125}$$

where we have used the variable $\tau = t-\frac{r}{c}-t'$ to represent the shifted value of time.

Let us now work at converting the remaining parts of each of the electric field dyadic Green function components one by one. Beginning with $G_{E_0\theta}^{(x)}$ we can write by inspection of equation (3.113) the function remaining to be converted as,

$$F_\theta^{(x)}(\omega)=-\frac{\mu}{2\pi r}\tau_\theta\frac{c}{d}\left[\frac{\sin(\omega\tau_\theta h)}{\tau_\theta\frac{c}{d}\sin(\omega\tau_\theta)-j\varepsilon_{rd}\cos\theta\cos(\omega\tau_\theta)}\right]\cos\theta\cos\phi \tag{3.126}$$

which when written in time domain form yields,

$$F_\theta^{(x)}(\tau)=-\frac{\mu}{2\pi r}\tau_\theta\frac{c}{d}\cos\theta\cos\phi I_\theta^{(x)}(\tau) \tag{3.127}$$

where,

$$I_\theta^{(x)}(\tau)=\frac{1}{2\pi}\int_{-\infty}^{\infty}\frac{\sin(\omega\tau_\theta h)}{\tau_\theta\frac{c}{d}\sin(\omega\tau_\theta)-j\varepsilon_{rd}\cos\theta\cos(\omega\tau_\theta)}e^{+j\omega\tau}d\omega \quad . \tag{3.128}$$

To begin solving this integral let us first expand the trigonometric functions containing omega. In so doing we arrive at,

$$I_\theta^{(x)}(\tau)=\frac{1}{2\pi}\int_{-\infty}^{\infty}\frac{e^{+j\omega\tau_\theta h}-e^{-j\omega\tau_\theta h}}{\tau_\theta\frac{c}{d}\left(e^{+j\omega\tau_\theta}-e^{-j\omega\tau_\theta}\right)+\varepsilon_{rd}\cos\theta\left(e^{+j\omega\tau_\theta}+e^{-j\omega\tau_\theta}\right)}e^{+j\omega\tau}d\omega \tag{3.129}$$

which when rearranged leaves,

$$I_\theta^{(x)}(\tau)=\frac{1}{2\pi}\int_{-\infty}^{\infty}\frac{e^{+j\omega\tau_\theta h}-e^{-j\omega\tau_\theta h}}{\left(\varepsilon_{rd}\cos\theta+\tau_\theta\frac{c}{d}\right)e^{+j\omega\tau_\theta}+\left(\varepsilon_{rd}\cos\theta-\tau_\theta\frac{c}{d}\right)e^{-j\omega\tau_\theta}}e^{+j\omega\tau}d\omega \ . \tag{3.130}$$

Dividing the top and bottom of the integrand by $\left(\varepsilon_{rd}\cos\theta+\tau_\theta\frac{c}{d}\right)e^{+j\omega\tau_\theta}$ and collecting exponents we then obtain the following representation of the integral,

$$I_\theta^{(x)}(\tau)=\frac{1}{\left(\varepsilon_{rd}\cos\theta+\tau_\theta\frac{c}{d}\right)}\left[\frac{1}{2\pi}\int_{-\infty}^{\infty}\frac{e^{+j\omega\tau_\theta(h-1)}-e^{-j\omega\tau_\theta(h+1)}}{1+x(\theta)}e^{+j\omega\tau}d\omega\right] \tag{3.131}$$

where,

$$x(\theta) = \frac{\left(\varepsilon_{rd}\cos\theta - \tau_\theta \frac{c}{d}\right)}{\left(\varepsilon_{rd}\cos\theta + \tau_\theta \frac{c}{d}\right)} e^{-j2\omega\tau_\theta} = \Gamma_v e^{-j2\omega\tau_\theta} \quad . \tag{3.132}$$

Examining $x(\theta)$, defined above, we should immediately notice that its magnitude will be less than one, unless $\theta = 90^o$. That is,

$$|x(\theta)| = \left|\frac{\left(\varepsilon_{rd}\cos\theta - \tau_\theta \frac{c}{d}\right)}{\left(\varepsilon_{rd}\cos\theta + \tau_\theta \frac{c}{d}\right)}\right| = |\Gamma_v| \leq 1 \quad . \tag{3.133}$$

Because of this, we can make use of the following identity [CRC],

$$\frac{1}{(1 + x(\theta))} = \sum_{n=0}^{\infty} (-1)^n x^n(\theta) \quad , \quad |x(\theta)| < 1 \tag{3.134}$$

and the definition of h (see the definitions prior to equation (3.107)) to rewrite equation (3.131) as follows.

$$I_\theta^{(x)}(\tau) = \frac{1}{\left(\varepsilon_{rd}\cos\theta + \tau_\theta \frac{c}{d}\right)} \left[\frac{1}{2\pi} \int_{-\infty}^{\infty} \left(e^{+j\omega\tau_\theta \frac{z'}{d}} - e^{-j\omega\tau_\theta\left(2 + \frac{z'}{d}\right)} \right) \sum_{n=0}^{\infty} \left\{ (-\Gamma_v)^n e^{-j2n\omega\tau_\theta} \right\} e^{+j\omega\tau} d\omega \right] \tag{3.135}$$

It should be noted at this point that this equation does not hold at $\theta = 90^o$ since the summation itself doesn't hold in this case. Now, interchanging the summation and integration, removing any constants from inside of the integration, and writing this integration separately for each term of the integrand we obtain the following much simplified integral.

$$I_\theta^{(x)}(\tau) = \frac{1}{\left(\varepsilon_{rd}\cos\theta + \tau_\theta \frac{c}{d}\right)} \sum_{n=0}^{\infty} \left\{ (-\Gamma_v)^n \left[\frac{1}{2\pi} \int_{-\infty}^{\infty} e^{+j\omega\left(\tau + \frac{z'}{d}\tau_\theta - 2n\tau_\theta\right)} d\omega - \frac{1}{2\pi} \int_{-\infty}^{\infty} e^{+j\omega\left(\tau - \frac{z'}{d}\tau_\theta - 2(n+1)\tau_\theta\right)} d\omega \right] \right\} . \tag{3.136}$$

The inverse Fourier transforms represented by the two integrals in this equation are well known using the property given in equation (3.124b). In the case when $F(\omega) = 1$ this

property becomes, $\delta(t-t') \Leftrightarrow e^{-j\omega t'}$ [MyintU], and so we see that equation (3.136) simply becomes,

$$I_{\theta}^{(x)}(\tau) = \frac{1}{\left(\varepsilon_{rd}\cos\theta + \tau_{\theta}\frac{c}{d}\right)} \sum_{n=0}^{\infty} \left\{ (-\Gamma_v)^n \left\{ \delta\left[\tau - \left(2n - \frac{z'}{d}\right)\tau_{\theta}\right] - \delta\left[\tau - \left(2(n+1) + \frac{z'}{d}\right)\tau_{\theta}\right] \right\} \right\} \quad . \text{(3.137)}$$

Substituting this equation into equation (3.127) and then in turn, into equation (3.125) and simultaneously substituting the value of τ we obtain the final time domain expression for the θ component of the x–directed electric field dyadic Green function as,

$$G_{E_0\theta}^{(x)}(t) = -\frac{\mu\tau_{\theta}\frac{c}{d}}{2\pi r\left(\varepsilon_{rd}\cos\theta + \tau_{\theta}\frac{c}{d}\right)} \sum_{n=0}^{\infty} \left\{ (-\Gamma_v)^n \left(\frac{d}{dt}\delta_n - \frac{d}{dt}\delta_{n+1} \right) \right\} \cos\theta\cos\phi \qquad \text{(3.138)}$$

where the two delta functions are defined as follows.

$$a)\ \delta_n = \delta\left[t - \frac{r}{c} - t' - \left(2n - \frac{z'}{d}\right)\tau_{\theta}\right] \quad b)\ \delta_{n+1} = \delta\left[t - \frac{r}{c} - t' - \left(2(n+1) + \frac{z'}{d}\right)\tau_{\theta}\right] \qquad \text{(3.139)}$$

Equation (3.138) is now obviously a closed form solution, (albeit an infinite summation), and we also already know that equation (3.96b) defines the same component due to a y–directed source in terms of this x–directed solution. So let us now try to put some significance to the two delta functions in this solution. Obviously, when we apply equation (3.138) to equation (3.119) to obtain the electric field due to a specific source at a specific point in time and space these differentiated delta functions serve to extract the time derivatives of the current at various points in previous time, a combination of which produce the field at the present time. Note that the extraction of current derivatives by use of the derivative of a dirac delta function can be accomplished in this case without a change in sign, (which would normally be present because of integration by parts) since the current derivative was present on the right hand side of the original wave equation, (2.2a). To see exactly how this current derivative extraction works we can look at the case when the source

is on the surface of the grounded dielectric. In this case $z' = 0$ and the first term of the summation, $n = 0$, yields $\delta_0 = \delta(t - r/c - t')$ and $\delta_1 = \delta(t - r/c - t' - 2\tau_\theta)$. Here we can see that $\frac{d}{dt}\delta_0$ will extract the current derivative at the present time less the direct propagation time (r/c) at a particular current position. This is the last current derivative that could possibly effect the field at the present time and can be viewed as that derivative which produces a wave that propagates directly from the source to the observation point. The time derivative of δ_1 however, moves yet further back in time by twice the amount of the variable τ_θ, which was defined in equation (3.107) and represents the propagation time through the substrate along a path dependent on the permittivity of the dielectric and the elevation angle to the observation point. The current derivative extracted by $\frac{d}{dt}\delta_1$ is the next to last current derivative which could possibly effect the field at the present time and can be viewed as that derivative which produces a wave that bounces once from the ground plane before propagating directly to the observation point. The contribution to the field at time t for this term of the summation is then proportional to the difference between these two current derivatives. For the next term of the summation, $n = 1$, $\delta_0 \rightarrow \delta_1$ and $\delta_1 \rightarrow \delta_2$ and the contribution to the field for this term of the summation is proportional to the difference between the current derivative whose wave bounces twice off the ground plane and the one that bounces only once. Now, since the summation is infinite we must mathematically proceed back in time to $-\infty$, but realistically we only need to go back to the start time of the waveform since before that we can assume the current derivatives to all be zero. Furthermore, because the $(-\Gamma_v)^n$ term (in which we remember that Γ_v is less than one) decays with increasing n we only need to go back enough terms in time until the contribution to the summation is negligible.

Let us now move on to solving for the $G^{(x)}_{E_0\phi}$ component of the electric field dyadic

Green function, defined in the frequency domain by equation (3.115). In this case, the function remaining to be converted within equation (3.125) can be written as,

$$F_{\phi}^{(x)}(\omega) = -\frac{\mu}{2\pi r}\left[\frac{\sin(\omega\tau_\theta h)}{\left(j\tau_\theta \frac{c}{d}\cos(\omega\tau_\theta) - \cos\theta\,\sin(\omega\tau_\theta)\right)}\right]\cos\theta\,\sin\phi \qquad (3.140)$$

which when written in time domain form yields,

$$F_{\phi}^{(x)}(\tau) = -\frac{\mu}{2\pi r}\cos\theta\,\sin\phi\, I_{\phi}^{(x)}(\tau) \qquad (3.141)$$

where,

$$I_{\phi}^{(x)}(\tau) = \frac{1}{2\pi}\int_{-\infty}^{\infty}\frac{\sin(\omega\tau_\theta h)}{\left(j\tau_\theta \frac{c}{d}\cos(\omega\tau_\theta) - \cos\theta\,\sin(\omega\tau_\theta)\right)}e^{+j\omega\tau}d\omega \quad . \qquad (3.142)$$

To solve this integral we proceed, as previously, to expand the trigonometric functions within the integral giving,

$$I_{\phi}^{(x)}(\tau) = \frac{1}{2\pi}\int_{-\infty}^{\infty}\frac{e^{-j\omega\tau_\theta h} - e^{+j\omega\tau_\theta h}}{\left(\tau_\theta \frac{c}{d}\left(e^{+j\omega\tau_\theta} + e^{-j\omega\tau_\theta}\right) + \cos\theta\left(e^{+j\omega\tau_\theta} - e^{-j\omega\tau_\theta}\right)\right)}e^{+j\omega\tau}d\omega \qquad (3.143)$$

which when rearranged leaves,

$$I_{\phi}^{(x)}(\tau) = \frac{1}{2\pi}\int_{-\infty}^{\infty}\frac{e^{-j\omega\tau_\theta h} - e^{+j\omega\tau_\theta h}}{\left(\left(\cos\theta + \tau_\theta \frac{c}{d}\right)e^{+j\omega\tau_\theta} - \left(\cos\theta - \tau_\theta \frac{c}{d}\right)e^{-j\omega\tau_\theta}\right)}e^{+j\omega\tau}d\omega \quad . \qquad (3.144)$$

Dividing the top and bottom of the integrand by $\left(\cos\theta + \tau_\theta \frac{c}{d}\right)e^{+j\omega\tau_\theta}$ and collecting exponents we obtain the following representation of the above integral,

$$I_{\phi}^{(x)}(\tau) = \frac{1}{\left(\cos\theta + \tau_\theta \frac{c}{d}\right)}\left[\frac{1}{2\pi}\int_{-\infty}^{\infty}\frac{e^{-j\omega\tau_\theta(h+1)} - e^{+j\omega\tau_\theta(h-1)}}{1 - x(\theta)}e^{+j\omega\tau}d\omega\right] \qquad (3.145)$$

where,

$$x(\theta) = \frac{\left(\cos\theta - \tau_\theta \frac{c}{d}\right)}{\left(\cos\theta + \tau_\theta \frac{c}{d}\right)}e^{-j2\omega\tau_\theta} = \Gamma_u\, e^{-j2\omega\tau_\theta} \quad . \qquad (3.146)$$

As previously, the magnitude of $x(\theta)$ can again be seen to be less than one, unless $\theta = 90^o$,

and we can therefore use the following identity [CRC],

$$\frac{1}{\left(1-x(\theta)\right)} = \sum_{n=0}^{\infty} x^n(\theta) \quad , \quad |x(\theta)| < 1 \tag{3.147}$$

and the definition of h (see the definitions prior to equation (3.107)) to rewrite equation (3.145) as follows.

$$I_{\phi}^{(x)}(\tau) = -\frac{1}{\left(\cos\theta + \tau_\theta \frac{c}{d}\right)}\left[\frac{1}{2\pi}\int_{-\infty}^{\infty}\left(e^{+j\omega\tau_\theta\frac{z'}{d}} - e^{-j\omega\tau_\theta\left(2+\frac{z'}{d}\right)}\right)\sum_{n=0}^{\infty}\left\{\Gamma_u^n e^{-j2n\omega\tau_\theta}\right\}e^{+j\omega\tau}d\omega\right] \tag{3.148}$$

Now, interchanging the summation and integration, removing any constants from the integration and writing this integration separately for each term of the integrand we obtain, the following much simplified integral.

$$I_{\phi}^{(x)}(\tau) = -\frac{1}{\left(\cos\theta + \tau_\theta \frac{c}{d}\right)}\sum_{n=0}^{\infty}\left\{\Gamma_u^n\left[\frac{1}{2\pi}\int_{-\infty}^{\infty} e^{+j\omega\left(\tau + \frac{z'}{d}\tau_\theta - 2n\tau_\theta\right)}d\omega\right.\right. \tag{3.149}$$

$$\left.\left. -\frac{1}{2\pi}\int_{-\infty}^{\infty} e^{+j\omega\left(\tau - \frac{z'}{d}\tau_\theta - 2(n+1)\tau_\theta\right)}d\omega\right]\right\} \quad . \tag{3.150}$$

These two inverse Fourier transforms are obviously the same as those used to solve equation (3.136) and so we can write the result of $I_{\phi}^{(x)}(\tau)$ directly by inspection of the above giving,

$$I_{\phi}^{(x)}(\tau) = -\frac{1}{\left(\cos\theta + \tau_\theta \frac{c}{d}\right)}\sum_{n=0}^{\infty}\left\{\Gamma_u^n\left\{\delta\left[\tau - \left(2n - \frac{z'}{d}\right)\tau_\theta\right]\right.\right.$$

$$\left.\left. -\delta\left[\tau - \left(2(n+1) + \frac{z'}{d}\right)\tau_\theta\right]\right\}\right\} \quad . \tag{3.151}$$

Finally, this component can be found in its entirety by substituting this equation into equation (3.141) and then in turn into equation (3.125) and simultaneously substituting the value of τ which yields,

$$G_{E_0\phi}^{(x)}(t) = \frac{\mu}{2\pi r\left(\cos\theta + \tau_\theta \frac{c}{d}\right)}\sum_{n=0}^{\infty}\left\{\Gamma_u^n\left(\frac{d}{dt}\delta_n - \frac{d}{dt}\delta_{n+1}\right)\right\}\cos\theta\sin\phi \tag{3.152}$$

where the two delta functions are defined as in equation (3.139) and the y–directed result

can be written in terms of this x–directed result using equation (3.96c).

Lastly then, we have to solve for the $G_{E_0\theta}^{(z)}$ component which is defined in the frequency domain by equation (3.117). In this case, the function remaining to be converted within equation (3.125) is written as,

$$F_\theta^{(z)}(\omega) = \frac{\mu}{2\pi r}\left[\frac{\cos(\omega\tau_\theta h)}{\left(\varepsilon_{rd}\cos\theta\cos(\omega\tau_\theta) + j\tau_\theta\frac{c}{d}\sin(\omega\tau_\theta)\right)}\right]\cos\theta\sin\theta \qquad (3.153)$$

which when written in time domain form yields,

$$F_\theta^{(z)}(\tau) = \frac{\mu}{2\pi r}\cos\theta\sin\theta I_\theta^{(z)}(\tau) \qquad (3.154)$$

where,

$$I_\theta^{(z)}(\tau) = \frac{1}{2\pi}\int_{-\infty}^{\infty}\frac{\cos(\omega\tau_\theta h)}{\left(\varepsilon_{rd}\cos\theta\cos(\omega\tau_\theta) + j\tau_\theta\frac{c}{d}\sin(\omega\tau_\theta)\right)}e^{+j\omega\tau}d\omega \quad . \qquad (3.155)$$

Again expanding the trigonometric functions within the integral yields,

$$I_\theta^{(z)}(\tau) = \frac{1}{2\pi}\int_{-\infty}^{\infty}\frac{e^{+j\omega\tau_\theta h} + e^{-j\omega\tau_\theta h}}{\left(\varepsilon_{rd}\cos\theta\left(e^{+j\omega\tau_\theta} + e^{-j\omega\tau_\theta}\right) + \tau_\theta\frac{c}{d}\left(e^{+j\omega\tau_\theta} - e^{-j\omega\tau_\theta}\right)\right)}e^{+j\omega\tau}d\omega \qquad (3.156)$$

which when rearranged gives,

$$I_\theta^{(z)}(\tau) = \frac{1}{2\pi}\int_{-\infty}^{\infty}\frac{e^{+j\omega\tau_\theta h} + e^{-j\omega\tau_\theta h}}{\left(\left(\varepsilon_{rd}\cos\theta + \tau_\theta\frac{c}{d}\right)e^{+j\omega\tau_\theta} + \left(\varepsilon_{rd}\cos\theta - \tau_\theta\frac{c}{d}\right)e^{-j\omega\tau_\theta}\right)}e^{+j\omega\tau}d\omega \quad . \qquad (3.157)$$

If we compare this equation with equation (3.130) it is immediately obvious that they are identical except that the exponential terms in the numerator of the integrand are added instead of subtracted. Because of this we can simply write down and slightly modify equation (3.137) to give the final form of this integral.

$$I_\theta^{(z)}(\tau) = \frac{1}{\left(\varepsilon_{rd}\cos\theta + \tau_\theta\frac{c}{d}\right)}\sum_{n=0}^{\infty}\left\{(-\Gamma_v)^n\left\{\delta\left[\tau - \left(2n - \frac{z'}{d}\right)\tau_\theta\right] + \delta\left[\tau - \left(2(n+1) + \frac{z'}{d}\right)\tau_\theta\right]\right\}\right\} \qquad (3.158)$$

Substituting this equation into equation (3.154) and then in turn into equation (3.125) along with the value of τ yields,

$$G_{E_0\theta}^{(z)}(t) = \frac{\mu}{2\pi r\left(\varepsilon_{rd}\cos\theta + \tau_\theta \frac{c}{d}\right)} \sum_{n=0}^{\infty} \left\{ (-\Gamma_v)^n \left(\frac{d}{dt}\delta_n + \frac{d}{dt}\delta_{n+1} \right) \right\} \cos\theta \sin\theta \quad (3.159)$$

where the two delta functions are defined as in equation (3.139). Note that in this case the contributions of the two current derivatives for each summation term are additive unlike in the previous results.

Now we have the final electric field dyadic Green function completely defined in the time domain by equations (3.138), (3.152), (3.96b) and (3.96c) for the x and y–directed results as well as by equation (3.159) for the only z–directed result, (note that these results correspond exactly with [Cicchetti]). These resulting time domain electric field dyadic components are then all that we require to numerically obtain time domain fields for any problem, that fits our problem definition, given that the time derivatives of the currents are known for each point along the printed circuit traces. Several typical problems will be examined in the following chapter for clarification of the method.

CHAPTER 4

NUMERICAL RESULTS AND DISCUSSION

4.1 Accuracy Considerations

In the two previous chapters we calculated the electric field dyadic Green function in the time domain by making use of the magnetic vector potential dyadic Green function, which was first calculated in the spectral–frequency domain and then converted into the frequency domain through the saddle point method. After this, the frequency domain electric field Green function was calculated and converted finally into the time domain. Following this immense amount of work a pressing concern needs to be addressed which pertains to the accuracy of our time domain results of section 3.2 as compared with the ones which would have been obtained without any approximations, (i.e. if direct integration had been used instead of the saddle point method in conversion from the spectral–frequency domain into the frequency domain). To address this concern in the easiest possible way we can simply compare the agreement of the exact inverse Fourier transform integration results of the electric field dyadic Green function in the spectral–frequency domain with its closed form approximate far field results which we obtained at the end of section 3.1.5. Such a check in the frequency domain is equally valid to a similar check in the time domain, (except at $\theta = 90^o$ where the time domain summation becomes invalid), since we used a direct mathematical transformation with no approximations to go from the frequency domain into the time domain. Furthermore, it is easier to test the frequency domain results since our approximate result is just a simple closed–form algebraic equation, not an infinite summation, and the exact result in the frequency domain does not require a semi–infinite integration with respect to time as it would in the time domain.

The first way to test our frequency domain results is to compare them with the well documented equations for a directed dipole source above ground and in free space. To do this we simply let $\varepsilon_{rd} = 1$ and $h = 1$, (since this depth ratio has no meaning for free space

conditions), in our resultant frequency domain equations of section 3.1.5. Consequently we obtain the same results as those documented in [Balanis] with a slight modification to the phase term due to the difference in origin, (ours being at the source and his being at the ground plane). This is a very good initial indication that the methods and procedures which we used to obtain our results are justified.

To now further assess the accuracy of our results we must calculate the exact electric field dyadic Green function and somehow compare it numerically with our approximate results. Doing this however, requires difficult and hence time consuming, integrations along the positive real k_ϱ axis, which was the reason for finding an approximate method in the first place. Difficulties aside however, we proceed in this way by first calculating $\overline{\mathbf{G}}_{E_0}$ in the spectral–frequency domain and then, through those time consuming inverse Fourier transform integrations, converting into the frequency domain. Note that this is the exact opposite of the procedure used in chapter 3 where we converted into the frequency domain before calculating $\overline{\mathbf{G}}_{E_0}$. Therefore, the electric field dyadic Green function is calculated from $\overline{\mathbf{G}}_{A_0}$ using equation (2.32a), which we have reiterated below,

$$\overline{\mathbf{G}}_{E_0} = \frac{1}{j\omega\varepsilon_0}\left(\nabla\nabla\cdot + k_0^2\right)\overline{\mathbf{G}}_{A_0} \tag{4.1}$$

and $\overline{\mathbf{G}}_{A_0}$ has been defined earlier as,

$$\overline{\mathbf{G}}_{A_0} = \begin{bmatrix} \dfrac{N_{h_0}}{D_{TE}} & 0 & 0 \\ 0 & \dfrac{N_{h_0}}{D_{TE}} & 0 \\ \dfrac{jk_x N_{h_0}(\varepsilon_{rd}-1)}{D_{TE}D_{TM}} & \dfrac{jk_y N_{h_0}(\varepsilon_{rd}-1)}{D_{TE}D_{TM}} & \dfrac{N_{v_0}}{D_{TM}} \end{bmatrix} E_d e^{-u_0 z} \quad . \tag{4.2}$$

Now, as we did in equation (2.33a) and (2.33c), equation (4.1) can easily be expanded for each column of $\overline{\mathbf{G}}_{E_0}$, as in equations (4.3) below, where the direction of the source is irrelevant and has not been explicitly shown in these equations.

$$a)\quad G_{E_{0x}} = \frac{1}{j\omega\varepsilon_0}\left(\frac{\partial^2 G_{A_{0x}}}{\partial x^2} + \frac{\partial^2 G_{A_{0y}}}{\partial x \partial y} + \frac{\partial^2 G_{A_{0z}}}{\partial x \partial z} + k_0^2 G_{A_{0x}}\right) \tag{4.3}$$

$$b)\quad G_{E_{0y}} = \frac{1}{j\omega\varepsilon_0}\left(\frac{\partial^2 G_{A_{0x}}}{\partial x \partial y} + \frac{\partial^2 G_{A_{0y}}}{\partial y^2} + \frac{\partial^2 G_{A_{0z}}}{\partial y \partial z} + k_0^2 G_{A_{0y}}\right)$$

$$c)\quad G_{E_{0z}} = \frac{1}{j\omega\varepsilon_0}\left(\frac{\partial^2 G_{A_{0x}}}{\partial x \partial z} + \frac{\partial^2 G_{A_{0y}}}{\partial y \partial z} + \frac{\partial^2 G_{A_{0z}}}{\partial z^2} + k_0^2 G_{A_{0z}}\right)$$

In the spectral domain then, these equations simply become, respectively,

$$a)\quad G_{E_{0x}} = \frac{1}{j\omega\varepsilon_0}\left\{\left(k_0^2 - k_x^2\right)G_{A_{0x}} - k_x k_y G_{A_{0y}} + jk_x \frac{dG_{A_{0z}}}{dz}\right\} \tag{4.4}$$

$$b)\quad G_{E_{0y}} = \frac{1}{j\omega\varepsilon_0}\left\{-k_x k_y G_{A_{0x}} + \left(k_0^2 - k_y^2\right)G_{A_{0y}} + jk_y \frac{dG_{A_{0z}}}{dz}\right\}$$

$$c)\quad G_{E_{0y}} = \frac{1}{j\omega\varepsilon_0}\left\{jk_x \frac{\partial G_{A_{0x}}}{\partial z} + jk_y \frac{dG_{A_{0y}}}{dz} + \left(\frac{\partial^2}{\partial z^2} + k_0^2\right)G_{A_{0z}}\right\}$$

and so, applying one column of $\overline{\mathbf{G}}_{A_0}$ at a time, we obtain for the first column (which as we remember is due to an x–directed source) the following components of $\overline{\mathbf{G}}_{E_0}$.

$$a)\quad G_{E_{0x}}^{(x)} = \frac{1}{j\omega\varepsilon_0}\left\{\frac{k_0^2 - k_x^2}{D_{TE}} + \frac{k_x^2 u_0(\varepsilon_{rd} - 1)}{D_{TE}D_{TM}}\right\}N_{h_0}E_d e^{-u_0 z} \tag{4.5}$$

$$b)\quad G_{E_{0y}}^{(x)} = \frac{1}{j\omega\varepsilon_0}\left\{\frac{-k_x k_y}{D_{TE}} + \frac{k_x k_y u_0(\varepsilon_{rd} - 1)}{D_{TE}D_{TM}}\right\}N_{h_0}E_d e^{-u_0 z}$$

$$c)\quad G_{E_{0z}}^{(x)} = \frac{1}{j\omega\varepsilon_0}\left\{\frac{-jk_x u_0}{D_{TE}} + \frac{jk_x\left(k_x^2 + k_y^2\right)(\varepsilon_{rd} - 1)}{D_{TE}D_{TM}}\right\}N_{h_0}E_d e^{-u_0 z}$$

Applying the second column, (due to a y–directed source) we obtain the next three similar components as,

$$a)\quad G_{E_{0x}}^{(y)} = \frac{1}{j\omega\varepsilon_0}\left\{\frac{-k_x k_y}{D_{TE}} + \frac{k_x k_y u_0(\varepsilon_{rd} - 1)}{D_{TE}D_{TM}}\right\}N_{h_0}E_d e^{-u_0 z} \tag{4.6}$$

$$b)\quad G_{E_{0y}}^{(y)} = \frac{1}{j\omega\varepsilon_0}\left\{\frac{k_0^2 - k_y^2}{D_{TE}} + \frac{k_y^2 u_0(\varepsilon_{rd} - 1)}{D_{TE}D_{TM}}\right\}N_{h_0}E_d e^{-u_0 z}$$

$$c)\quad G_{E_{0z}}^{(y)} = \frac{1}{j\omega\varepsilon_0}\left\{\frac{-jk_y u_0}{D_{TE}} + \frac{jk_y\left(k_x^2 + k_y^2\right)(\varepsilon_{rd} - 1)}{D_{TE}D_{TM}}\right\}N_{h_0}E_d e^{-u_0 z}$$

and finally, for the last column (due to a z–directed source) we obtain,

$$a)\quad G_{E_0x}^{(z)} = \frac{1}{j\omega\varepsilon_0}\left\{\frac{-jk_x u_0}{D_{TM}}\right\}N_{v_0}E_d e^{-u_{0z}} \quad b)\quad G_{E_0y}^{(z)} = \frac{1}{j\omega\varepsilon_0}\left\{\frac{-jk_y u_0}{D_{TM}}\right\}N_{v_0}E_d e^{-u_{0z}} \tag{4.7}$$

$$c)\ G_{E_0z}^{(z)} = \frac{1}{j\omega\varepsilon_0}\left\{\frac{\left(k_x^2+k_y^2\right)}{D_{TM}}\right\}N_{v_0}E_d e^{-u_{0z}} \quad .$$

We now proceed to convert these nine components from the spectral–frequency domain back into the frequency domain by applying, (as in chapter 3), the inverse Fourier transform given in equation (2.34b). In so doing we use,

$$\overline{\mathbf{G}}_{E_0}(x,y,z) = \frac{1}{4\pi^2}\int_{-\infty}^{\infty}\int_{-\infty}^{\infty}\overline{\mathbf{G}}_{E_0}(k_x,k_y,z)e^{+j[k_x(x-x')+k_y(y-y')]}dk_x dk_y \tag{4.8}$$

and apply this integral to each of the nine dyadic components in turn. To do this we first make the same substitutions defined in equations (3.7) to (3.9) which again allow us to convert the double integrals of equation (4.8) into single integrals containing Bessel functions in place of the complex exponential. The procedure to obtain these integrals will not be reiterated here due to its distinct similarity to the procedure given previously in section 3.1.1 and its length of derivation, however, the final integrals for the nine components are given in equations (4.9) to (4.14), below.

$$G_{E_0x}^{(x)}(k_\varrho) = \frac{1}{j\omega\varepsilon_0}\left\{\frac{1}{2\pi}\int_0^{\infty}\frac{k_0^2}{D_{TE}}N_{h_0}J_0(k_\varrho\varrho)e^{-u_{0z}}k_\varrho dk_\varrho\right.$$
$$\left.-\frac{1}{4\pi}\int_0^{\infty}\left(\frac{1}{D_{TE}}-\frac{u_0(\varepsilon_{rd}-1)}{D_{TE}D_{TM}}\right)N_{h_0}\left(J_0(k_\varrho\varrho)-\cos 2\phi J_2(k_\varrho\varrho)\right)e^{-u_{0z}}k_\varrho^3 dk_\varrho\right\} \tag{4.9}$$

$$G_{E_0y}^{(x)}(k_\varrho) = G_{E_0x}^{(y)}(k_\varrho) = \frac{1}{j\omega\varepsilon_0}\left\{\frac{\sin 2\phi}{4\pi}\int_0^{\infty}\left(\frac{1}{D_{TE}}-\frac{u_0(\varepsilon_{rd}-1)}{D_{TE}D_{TM}}\right)N_{h_0}J_2(k_\varrho\varrho)e^{-u_{0z}}k_\varrho^3 dk_\varrho\right\} \tag{4.10}$$

$$G_{E_0y}^{(y)}(k_\varrho) = \frac{1}{j\omega\varepsilon_0}\left\{\frac{1}{2\pi}\int_0^{\infty}\frac{k_0^2}{D_{TE}}N_{h_0}J_0(k_\varrho\varrho)e^{-u_{0z}}k_\varrho dk_\varrho\right.$$
$$\left.-\frac{1}{4\pi}\int_0^{\infty}\left(\frac{1}{D_{TE}}-\frac{u_0(\varepsilon_{rd}-1)}{D_{TE}D_{TM}}\right)N_{h_0}\left(J_0(k_\varrho\varrho)+\cos 2\phi J_2(k_\varrho\varrho)\right)e^{-u_{0z}}k_\varrho^3 dk_\varrho\right\} \tag{4.11}$$

$$G_{E_{0z}}^{(x)}\left(k_\varrho\right) = \cot\phi G_{E_{0z}}^{(y)}\left(k_\varrho\right) = \frac{1}{j\omega\varepsilon_0}\left\{\frac{\cos\phi}{2\pi}\int_0^\infty\left(\frac{u_0}{D_{TE}} - \frac{k_\varrho^2(\varepsilon_{rd}-1)}{D_{TE}D_{TM}}\right)N_{h_0}J_1\left(k_\varrho\varrho\right)e^{-u_0 z}k_\varrho^2 dk_\varrho\right\} \quad (4.12)$$

$$G_{E_{0x}}^{(z)}\left(k_\varrho\right) = \cot\phi G_{E_{0y}}^{(z)}\left(k_\varrho\right) = \frac{1}{j\omega\varepsilon_0}\left\{\frac{\cos\phi}{2\pi}\int_0^\infty\frac{u_0}{D_{TM}}N_{v_0}J_1\left(k_\varrho\varrho\right)e^{-u_0 z}k_\varrho^2 dk_\varrho\right\} \quad (4.13)$$

$$G_{E_{0z}}^{(z)}\left(k_\varrho\right) = \frac{1}{j\omega\varepsilon_0}\left\{\frac{1}{2\pi}\int_0^\infty\frac{1}{D_{TM}}N_{v_0}J_0\left(k_\varrho\varrho\right)e^{-u_0 z}k_\varrho^3 dk_\varrho\right\} \quad (4.14)$$

Examining these equations we find that there are only six components which require the solution of an integral since three components can be obtained easily from others through simple trigonometric equalities. Examining these six equations more closely we find eight integrations are required to solve for all of them. However, these eight integrals can be obtained through the superposition of several of only six distinct integrals as an observant reader might notice. Regardless of how the integrations are rearranged for programming or numerical expediency these are the integrations which must be performed in order to obtain a solution for the frequency domain electric field dyadic Green function [Sphicopoulos].

The integration of the previous integrals is exceedingly difficult in many instances so let us examine some of the properties of these integrals to get a better feeling for their integration difficulties. The first thing to notice is that each of the integrals contains an exponential term $e^{-u_0 z}$ which oscillates when u_0 is purely imaginary, decays when u_0 is real and positive, and yields a damped oscillation when u_0 is complex with a positive real part. Now, for our purposes the sign of u_0 was chosen to be positive to ensure the satisfaction of the radiation condition and so we know that this exponential will either oscillate, decay or both. From the definition of $u_0 = \sqrt{k_\varrho^2 - k_0^2}$ then, we can see that along the real axis the exponential will oscillate for $0 \leq \lambda < k_0$ while it will decay for $\lambda \geq k_0$ and furthermore the larger the height, z, of the observation point above the dielectric surface the smaller the period of the oscillation or the faster the decay with respect to the integration variable k_ϱ.

The next thing to notice is that each integral contains a Bessel function of some order, each of which has a domain which increases with ϱ, which we know is simply the transverse distance from the source to the observation point. Now, as the domain of these Bessel functions increases, more oscillations of these functions are consequently realized in the integrations. Therefore we can see that the Bessel functions and the exponential have a combined detrimental effect as the vertical distance from the source to the observation point decreases and the transverse distance increases, since the exponential decays more and more slowly as $z \rightarrow 0$, until it doesn't decay at all when $z = 0$, while the Bessel functions will ensure more and more oscillations are present as ϱ increases. We can now see why the integrals which we are required to evaluate become very memory and time intensive at angles of θ approaching 90 degrees. To make matters worse, in addition to the above behavior we still have the poles of the numerator and denominator functions to deal with!

Considering then the difficulties inherent in calculating these integrals we must proceed with caution. As a first attempt at a solution we can simply use a very high order gauss quadrature [Recipes], or some such integration technique, and break the range of the integral into many smaller ranges. This however, produces time consuming and highly memory intensive integrations but should give adequate results if the segmentation is done with the period of the oscillations in mind, (excepting the segments near the poles). By a simple integration trick however, we can improve the accuracy of these integrations and side step the problems caused by those pesky poles altogether. This so called trick is simply not to integrate along the real axis but instead integrate off the real axis in the complex k_ϱ plane. This can be done since we know that any such modification of the integration path is valid and will yield the same answer as long as no poles or branch points are crossed in the act of deforming the path [Trim1]. Now, as we have previously discussed, all the poles on the proper Riemann sheet occur on the real axis for a lossless substrate and beneath this axis for a lossy substrate and so we can be confident that no poles will be crossed in any upward

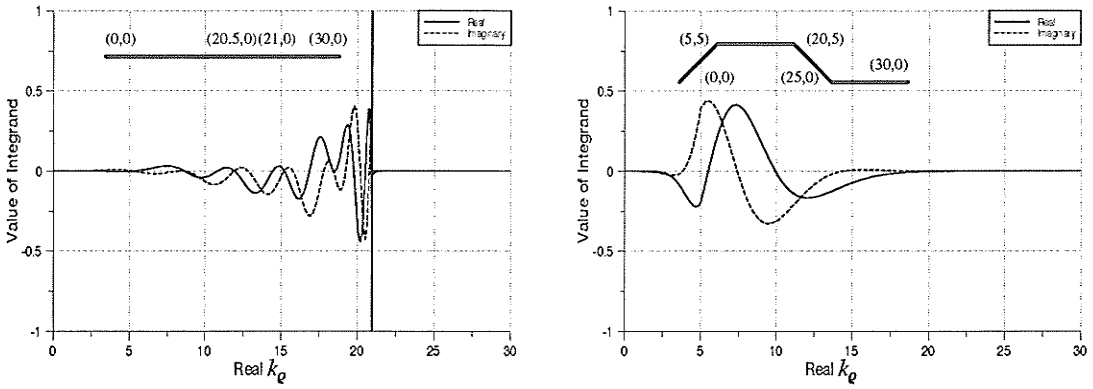

a) Real Path *b) Complex Path*

Figure 8: The Value of the $G_y^{(x)}$ Integrand Along Two Different Paths in the Complex Plane

deformation of the path that we choose. This new path of integration will in effect avoid integrating over the poles entirely and furthermore will also help lessen the oscillations due to the Bessel functions which have to be integrated since the exponential will always contain a decaying term when k_ϱ is complex.

To integrate along such a complex path a C++ program was written which obviously entailed the calculation of Bessel functions of complex argument [Abramowitz]. This program was also designed to draw the integrand with respect to k_ϱ and an example of the difference in the integrands along the real axis and one deformed path is shown in Fig. 8 for a substrate of thickness $1.5mm$, relative permittivity of 2.55, a frequency of 1GHz and a source residing at the exact middle of the substrate. Notice first of all that the pole occurring at $1.000183\,k_0$ (which was found numerically) due to the D_{TM} denominator function results in a sharp peak in Fig. 8a where the path is along the real axis. Furthermore, the integrand along the deformed integration path will obviously be much easier to integrate and use much less memory and time, with excellent accuracy.

Given the previous equations for the electric field dyadic Green function components in cartesian coordinates we now require the spherical components for direct comparison with our approximate results of section 3.1.5. To obtain these components we can either calculate

the cartesian components and then convert into spherical components or convert the integrals first and directly calculate the spherical components. The transformations needed to do this conversion were given in equations (3.93) to (3.95) and so the transformed integrals are simply given below for completeness, with $G_{E_0\phi}^{(z)} = 0$ as defined in the previous chapter.

$$G_{E_0r}^{(x)}(k_\varrho) = \cot\phi G_{E_0r}^{(y)}(k_\varrho) = \frac{1}{j\omega\varepsilon_0}\left\{\left\{\frac{1}{2\pi}\int_0^\infty \frac{k_0^2}{D_{TE}} N_{h_0} J_0(k_\varrho\varrho) e^{-u_{0z}} k_\varrho dk_\varrho \right.\right.$$

$$\left. - \frac{1}{4\pi}\int_0^\infty \left(\frac{1}{D_{TE}} - \frac{u_0(\varepsilon_{rd}-1)}{D_{TE}D_{TM}}\right) N_{h_0}\left(J_0(k_\varrho\varrho) - J_2(k_\varrho\varrho)\right) e^{-u_{0z}} k_\varrho^3 dk_\varrho \right\} \sin\theta$$

$$\left. + \frac{\cos\theta}{2\pi}\int_0^\infty \left(\frac{u_0}{D_{TE}} - \frac{k_\varrho^2(\varepsilon_{rd}-1)}{D_{TE}D_{TM}}\right) N_{h_0} J_1(k_\varrho\varrho) e^{-u_{0z}} k_\varrho^2 dk_\varrho \right\} \cos\phi \quad (4.15)$$

$$G_{E_0\theta}^{(x)}(k_\varrho) = \cot\phi G_{E_0\theta}^{(y)}(k_\varrho) = \frac{1}{j\omega\varepsilon_0}\left\{\left\{\frac{1}{2\pi}\int_0^\infty \frac{k_0^2}{D_{TE}} N_{h_0} J_0(k_\varrho\varrho) e^{-u_{0z}} k_\varrho dk_\varrho \right.\right.$$

$$\left. - \frac{1}{4\pi}\int_0^\infty \left(\frac{1}{D_{TE}} - \frac{u_0(\varepsilon_{rd}-1)}{D_{TE}D_{TM}}\right) N_{h_0}\left(J_0(k_\varrho\varrho) - J_2(k_\varrho\varrho)\right) e^{-u_{0z}} k_\varrho^3 dk_\varrho \right\} \cos\theta$$

$$\left. - \frac{\sin\theta}{2\pi}\int_0^\infty \left(\frac{u_0}{D_{TE}} - \frac{k_\varrho^2(\varepsilon_{rd}-1)}{D_{TE}D_{TM}}\right) N_{h_0} J_1(k_\varrho\varrho) e^{-u_{0z}} k_\varrho^2 dk_\varrho \right\} \cos\phi \quad (4.16)$$

$$G_{E_0\phi}^{(x)}(k_\varrho) = -\tan\phi G_{E_0\phi}^{(y)}(k_\varrho) = \frac{1}{j\omega\varepsilon_0}\left\{\left\{\frac{-1}{2\pi}\int_0^\infty \frac{k_0^2}{D_{TE}} N_{h_0} J_0(k_\varrho\varrho) e^{-u_{0z}} k_\varrho dk_\varrho \right.\right.$$

$$\left. + \frac{1}{4\pi}\int_0^\infty \left(\frac{1}{D_{TE}} - \frac{u_0(\varepsilon_{rd}-1)}{D_{TE}D_{TM}}\right) N_{h_0}\left(J_0(k_\varrho\varrho) + J_2(k_\varrho\varrho)\right) e^{-u_{0z}} k_\varrho^3 dk_\varrho \right\} \sin\phi \quad (4.17)$$

$$G_{E_0 r}^{(z)}\left(k_\varrho\right)=\frac{1}{j\omega\varepsilon_0}\left\{\frac{1}{2\pi}\int_0^\infty \frac{N_{v_0}}{D_{TM}}\left(\cos\theta k_\varrho J_0\left(k_\varrho\varrho\right)+\sin\theta u_0 J_1\left(k_\varrho\varrho\right)\right)e^{-u_0 z}k_\varrho^2 dk_\varrho\right\} \tag{4.18}$$

$$G_{E_0\theta}^{(z)}\left(k_\varrho\right)=\frac{1}{j\omega\varepsilon_0}\left\{\frac{-1}{2\pi}\int_0^\infty \frac{N_{v_0}}{D_{TM}}\left(\sin\theta k_\varrho J_0\left(k_\varrho\varrho\right)-\cos\theta u_0 J_1\left(k_\varrho\varrho\right)\right)e^{-u_0 z}k_\varrho^2 dk_\varrho\right\} \tag{4.19}$$

Let us now look at some electric fields results given a dipole of constant magnitude equal to $\bar{J}=(\hat{x}+\hat{y}+\hat{z})/dl$, (where dl is the component length of the dipole), at the middle of a $1.5mm$ thick substrate of permittivity, $\varepsilon_{rd}=2.55$. Let us choose to observe these fields along the E–Plane half cut, ($\phi=0,\ 0\le\theta\le 90$), at distances of one, three and five lambda with the dipole operating at, first 1GHz and then 10GHz. Therefore, substituting $\phi=0$ into equations (4.15) to (4.19) and looking only at the θ and ϕ components, (since the radial components are zero in the approximate case), we find that only three components are non–zero, namely, $E_\theta^{(x)}$, $E_\phi^{(y)}$ and $E_\theta^{(z)}$. The results for these components are shown in Figs. 9–11 for the 1GHz case and Figs. 12–14 for the 10GHz case where, for each case and for each component the results are displayed together with a graph of the error. This error has been defined as,

$$Err(\%)=\frac{|E_I|-|E_{CF}|}{|E_I|}\times 100\% \tag{4.20}$$

where $|E_I|$ is the magnitude of the field calculated through integration of the six required transform integrals and $|E_{CF}|$ is the magnitude of field obtained from the approximate closed form equations. Now, observing these results we can see that, as expected, those calculated using the closed–form equation agree more and more closely with the integrated results as the electrical distance from the source increases. Furthermore, all the results show that the error (which was only displayed up to 10% since any greater error value is unacceptable) increases with θ until it goes off the scale. Note also that the error for the 1GHz field results at a distance of five lambda remains under 2% for all three field components until θ exceeds approximately 74^o. Similarly for the 10GHz case, at a distance of five lambda the 2% error mark is not exceeded by any of the three components until θ

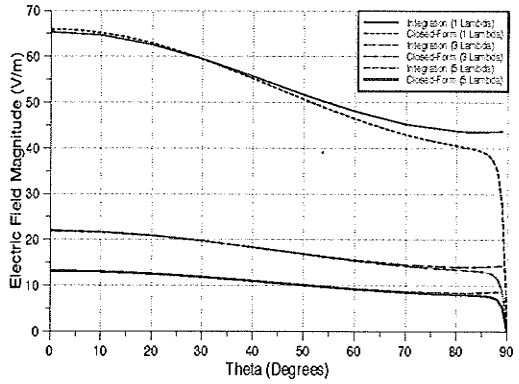

a) Magnitude

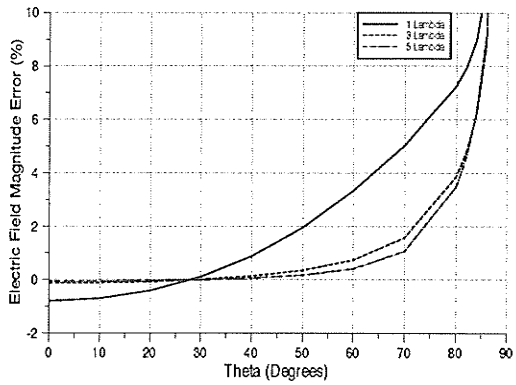

b) Error

Figure 9: A Comparison Between the Integration and Closed–Form Results for the $E_{\theta}^{(x)}$ Component at 1 GHz

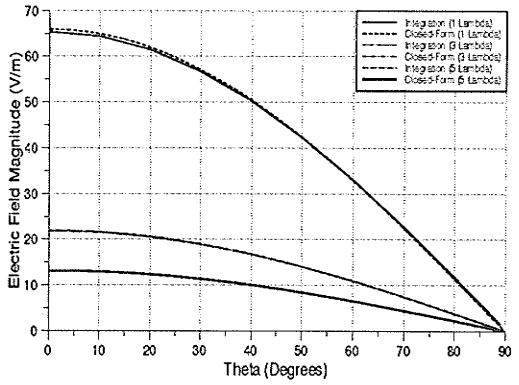

a) Magnitude

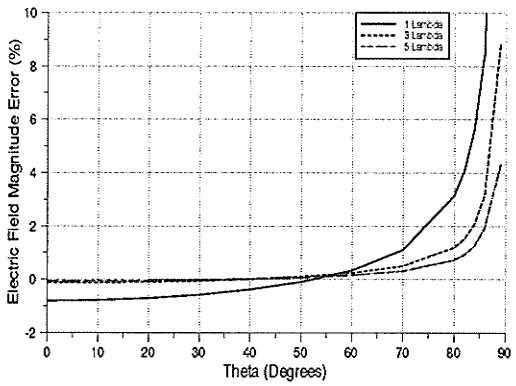

b) Error

Figure 10: A Comparison Between the Integration and Closed–Form Results for the $E_{\phi}^{(y)}$ Component at 1 GHz

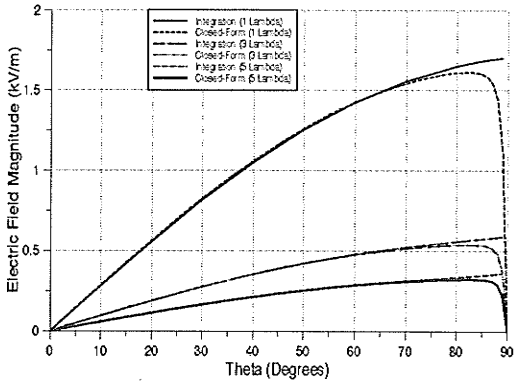

a) Magnitude

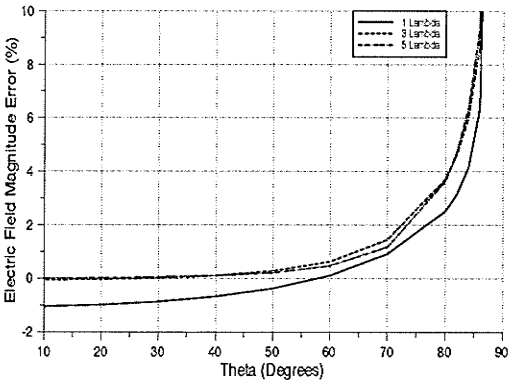

b) Error

Figure 11: A Comparison Between the Integration and Closed–Form Results for the $E_{\theta}^{(z)}$ Component at 1 GHz

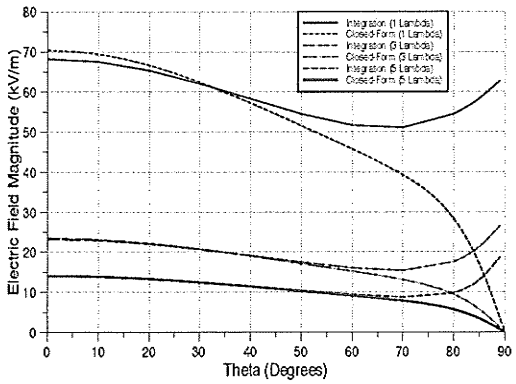

a) Magnitude

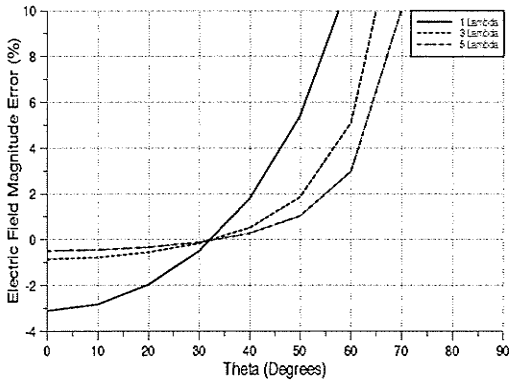

b) Error

Figure 12: A Comparison Between the Integration and Closed–Form Results for the $E_{\theta}^{(x)}$ Component at 10 GHz

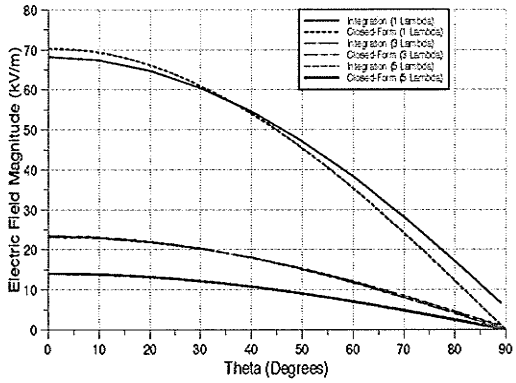

a) Magnitude

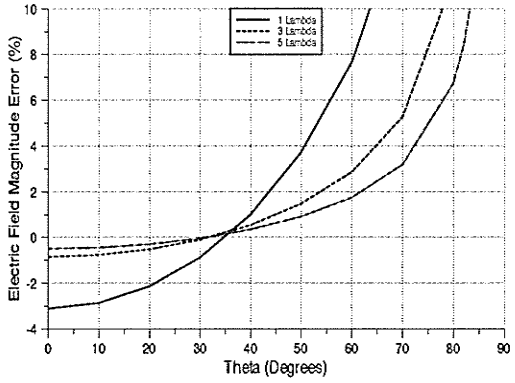

b) Error

Figure 13: A Comparison Between the Integration and Closed–Form Results for the $E_{\phi}^{(y)}$ Component at 10 GHz

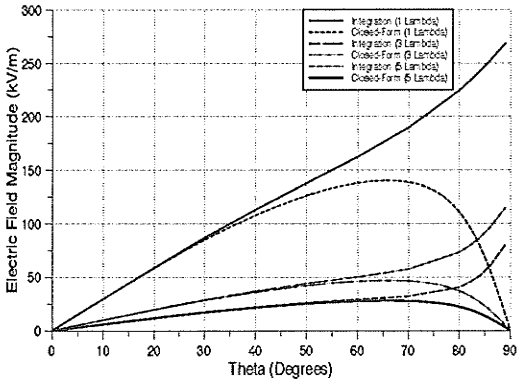

a) Magnitude

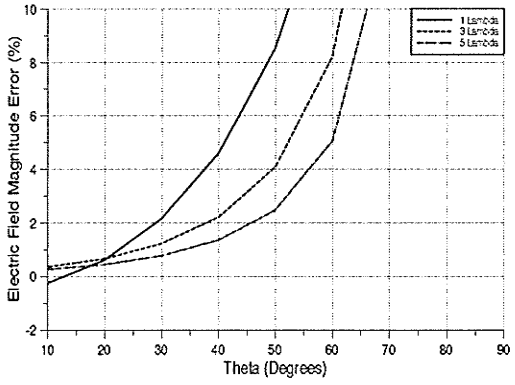

b) Error

Figure 14: A Comparison Between the Integration and Closed–Form Results for the $E_{\theta}^{(z)}$ Component at 10 GHz

becomes larger than 55^o. This increase in error as the frequency increases and/or the elevation angle decreases is also an expected result since eventually the steepest descent path gets too close to a pole so that the contribution by the saddle point is no longer the only contributor to the field result.

Now, as θ increases, the steepest descent path will eventually cross directly over a pole. The value of θ at this point (denoted θ_{crit}) serves as a minimum elevation angle indicator since as θ approaches this value the error will begin to increase at an increasing rate and once the pole is crossed the error becomes much too large for the closed–form result to be useful due to the exclusion of an entire pole contribution. Finding the value of θ_{crit} is quite straight forward assuming we know the value of k_ϱ at which these poles occur, (recall that the pole locations for the numerator functions are simply defined by equations (3.41) and (3.48) while the pole locations for the denominator functions must be found numerically). Now, beginning with the denominator poles, remember that they occur in the range $k_0 < \left|k_\varrho\right| < \sqrt{\varepsilon_{rd}}k_0$ in the k_ϱ plane, (or correspondingly between $\Psi = \pm\ \pi/2$ and $\Psi = \pm\ \pi/2\ \pm j\sin^{-1}\left(\sqrt{\varepsilon_{rd}}\right)$ in the Ψ plane) for a lossless substrate. Therefore, observing Fig. 7 in section 3.1.4 we notice that since the steepest descent path in the Ψ plane crosses the line $\Psi = \pi/2$ with a decreasing imaginary value of Ψ as θ increases, the steepest descent paths first possible encounter with a denominator pole occurs at the upper end of the range of possible Ψ. To then obtain the actual value of θ_{crit} corresponding to the value of k_ϱ (or Ψ) at which such a pole is crossed we simply take equation (3.76) and substitute therein, $\Psi = \pi/2 + j\beta$ giving,

$$\cos\left(\frac{\pi}{2} - \theta_{crit}\right) = \frac{1}{\cosh(\beta)} \tag{4.21}$$

or [CRC],

$$\theta_{crit} = \sin^{-1}\left[\frac{1}{\cosh(\beta)}\right] . \tag{4.22}$$

Then, since $k_\varrho = k_0 \sin\Psi$ we have,

$$k_{\varrho p} = k_0 \sin\left(\frac{\pi}{2} + j\beta\right) = k_0 \cosh(\beta) \tag{4.23}$$

and therefore,

$$\theta_{crit} = \sin^{-1}\left(\frac{k_0}{k_{\varrho p}}\right) . \tag{4.24}$$

Note that this expression for θ_{crit} is also valid for any numerator poles which occur in the range $k_0 < |k_\varrho| < \sqrt{\varepsilon_{rd}}\,k_0$. For the numerator poles which occur in the range $-k_0 \le |k_\varrho| \le k_0$ in the k_ϱ plane (or correspondingly lie on the real Ψ axis) we simply obtain the equation $\theta_{crit} = \alpha$ from substituting $\beta = 0$ into equation (3.76) and obtain,

$$\theta_{crit} = \sin^{-1}\left(\frac{k_{\varrho p}}{k_0}\right) \tag{4.25}$$

for the value of θ_{crit} given the pole location in the k_ϱ plane.

Finally, for the numerator poles which are situated on the negative imaginary k_ϱ (or Ψ) axis we can substitute $\Psi = j\beta$ into equation (3.76) to yield a similar result to equation (4.22), namely,

$$\theta_{crit} = -\cos^{-1}\left[\frac{1}{\cosh(\beta)}\right] . \tag{4.26}$$

This time however, $k_{\varrho p}$ becomes $k_{\varrho p} = k_0 \sin\Psi = jk_0 \sinh\beta$ and substituting this into the above equation gives the following, where several familiar trigonometric identities have been used [CRC].

$$\theta_{crit} = -\cos^{-1}\left[1/\cosh\left[\sinh^{-1}\left(\frac{k_{\varrho p}}{jk_0}\right)\right]\right] = -\cos^{-1}\left[1/\sqrt{1-\left(\frac{k_{\varrho p}}{k_0}\right)^2}\right] \tag{4.27}$$

In this case $k_{\varrho p}$ is purely imaginary and negative. Therefore substituting $k_{\varrho p} = jk'_{\varrho p}$ into the above equation and applying another well documented identity [CRC], we obtain the final

definition for θ_{crit} due to poles on the negative imaginary k_ϱ (or Ψ) axis as,

$$\theta_{crit} = \tan^{-1}\left(-\frac{k'_{\varrho p}}{k_0}\right) \quad . \tag{4.28}$$

Armed with this new information we can now calculate a minimum elevation angle indicator for our substrate and operating frequencies. Table 1 therefore, shows the location of the first denominator pole encountered at the required operating frequencies, the corresponding value of θ_{crit} and the elevation angle. It also includes the largest possible pole

Frequency (f)	Pole Position ($k_{\varrho p}$)	θ_{crit}	Elevation Angle
1GHz	1.000183 k_0	88.90°	1.10°
10GHz	1.019068 k_0	78.90°	11.10°
All	$\sqrt{\varepsilon_{rd}}\,k_0 = 1.596872\,k_0$	38.77°	51.23°

Table 1 : The Relevant Denominator Poles

location (which occurs at $k_\varrho = \sqrt{\varepsilon_{rd}}\,k_0$ or $\Psi = \pi/2 + j\sin^{-1}\left(\sqrt{\varepsilon_{rd}}\right)$ as mentioned earlier) with its corresponding angles since this is valid for any frequency. A numerical root solver was written in FORTRAN to find these poles and it should be noted that the poles given in Table 1 at our desired operating frequencies are the only denominator poles present at these frequencies and are due to the D_{TM} function. Now, Table 2 is similar to Table 1 but shows

Frequency (f)	Pole Position ($k'_{\varrho p}$)	θ_{crit}	Elevation Angle
1GHz	– 49.974493 k_0	88.85°	1.15°
10GHz	– 4.738143 k_0	78.08°	11.92°

Table 2 : The Relevant Numerator Poles

the locations and corresponding angles of the numerator functions. Note that these pole locations will change not only with frequency, as for the denominator poles, but also with the depth of the source within the substrate. Finally, comparing these two tables we find that,

for both frequencies, the numerator pole is encountered first. It should be stressed at this point, that the minimum elevation angle indicators should only be used as an indication of where the error becomes much too large for the result to be acceptable. The actual value of θ_{crit} at which the result becomes unacceptable may be much smaller than the one indicated by the minimum elevation angle and is dependent on the accuracy desired. This is obvious when comparing the points at which our results exceed 2% error with the values given in the above tables. Remember that only proximity to a pole is required to throw off the accuracy of the results, not just actual pole exclusion.

The above discussion of the numerator and denominator poles is important but since our steepest descent path does not remain on the proper Riemann sheet for its entirety we can also encounter improper poles whose contribution should be accounted for. These poles are usually termed leaky wave poles [Felsen1], and their positions must be found numerically. Given their location however we can also calculate their θ_{crit} and elevation angle indicators in a similar way to that used for the proper poles.

Before ending this section it is interesting to note from Figs. 9–14 that the integrated E_θ results for both the x and z directed dipoles increase as θ approaches the substrate surface while the corresponding closed–form results become zero at the surface. This is due to the fact that the closed–form equation assumes that no poles of any kind are present while the integration obviously takes them into account. The reason for the increase in field result is that the denominator poles are responsible for the launching of surface waves, so called since they propagate along the surface of the substrate and decay much more slowly than the regular space waves with a decay proportional to $1/\sqrt{r}$ [Felsen1].

4.2 Time Domain Results

In this section we will examine and discuss time domain electric field waveforms radiated from several different microstrip structures. Before we do however, it should be noted that simple dipole results were compared with [Cicchetti] and found to be identical so we will

only deal with more complex structures here. Now, as was mentioned early on in this document, our solution depends on the knowledge of the current derivatives present on each part of a radiating structure for all points in time up to the present. These current derivatives will be obtained here using a two dimensional Finite Difference Time Domain (FDTD) algorithm which uses square cells and assumes a constant propagation time for all lines, equal to 2/3 the speed of light. This propagation time would in actuality vary depending on the permittivity of the dielectric and the depth of the source within the substrate ([Pramanick], [Schneider]), but is not relevant for our purposes since the required current derivatives can be obtained using any desired current simulator, (if it can calculate derivatives), and therefore accuracy of these current derivatives in not our major concern.

The equation which sums the field contributions from each radiating current cell at a particular time and source point was given in equation (3.119) and was discussed in section 3.2. In our development and consequent solution of this equation we chose to do the time integration first for convenience sake and are now left with a volume integration to take into account the contributions from each radiating current element. As we know, there are many ways to perform this integration with varying degrees of accuracy. For simplicity of programming and since our current derivatives were obtained using equally spaced square cells we have chosen a simple rectangular rule of integration. If more accuracy is desired this integration can easily be changed or the number of cells in the FDTD current calculation program increased. It is important to stress again that the currents derivatives can be obtained using any available current calculation software as long as it can calculate the current derivatives at each point required by the chosen integration scheme. Furthermore the accuracy of the fields is directly dependent on the accuracy of the current calculation software and so for large problems a fairly rough (but generally quick) current calculation can be adequate to give a general idea of the time domain radiation, and if increased accuracy is then desired a more robust (but usually slower) current calculation can be used.

Let us begin by looking at some simple, one–dimensional, straight line, x–directed,

and lossless interconnect examples. To be more specific, let us compare the radiated electric field for three similar lines residing in (or on) a $1.5mm$ thick substrate of relative permittivity 2.55 at three spatial observation points and for two different voltage waveforms. Let all three lines have a characteristic impedance of $50\,\Omega$, a length of 4cm and be matched at both the source and load. Then, let one line reside on the surface of the substrate, another be buried inside the substrate at a depth equal to 44.44% the thickness and the last be similarly buried but with vias reaching the surface. Let our excitation current waveforms be gaussian pulses defined as,

$$v_s(t) = 10\exp\left(-t^2/\tau_s^2\right) V \tag{4.29}$$

where in the first case $\tau_s = 20ps$ and in the second $\tau_s = 200ps$ and let us compare their radiation waveforms at a distance of 1m and spherical angles, $\theta = 0^o, \phi = 0^o$, $\theta = 45^o, \phi = 0^o$ and $\theta = 45^o, \phi = 180^o$. The current waveform and its derivative multiplied by the width of a single cell are shown in Fig. 15 where the current is shown at a point just after it has entered the line while its derivative is shown at a point just before it leaves the line. This was done for two reasons, the first being simply to clarify the picture while the second was to show that the line has a 200ps propagation time as we would expect for the given line length and propagation velocity. This particular choice of where to examine these waveforms does not cause a problem since the line is lossless and matched so we know that the current waveform and its derivative will be identical along the entire length of the line. Note also that the maximum current value is 100mA as we would expect for a 10v source with a $50\,\Omega$ source resistance feeding a $50\,\Omega$ line.

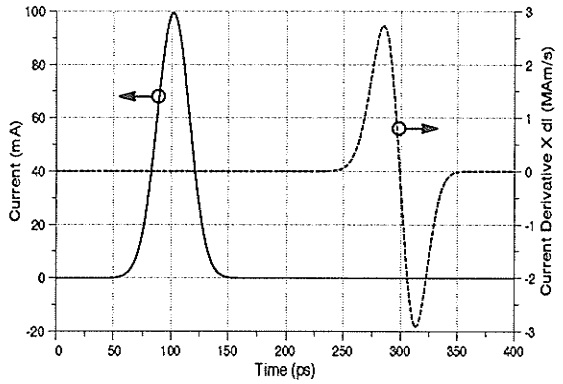

Figure 15: The Transmission Line Current and its Derivative for a Straight, One–Dimensional, Lossless Line

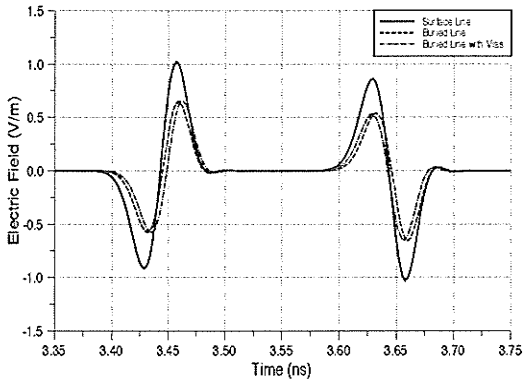

Figure 16: The E_θ Field Component at Spherical Position $(1m, 0^o, 0^o)$ Due to a 20 ps Gaussian Excitation

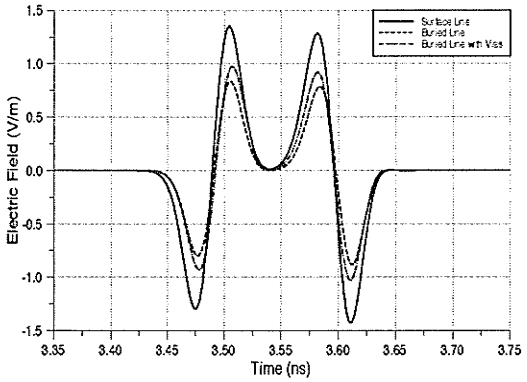

Figure 17: The E_θ Field Component at Spherical Position $(1m, 45^o, 0^o)$ Due to a 20 ps Gaussian Excitation

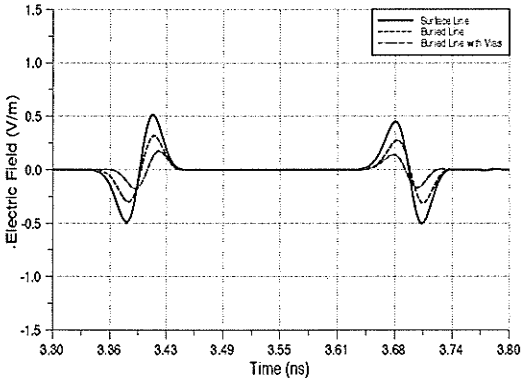

Figure 18: The E_θ Field Component at Spherical Position $(1m, 45^o, 180^o)$ Due to a 20 ps Gaussian Excitation

Now, knowing the waveform of the current derivative multiplied by the cell width allows us to perform our spatial numerical integration by simply summing this derivative value for each cell over all the cells. To do both the time and space summations a FORTRAN program was written together with an openlook windows program for ease of data entry. The results we obtained for the preceding lines are shown in Fig. 16 for the broadside case, ($\theta = 0^o, \phi = 0^o$), Fig. 17 for the 45 degree forward radiating case, ($\theta = 45^o, \phi = 0^o$), and Fig. 18 for the 45 degree backward radiating case, ($\theta = 45^o, \phi = 180^o$). The first thing that we should notice in examining these three figures is that for the broadside case the time interval between the first gaussian derivative waveform and the second is exactly 200ps, (except in the case of the buried line with vias which looks slightly shorter spatially and so the time interval is about 196ps). This duration is exactly the propagation time of the current waveform down the line and goes to show that, as

expected for a lossless line, the only current values which contribute to the radiated electric field are those occurring at entry and exit points of the line as well as at any geometrical discontinuities on the line [Schelkunoff]. This occurs because the field contribution from each segment of the line is just a time shifted version of the same electric field waveform, causing all of the individual contributions to add at the propagation times corresponding to the propagation from the beginning and end of the line to the observation point but cancel at all other times. This cancellation is also responsible for the opposite signs of the two waveforms radiated from each end of the line. It should be mentioned before proceeding that, in actuality the buried line with vias has added discontinuities at the joints between the vias and the horizontal line but since we used a two–dimensional FDTD method to obtain the currents these discontinuities are not present and so their contribution to the radiated fields is not present either.

Now, comparing the broadside results with the results of the forward radiating case, Fig. 17, we find that in this case the field magnitude has increased and the time duration has compressed by approximately 94ps. This time compression is due to the difference in the distance from the end–points of the line to the observation point, (which can be proved trigonometrically), and to the fact that the current pulse is traveling in the direction of the observation point forcing the field due to the final current to travel a smaller distance than the field from the initial current. This same phenomenon also accounts for the increase in field magnitude since the waveforms of the fields radiated by each current element occur closer together causing their magnitudes to add up to a greater degree. The exact opposite is true for the backward radiating case, Fig. 18, in which the field magnitude has decreased and the time duration has expanded by 94ps as compared to that of the broadside case. This expansion and decrease in magnitude is similarly due to the fact that the current pulse is traveling away from the observation point so that the field due to the final current has a larger distance to travel than the field from the initial current.

It should be noticed that the surface trace radiates more than the buried traces in all

cases as would be expected. We also find that the buried line with vias radiates a field of the same magnitude as the buried line at broadside which is reasonable since as we saw in the the previous section vertical elements do not radiate in this direction. The two $\theta = 45^o$ cases are interesting however since the buried line with vias radiates a greater field strength than the buried line, for the $\phi = 0^o$ case and less for the $\phi = 180^o$ case. This is due to the fact that in the first case the positively directed via is closer to the observation point and so the fields due to the two vias end up adding to the radiation from the horizontal line while in the other case the negatively directed via is closer and the two vias end up subtracting from the radiation due to the horizontal line. Finally, we should also note that in the case of a buried line with vias the same expansion and compression as was discussed earlier is obvious but since the line looks slightly smaller the change in time duration does not keep in step with that of the two straight lines, as can be seen from the figures.

Now since we found in the preceding section that the accuracy of our results increases with electrical distance but decreases with frequency and an increasing θ angle we should try to get a handle on our accuracy in the time domain. Since we have excited the line with a 20ps Gaussian voltage source we can perform a Fourier transform on this equation to obtain the frequency domain representation of this source voltage waveform. This is a well known Fourier transform [Trim2], and so we will simply state its frequency domain equivalent to be,

$$v_s(\omega) = 10\tau_s\sqrt{\pi}\exp\left(-\omega^2\tau_s^2/4\right) = \frac{20\sqrt{\pi}}{\tau_\omega}\exp\left(-\omega^2/\tau_\omega^2\right) V \qquad (4.30)$$

were $\tau_\omega = 2/\tau_s$. Now letting $\omega = 2\pi f$, $\tau_\omega = 2\pi\tau_f$ and substituting into the previous expression we obtain finally,

$$v_s(f) = \frac{10}{\sqrt{\pi}\tau_f}\exp\left(-f^2/\tau_f^2\right) V \qquad (4.31)$$

where $\tau_f = 1/\tau_s\pi$. This final Frequency Domain result looks very similar to our original time

domain waveform except for a change in magnitude. Now from statistical analysis [Devore], we know that a Gaussian distribution takes on the form,

$$\frac{1}{\sqrt{2\pi}\sigma}\exp\left(-f^2/2\sigma^2\right) \tag{4.32}$$

where σ is the the standard distribution and where $\pm\,\sigma$ occur at the inflection points of the waveform. It can furthermore be shown that, for a one sided distribution, 68.26% of the area under this curve occurs in the range $0 \le t \le \sigma$. Therefore we can use the standard deviation as an indicator of the frequency content of a Gaussian. In the case of our time domain Gaussian the frequency domain spectrum given in equation (4.31) has a standard deviation which can be found by equating τ_f to $\sqrt{2}\sigma$ giving $\sigma = 1/\sqrt{2}\pi\tau_s$.

In our present case of a 20ps Gaussian we find that the standard deviation in the frequency domain is 11.25GHz. We then know that the spectrum decays beyond this point and contains only 31.74% of the area under the waveform. In the previous section we graphed error results for 10GHz and so we shall use this error for our standard deviation error. The wavelength at 10GHz is 3cm which for our 100cm distance makes the observation point 33.33 wavelengths distant. We will therefore read off the 5 lambda curves for the component $E_\theta^{(x)}$ which gives us a maximum error of about 1%. This error is more than acceptable and would only be better for our actual distance and only slightly worse for our actual standard deviation frequency. In fact it seems to indicate that our error would remain acceptable for many frequencies beyond our standard deviation frequency. At frequencies below this frequency our error decreases since the number of denominator poles decreases until there are none. However at low frequencies such as those below 300MHz, (which has a wavelength of 1m making the electrical distance one lambda for our observation distance) the error will increase again since our distance from the source is no longer in the far field.

Let us now look at the same results for the case of the 200ps time domain Gaussian. These results are shown in Figs. 19–21 from which we now see that there is no obvious

separation between the radiation from the beginning and end of the line, as there was for the 20ps case. This is simply due to the fact that the transit time along the line is much less than the duration of the waveform. This accounts for all the waveforms looking identical in shape and duration but having varying magnitudes. Looking more closely however we find, as in the 20ps case, a slight time compression in the forward radiating case and a slight expansion in the backward radiating case but since this time variation is, as previously, 94ps and the graphs are displayed in nanoseconds these shifts are understandably hard to see. Other than this the behavior is basically the same as that in the 20ps case.

Now, as we did previously, we can again find the standard deviation for this excitation waveform, which turns out to be 1.125GHz. In the preceding section we obtained results for the 1GHz case which has a wavelength of 30cm. For our 1m observation distance this turns out to be 3.33 lambda distant and so we read off the 3 lambda curve for the component $E_\theta^{(x)}$

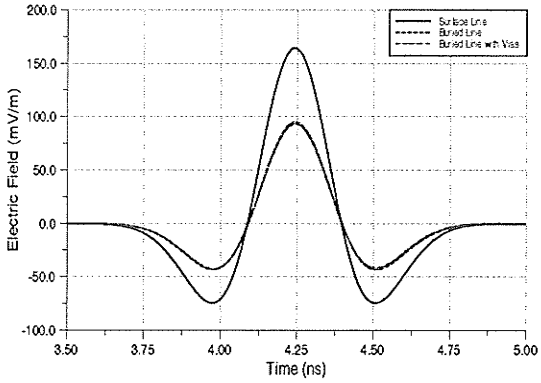

Figure 19: The E_θ Field Component at Spherical Position $(1m, 0^o, 0^o)$ Due to a 200 ps Gaussian Excitation

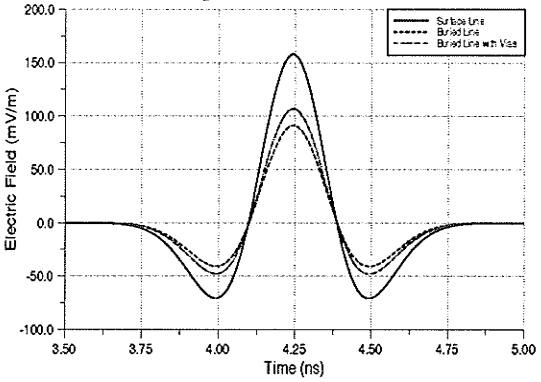

Figure 20: The E_θ Field Component at Spherical Position $(1m, 45^o, 0^o)$ Due to a 200 ps Gaussian Excitation

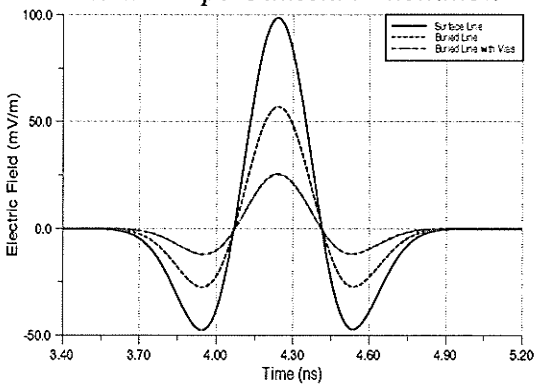

Figure 21: The E_θ Field Component at Spherical Position $(1m, 45^o, 180^o)$ Due to a 200 ps Gaussian Excitation

which yields an error of approximately 0.1% which would again seem to indicate that the error would remain more than reasonable for many frequencies beyond our standard deviation frequencies.

Let us now examine a few, more difficult cases using one–dimensional lines. In all cases we will use a $1.578mm$ thick substrate with a relative permittivity of 2.55. The first case we will look at is again a 4cm transmission line printed on the surface of the substrate but with an open circuit at the end of the line and a mismatch at the beginning. The characteristic impedance of the line is $50\,\Omega$ and the source resistance is $20\,\Omega$ creating the mismatch. We then excite the line using an exponential rise with a steady state value of one volt. This waveform is defined as,

$$v_s(t) = \left[1 - \exp(-t/\tau_s)\right] V \quad (4.33)$$

where $\tau_s = 100ps$. The voltage waveform at the beginning of the line and the θ component of the electric field at a distance of one meter directly above the center of the line are shown in Fig. 22 where the field component has been shifted back in time, by the transit time, to the observation point. Observing first of all the voltage waveform we should note that the current entering the line is $5/7v_s(t)$ due to the voltage division caused by the source resistance and the line characteristic impedance. We then observe several exponential curves occurring on top of one another but each delayed by 400ps from the previous. This delay is simply equal to the propagation time to the end of the line and back. Therefore we see in the the first 400ps interval the exponential trying to reach 5/7V, (0.71V). At the end of this interval the reflected wave from the end of the line adds to the existing voltage, (note that this waveform is identical to the waveform initially launched since the

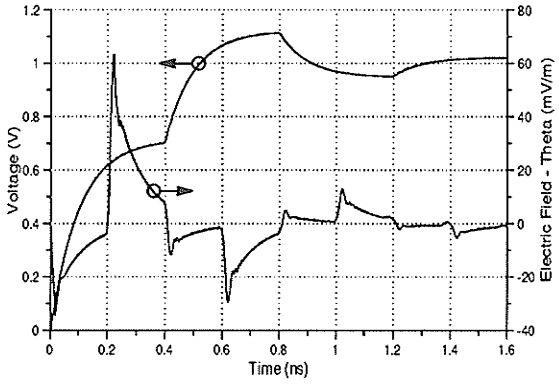

Figure 22: The Voltage and Electric Field Waveforms at Broadside for a Lossless Line Displaying Ringing Effects

end of the line has a reflection coefficient of 1). However, since we are observing the voltage waveform at the beginning of the line we also have another reflected wave from the beginning of the line adding its contribution simultaneously. The voltage reflection coefficient at the beginning of the line can be calculated to be –3/7 and so the overall effect of the incoming and reflected wave is only $5/7(1-3/7)v_s(t)$, which has a peek of 0.41V. Adding this voltage to the initial voltage we obtain 1.12V which we can see is what the waveform is trying to reach after another 400ps interval. At this time the incoming wave is equal to the last wave reflected from the beginning of the line or $5/7(-3/7)v_s(t)$ while the next reflected wave is equal to $5/7(-3/7)(-3/7)v_s(t)$ giving us an overall effect of $5/7(-3/7)(1-3/7)v_s(t)$ which tends toward –0.17. Adding this to the first two exponentials yields 0.95 and now this is the value that the waveform is trying to reach after the next 400ps interval. As this oscillation continues we can see the wave approaching a steady state value of one volt which would also have been the case had the line been matched. Now that we understand the behavior of the voltage we see that the field results follow a similar pattern. This time however we obtain a jump in the field value at the beginning of every 200ps interval followed by an exponential decay. This again is due to the radiation from the ends of the line which we know have propagation times differing by 200ps. The ringing which is apparent on top of the exponential decay is most likely due to numerical inaccuracies in the calculation of the current derivative which is close to being infinite at the beginning of each exponential decay. Note that these results are identical to the ones obtained by [Bridges2].

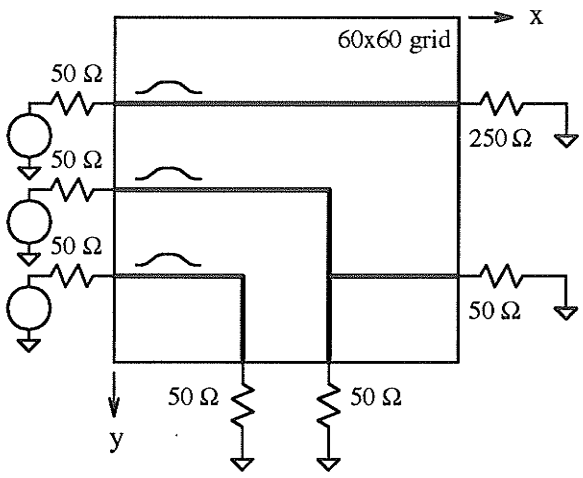

Figure 23: The Geometry of a Complex, One–Dimensional Interconnect Example

Moving on to a slightly more

complicated case let us examine the radiation from a combination of lines printed on the substrate and having both x and y directed sections. Let us excite each of these lines simultaneously with identical 50ps Gaussian pulses. The geometry of these lines is shown in Fig. 23 from which we can see several discontinuities which will add to the overall radiation. The board that these lines are printed on is centered about the origin, has an overall size of $4cm \times 4cm$ and has been modeled using an FDTD grid of 60×60 cells to obtain the current derivatives along the lines. The current simulation was run for 698ps to allow all the waveforms to die down and the current waveforms present on these lines at two instants in time are shown in Figs. 24 and 25. Fig. 24 shows us these waveforms as the T–junction on the middle line is reached while Fig. 25 shows us the waves being reflected by the unmatched load on the upper line and the T–junction on the middle line as well as the absorption of the currents approaching the ends of the two bent lines. The θ and ϕ components of the electric field for several θ angles in the E–plane are shown in Fig. 26 where the time duration of each of the graphs is from 320ps to 420ps. We again notice the familiar compression and expansion of the θ component depending on if the waveforms are propagating toward the observation point or away from the observation point. It is interesting to note that the ϕ component has a slightly later starting time than the θ component which is due to the fact that only the x–directed sections of line radiate E_θ while only the y–directed sections radiate E_ϕ and obviously all the lines begin in the x–direction.

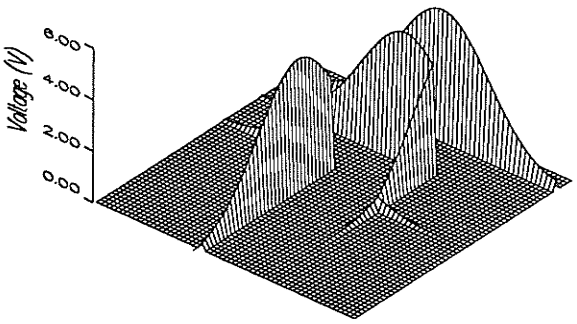

Figure 24: The Gaussian Waveforms for the Complex Example at a Time of 262 ps

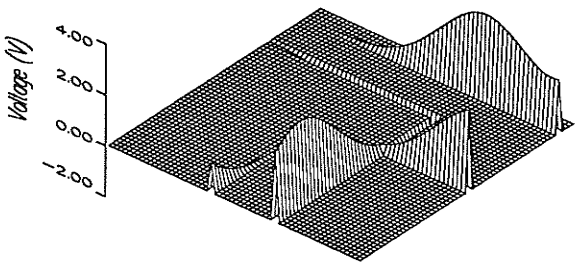

Figure 25: The Gaussian Waveforms for the Complex Example at a Time of 409 ps

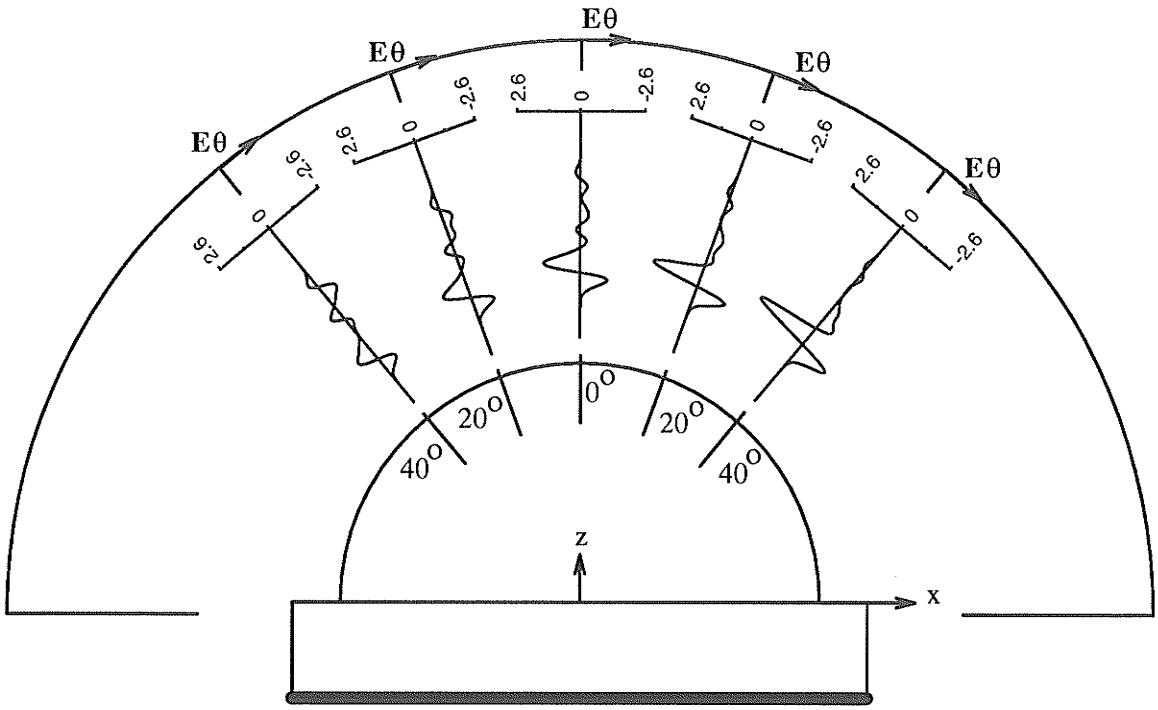

a) Theta Component

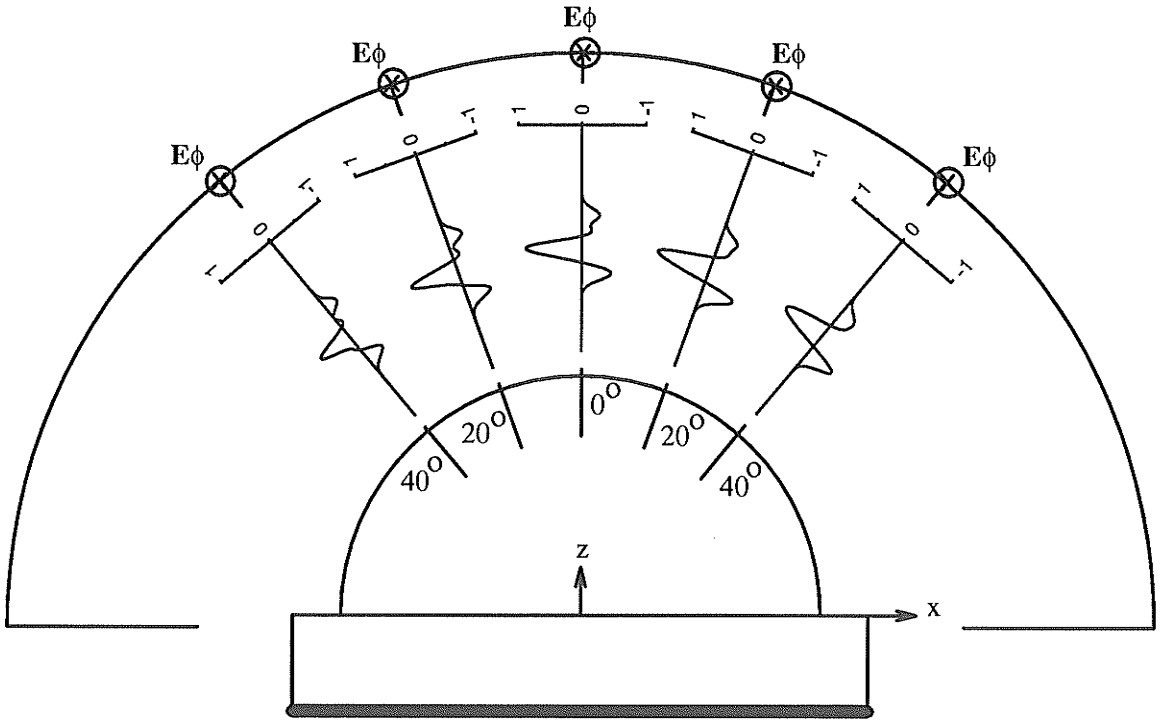

b) Phi Component

Figure 26: The E–Plane Radiated Electric Fields for the Complex Example at Several Values of Theta

The final case which we will look at is that of a bent 'fat–line'. This line is basically identical to the bent line in the previous example and is printed on the same substrate. This line has the same center length as the previous line but is 4mm or 6 cells wide. Now, as the line becomes wide with respect to the pulse duration the waveforms begin to reflect between the walls of the line and not only directly back on themselves. For our purposes we have excited this 'fat–line' with a 30ps Gaussian pulse. This pulse width begins to show the preceding property but not to such an extent that the reflections take an extremely long time to die down. In this case the current simulation was run for 931ps to allow the line to settle down and the current waveforms present on the lines at two instants in time are shown in Figs. 27 and 28. Figure 27 shows the waveform just after it has hit the corner while Fig. 28 shows the reflection and transmission from the corner as they are about to be absorbed.

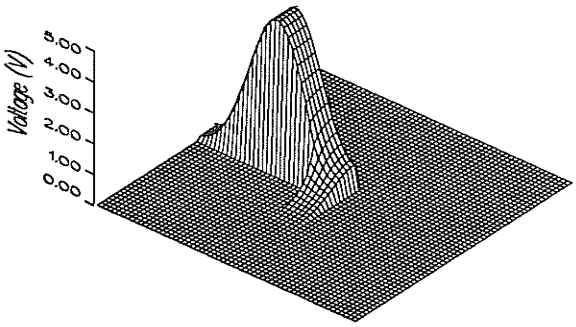

Figure 27: The Gaussian Waveforms for the Fat–Line Example at a Time of 210 ps

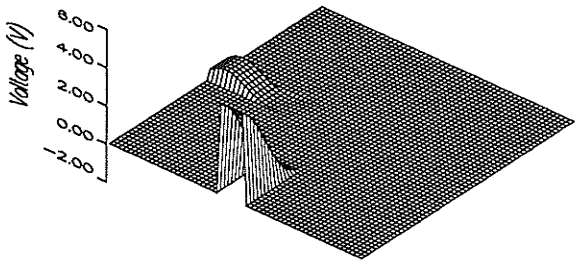

Figure 28: The Gaussian Waveforms for the Fat–Line Example at a Time of 350 ps

The θ and ϕ components of the electric field for several θ angles in the E–plane are shown in Fig. 29 where, as in the previous example, the time duration of each of the graphs is from 320ps to 420ps. As before we again notice the familiar compression and expansion of the θ component depending on if the waveforms are propagating toward the observation point or away from the observation point. The ϕ component again has a slightly later starting time than the θ component since our Gaussian propagates down the x–directed section of line first. We notice however that this time the ϕ components of field look basically identical to each other but their magnitude decreases with the elevation angle. This

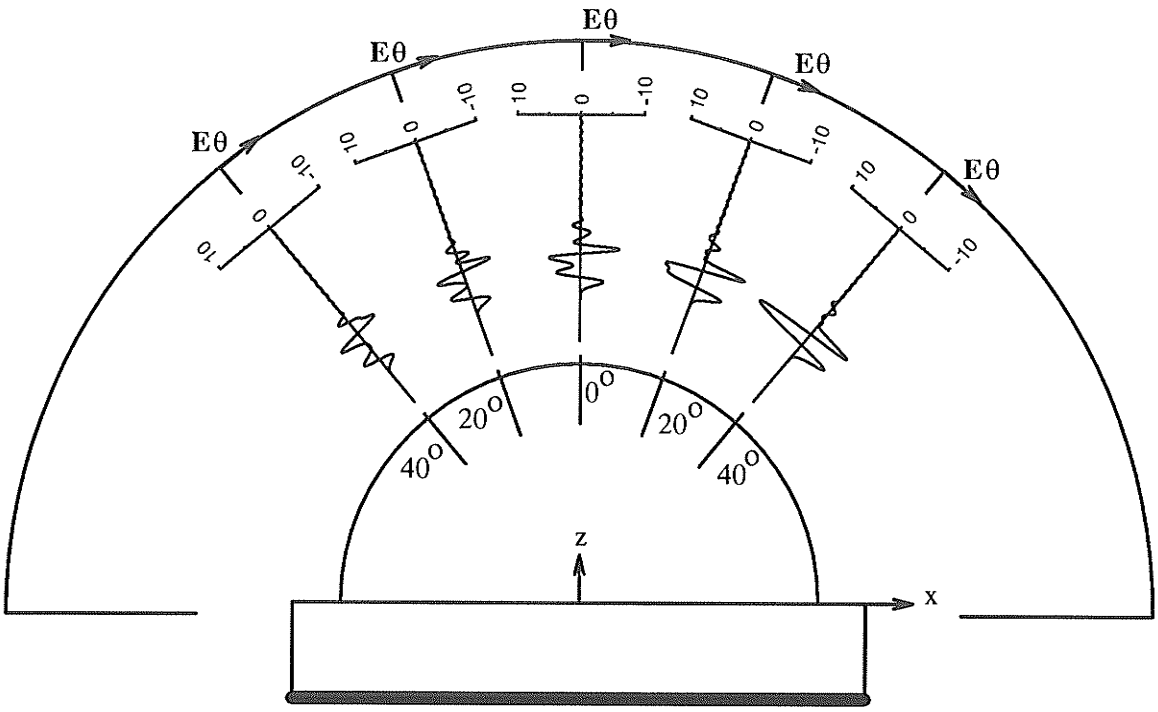

a) Theta Component

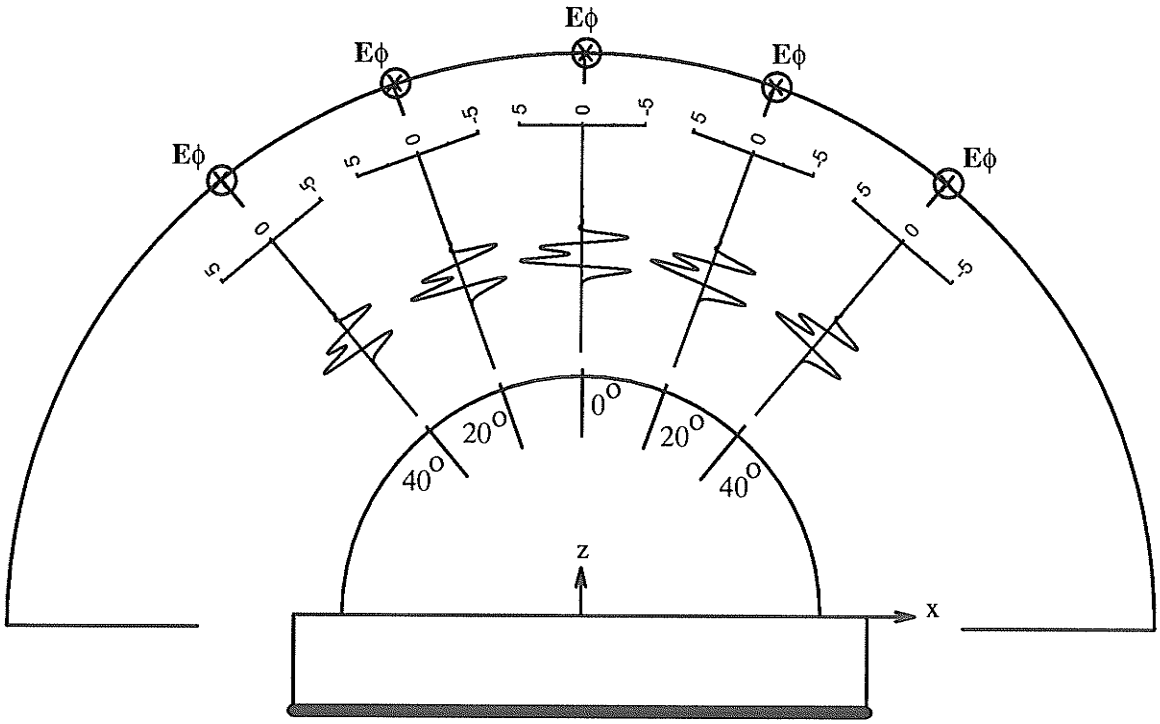

b) Phi Component

Figure 29: The E–Plane Radiated Electric Fields for the Fat–Line Example at Several Values of Theta

is due to the fact that now the waveform is propagating away from all of the observation points in the exact same manner where the change in magnitude is simply caused by the formula for this field component which decays as $\cos\theta$. Many more examples could be demonstrated in this section, however the ones already shown have one or more of the general characteristics of any lossless example we could probably think of. Besides, the idea here was to show the merit of the method and not to grind out one example after another.

Before concluding this chapter though, it is worthwhile to note some approximate computation times for the previous results. All of the following times are for the broadside instances, were calculated by the /usr/bin/time command on a Sun Sparc 10 workstation and include the actual user cpu times only. The first set of examples for the 20ps Gaussian travelling along the surface and buried lines took an average of approximately 6.15 seconds.These lines consisted of 60 cells and the results were calculated for 200 time points giving us an average incremental time (time/(cell*timepoints)) of 512μ s. The 200ps examples on these same lines took an average of approximately 1 minute 23.75 seconds and since we now used 800 time points we get an average incremental time of 1.75ms. It is interesting to note from this that the average incremental time increased from the previous by a factor of 3.4. Since the number of cells remained constant for these two cases this means that as the number of time points increases more time is spent for each time point, (on average). We can see that this must be the case by remembering that the result for each component of field at each point in time is due to a summation from the start of the waveform to the present time. Therefore as the present time increases a greater number of terms are included in the summation. These summations could be made more efficient however since they decay with the factors $(-\Gamma_v)^n$ and Γ_u^n and so eventually the contributions of any added terms makes only negligible difference to the answer. This was not implemented here since accuracy and not speed was desired. As for the remaining examples we find that the exponential took the longest since it had the largest number of time points at 1370. Together

with this it used 120 cells (rather than 60) for increased accuracy (the line length remained unchanged at 4cm) and took an average of 9 minutes 44.7 seconds to execute. Then the 'fat–line' consisting of 720 cells and 400 time points took 5 minutes 20.6 seconds and finally the complex one dimensional case consisting of 228 cells and 300 time points took on average 2 minutes 14.5 seconds. In closing it should be mentioned that these times will increase for angles of θ greater than zero since the value of τ_θ decreases with θ and so the number of terms in each summation will increase since the time between the two adjacent time derivatives of the current decreases. A similar effect occurs for buried lines and was evident for the preceding buried line examples for which we took the average between the buried and surface lines. The effect was extremely small for the 20ps Gaussian pulse and about a second in the case of the 200ps pulse.

CHAPTER 5

CONCLUSION

5.1 Summary and Conclusions

In this document we have developed, in detail, the procedure for obtaining a closed form far field approximation to the time domain electric field dyadic Green function for a single dielectric, PCB problem. To do this the frequency domain dyadic Green function was developed first and although parts of that development have been done before, they were included, discussed and explained herein so as to aid future researchers in this area. This was deemed important since no detailed explanations of such developments seem to exist, (at least not one that someone new to the area can understand). The method used thereafter to obtain the time domain dyadic Green function from the frequency domain Green function was developed by the author and the results were shown to be identical to those of [Cicchetti]. The time domain dyadic Green function was then implemented in a FORTRAN and openlook program and several results of lossless lines and collections of lines were displayed and discussed. Some results of this work have already been published, [Lohse1], or will be published in the near future, ([Lohse2], [Lohse3]).

Following the actual development of the method we demonstrated that the saddle point method, which was used to obtain the closed form result, yielded excellent results when compared with the actual integrated results in the frequency domain. For example, at a distance of one wavelength from the source we found that the results had an error of less than 2% for a frequency of 1 GHz and quite a large range of θ, (up to about 50^o or better depending on the component). We also found that as the frequency increases the error increases due to the steepest descent paths approach on one or more poles or branch points. The locations and effects of these poles were discussed throughout the document and even though their contributions were not included in the saddle point approximation to the inverse (spectral–frequency to frequency domain) Fourier transform integral it was shown that these poles have a negligible effect at frequencies up to and beyond 1 GHz at observation distances

greater than one wavelength. Furthermore, at very small elevation angles it is only the branch point that causes this error to occur. Then, in the time domain we proved that our closed form method yielded physically interpretable results very quickly.

It should be obvious that more complex structures than the ones analyzed in this document could be addressed without modifying the existing method. For instance, PCBs consisting of many traces or multiple layers of the same or similar dielectric material could be easily analyzed with good results. Furthermore, the method has shown distinct advantages over frequency domain methods, one of which was that current waveforms which have a wide band frequency content can be evaluated with one simple summation instead of requiring the solution of the radiated field at many frequency components. For similar reasons, using this method to obtain time domain results and follow that by an FFT to obtain the frequency domain spectrum is also a reasonable and desirable approach to analyzing wide band waveforms. The ease in programming these results was evident from the simplicity of the resulting time domain dyadic Green function and so the fact that such a program can easily be written to take current results from any available signal integrity software and compute the time domain fields in a short time is a definite asset to circuit designers and EMC engineers alike.

The down side of this method is its restriction to board level radiation only since this type of radiation is completely unrealistic in most real word problems where enclosures, cabling and other scatterers are present. Having said this, it is perhaps possible to incorporate this method into many, more general, applications to increase its scope and extend it usefulness.

5.2 Recommendations for Future Work

Future research in this area is definitely warranted since quick, approximate methods are always required even with the ever increasing computer power that is available today. For instance, to rigorously solve a printed circuit board problem where the board contains

thousands of current traces or elements would take many days or more. Therefore a quick approximate method which has a reasonable error over a certain range of some variable can be invaluable. To the circuit designer or EMC engineer, who doesn't care about a perfect answer (which is realistically unattainable anyway), an indication in a reasonable amount of time, of where an EMC problem may occur may be more desirable.

Future work which is a direct extension to this written document could be to further analyze the effects of the surface wave (denominator) poles, the numerator poles and the leaky wave poles which were discussed herein. A novel way of incorporating the effects of all these poles in the time domain summation would be extremely valuable in increasing the accuracy of the method. Other than further pole analysis, numerical methods to account for more realistic finite transverse dimensions or multiple layers of different dielectric material could be very useful. Finally, a parallel development using a lossy dielectric and/or ground plane would be warranted to make the method more robust.

Lastly, it would be interesting to further investigate the result obtained in section 2.7 to determine if this is a physical phenomenon or simply some sort of mathematical discrepancy. Such an investigation would perhaps bring greater understanding to the radiation principles of printed circuit structures.

REFERENCES

[Abramowitz] M. Abramowitz, I. A. Stegun, 'Handbook of Mathematical Functions with Formulas, Graphs and Mathematical Tables', U. S. Department of Commerce, National Bureau of Standards, 1964.

[Aksun] M. I. Aksun, R. Mittra, 'Spurious Radiation from Microstrip Interconnects', IEEE Trans. EMC, Vol. 35, No. 2, pp. 148–158, May 1993.

[Archambeault] B. Archambeault, 'The World of EMI Modeling', Interference Technology Engineers' Master (ITEM), pp. 47–54 & 246–248, 1995.

[Balanis] C. A. Balanis, 'Antenna Theory – Analysis and Design', John Wiley & Sons Inc., 1982.

[Barkeshli] S. Barkeshli, P. H. Pathak, 'Radial Propagation and Steepest Descent Path Integral Representations of the Planar Microstrip Dyadic Green's Function', Radio Science, Vol. 25, No. 2, pp. 161–174, March–April 1990.

[Bridges1] G. E. Bridges, 'Theory of Guided Waves for Cylindrical Structures Embedded in Stratified Media', Ph. D. Dissertation, University of Manitoba, 1989.

[Bridges2] G. E. Bridges, 'Radiated Fields from Transient Signals on Open Microstrip', in Proc. of ANTEM, 1992 Symposium, Winnipeg, pp. 191–196, July 1992.

[Cabral] S. W. Cabral, 'A Survey of Commercially Available Electromagnetic Modeling Software', in Proc. of IEEE International EMC Symposium, Dallas, pp. 284–288, August 1993.

[Campbell] S. L. Campbell, 'An Introduction to Differential Equations and Their Applications', Longman Inc., 1986.

[Cicchetti] R. Cicchetti, 'Transient Analysis of Radiated Field from Electric Dipoles and Microstrip Lines', IEEE Trans. Antennas and Prop., Vol. 39, No. 7, pp. 910–918, July 1991.

[Choi] I. Choi, 'An Efficient Representation for the Planar Microstrip Green's Function', Ph. D. Dissertation, Ohio State University, 1986.

[Collin] R. E. Collin, 'Field Theory of Guided Waves – Second Edition', IEEE Press Inc., 1991.

[CRC] W. H. Beyer, 'CRC Standard Mathematical Tables – 26th Edition', CRC Press Inc., 1981.

[Devore] J. L. Devore, 'Probability and Statistics for Engineering and the Sciences – Second Edition', Wadsworth Inc., 1987.

[Felsen1] L. B. Felsen, N. Marcuvitz, 'Radiation and Scattering of Waves', Prentice–Hall Inc., 1973.

[Felsen2] L. B. Felsen, F. Niu, 'Spectral Analysis and Synthesis Options for Short Pulse Radiation from a Point Dipole in a Grounded Dielectric Layer', IEEE Trans. Antennas and Prop., Vol. 41, No. 6, pp. 747–754, June 1993.

[Goyal] R. Goyal, 'Managing Signal Integrity', IEEE Spectrum, pp. 54–58, March 1994.

[Gravelle] L. B. Gravelle, P. F. Wilson, 'EMI/EMC in Printed Circuit Boards – A Literature Review', IEEE Trans. EMC, Vol. 34, No. 2, pp. 109–116, May 1992.

[Harrington] R. F. Harrington, 'Time–Harmonic Electromagnetic Fields', McGraw–Hill Book Co. Inc., 1961.

[Herault] J. Herault, R Moini, A. Reineix, B. Jecko, 'A New Approach to Microstrip Antennas Using a Mixed Analysis: Transient–Frequency', IEEE Trans. Antennas and Prop., Vol. 38, No. 8, pp. 1166–1175, August 1990.

[Jackson] J. D. Jackson, 'Classical Electrodynamics – Second Edition', John Wiley & Sons Inc., 1975.

[Kong] J. A. Kong, 'Theory of Electromagnetic Waves', John Wiley & Sons Inc., 1975.

[Lohse1] R. D. Lohse, G. E. Bridges, 'Calculation of Transient Radiated Fields from High Speed Interconnects', in Proc. of Canadian Conference on VLSI, Banff, pp. 1A 6–11, November 1993.

[Lohse2] R. D. Lohse, G. E. Bridges, 'Calculation of Transient Radiated Fields from High Speed Interconnects', IEEE Trans. EMC, Accepted for Publication.

[Lohse3] R. D. Lohse, G. E. Bridges, 'An Efficient Algorithm for the Calculation of Transient Radiated Fields from Printed Circuit Interconnects', in Proc. of ANTEM, 1996 Symposium, Montreal, pp 295–298, August 1996.

[Marin1] M. Marin, S. Barkeshli, P. H. Pathak, 'Efficient Analysis of Planar Microstrip Geometries Using a Closed–Form Asymptotic Representation of the Grounded Dielectric Slab Green's Function', IEEE Trans. Microwave Theory and Tech., Vol. 37, No. 4, pp. 669–679, April 1989.

[Marin2] M. A. Marin, S. Barkeshli, P. H. Pathak, 'On the Location of Proper and Improper Surface Wave Poles for the Grounded Dielectric Slab', IEEE Trans. Antennas and Prop., Vol. 38, No. 4, pp. 570–572, April 1990.

[Mosig] J. R. Mosig, F. E. Gardiol, 'Analytical and Numerical Techniques in the Green's Function Treatment of Microstrip Antennas and Scatterers', IEE Proc., Vol 130, Pt. H, No. 2, pp. 175–182, March 1983.

[MyintU] T. Myint–U, L. Debnath, 'Partial Differential Equations for Scientists and Engineers – Third Edition', Elsevier Science Publishing Co. Inc., 1987.

[Naishadham] K. Naishadham, J. B. Berry, H. A. N. Hejase, 'Full–Wave Analysis of Radiated Emission from Arbitrarily Shaped Printed Circuit Traces', IEEE Trans. EMC, Vol. 35, No. 3, pp. 366–377, August 1993.

[Pramanick] P. Pramanick, P. Bhartia, 'An Accurate Description of Dispersion in Microstrip', Microwave Journal, pp. 89–96, December 1983.

[Rana] I. E. Rana, 'Theory and Design of Printed Antennas', Ph. D. Dissertation, University of California, 1979.

[Recipes] W. H. Press, 'Numerical Recipes in Fortran: the Art of Scientific Computing', Cambridge University Press Inc., 1992.

[Schelkunoff] S. A. Schelkunoff, 'Electromagnetic Waves', D. Van Nostrand Co. Inc, 1943.

[Schneider] M. V. Schneider, 'Microstrip Dispersion', Proc. IEEE, Vol. 60, pp. 144–146, January 1972.

[Sphicopoulos] T. Sphicopoulos, V. Teodoridis, F. E. Gardiol, 'Dyadic Green Function for the Electromagnetic Field in Multilayered Isotropic Media: an Operator Approach', IEE Proc., Vol. 132, Pt. H, No. 5, pp. 329–334, August 1985.

[Tai] C. T. Tai, 'Dyadic Green's Functions in Electromagnetic Theory', International Textbook Co. Inc., 1971.

[Trim1] D. W. Trim, 'Engineering Mathematics', Ruskin Publishing Co., 1989.

[Trim2] D. W. Trim, 'Applied Partial Differential Equations', PWS–Kent Publishing Co., 1990.

[Tsandoulas] G. N. Tsandoulas, 'Excitation of a Grounded Dielectric Slab by a Horizontal Dipole', IEEE Trans. Antennas and Prop., Vol. AP–17, No. 2, pp. 156–161, March 1969.

[Uzunoglu] N. K. Uzunoglu, N. G. Alexopoulos, J. G. Fikioris, 'Radiation Properties of Microstrip Dipoles', IEEE Trans. Antennas and Prop., Vol. AP–27, No. 6, pp. 853–858, November 1979.

[Vegni] L. Vegni, R. Cicchetti, P. Capece, 'Spectral Dyadic Green's Function Formulation for Planar Integrated Structures', IEEE Trans. Antennas and Prop., Vol. 36, No. 8, pp. 1057–1065, August 1988.